中国科学院北京天文台
博士后研究工作报告

电流螺度与太阳周.
耀斑活动等相关性的研究

包曙东

二〇〇〇年四月六日
中国科学院北京天文台(北京)

分类号_____ 密级_____

UDC_____ 编号_____

中国科学院北京天文台
博士后研究工作报告

电流螺度与太阳周、耀斑活动等相关性的研究

包曙东

研究工作起止时间：1998年7月15日—2000年3月31日

中国科学院北京天文台（北京）

二零零零年四月六日

电流螺度与太阳周、耀斑活动等相关性的研究

『THE STUDIES OF CURRENT HELICITY ASSOCIATED WITH SOLAR CYCLES AND FLARE ACTIVITIES』

博士后姓名： 包 曙 东

博士后流动站单位：中科院北京天文台

博士学位授予单位： 北京师范大学

学科（一级学科）名称： 天文学

专业（二级学科）名称：天体物理

研究工作开始时间：1998 年 7 月 15 日

研究工作期满时间：2000 年 3 月 31 日

中国科学院北京天文台

二零零零年四月六日

目 录

第一篇　概 况

1.1 本课题研究的意义

首先，我们知道磁场已被称作为太阳上的第一物理量，太阳表面上众多的活动现象(如太阳黑子、耀斑爆发等)无不与太阳磁场有关。因此，太阳活动区磁场非势特征的研究对理解太阳表面上各种活动现象的物理机制及动力学过程有着十分重要的意义。这种所谓的非势特征实际上就是磁力线的强扭曲和互嵌套，可以说磁螺度（或电流螺度）是这种非势特性的最好表述。磁螺度在磁重联现象当中也扮演着重要的角色。

其次，我们也知道，如何解释太阳活动的周期性问题是太阳物理上的一个重大问题，这个问题的回答离不开太阳发电机理论。在不同的发电机模型当中，有两个重要参数的选取（$\alpha > 0$，$d\omega/dr < 0$ 或 $\alpha < 0$，$d\omega/dr > 0$），$d\omega/dr < 0$ 还是 $d\omega/dr > 0$ 得依赖于日震学的观测；而 $\alpha < 0$ 还是 $\alpha > 0$ 可取决于太阳表面电流螺度的观测。事实上，磁螺度的概念也正被应用于恒星、星系和宇宙发电机理论当中，它的重要性越来越明显。此外，每一个研究工作的目的和意义也可从它们各自的引言中发现到。

1.2 研究工作的内容提要

越来越多的研究表明，太阳表面被观测到的各式各样的图案在南、北两个半球上各自呈现出以一种手性（左手系，或者右手系）为主导的扭曲，且与太阳活动周无关。比如，(1) 位于北半球的绝大多数太阳黑子的半影或超半影纤维结构具有逆时针方向的旋转，而南半球的却以顺时针走向为主；(2) 出现在极冠区或中等纬度区的宁静暗条大约 80%在北半球属于 Dextral 型，而在南半球的为 Sinistral 型；(3) 北半球中反 S 形状的 X 射线日冕环的数目远高于 S 形状的数目，而这种环在南半球中则主要是以 S 形状的样子存在。所有这些图案的形态在南、北半球上所表现出的反对称性实际上也就是太阳大气中不同磁结构的位形具有南北反对称性的体现。如果用螺度这个量来描述磁场拓扑结构的复杂性，那么人们至少可以推断局域在北半球中的大多数磁结构具有负的磁螺度(左手扭曲)，而南半球中的具有正的磁螺度（右手扭曲)。更有趣的是，一些作者还采用了各自的方法定量地计算了太阳活动区光球磁场的平均电流螺度，其结果与上述形态分析的结论一致。这就是已被大家接受的所谓半球螺度符号定则。

近年来，我们利用北京天文台怀柔太阳磁场望远镜观测到的跨越一个活动周 (1988—2000) 的资料，对活动区电流螺度符号在南北两个半球上、在不同太阳纬度上和在不同卡林顿经度上的分布，电流螺度的变化与耀斑爆发以及电流螺度与太阳活动周的相关性等问题进行了初步的分析和研究，其主要结果如下：

1．我们分别计算了 422 个活动区的光球电流螺度，发现在北半球大约有 84%的活动区的螺度是负的，南半球 79%是正的，这进一步证实了半球螺度符号定则。这个结论的产生必将严重地威胁着人们多年来所偏爱的太阳对流区内部的 α-ω 运动学发电机理论。按照这个理论，要想得到与我们在太阳表面所观测到的事实（比如，黑子的蝴蝶图）相一致的结果，两个重要参数的选取必须为 $\alpha > 0$（在北半球），$d\omega/dr < 0$。由此可见，$\alpha > 0$（螺度为正）与上述观测到的电流螺度符号规则相反。另一方面，基于地面的 Global Oscillation Network Group（GONG）和空间 SOHO 的 Michelson Doppler Imager（MDI）资料，日震学研究表明 $d\omega/dr > 0$。因此，运作在太阳对流过冲区新近的动力学发电机模型（$\alpha < 0$，$d\omega/dr > 0$）目前越来越受到人们的重视。此外，经过仔细的分析，我们认为这种半球螺度符号的倾向性可能与柯里奥利力的作用是分不开的。由太阳较差自转引起的大尺度的光球运动对活动区电流螺度的贡献只会减弱上述半球螺度符号的倾向性。

2．每一个活动区都包含着电流螺度的混合符号，但这种有正和有负的混合符号只有少数情况表现为相互均衡的，绝大多数活动区都是以某一种符号占据着绝对的优势。这个结果表明虽然在一个活动区内各种扭曲和缠绕的磁流管都可能存在，但以某一种扭曲方式（或者是左手性，或者是右手性）为主的现象则是普遍的。换句话说，这种以一种扭曲方式为主的磁结构不仅仅发生在有明显旋涡结构的单极黑子中，在其它类型的复杂活动区中也一样。当然，每一个活动区本身都在不断地随时间发生变化，在它的演变过程中，不可避免地有来自光球下面的新的磁流的浮现，如果这种新浮现的磁流比较强，而且是反常扭曲的，那么原先是一种符号的螺度占主导地位的，现在有可能正负两种成份掺半，甚至使得该活动区的螺度符号发生反转。

3．我们首次给出了太阳活动第 22 周期间太阳日面上总的活动区的绝对平均电流螺度随不同卡林顿旋转的变化，把它同这一活动周的每月平均黑子数比较，结果发现它们有很好的相关性，特别是它们变化的总趋势是一致的，而且都有两个峰值，不过也显露出一些差异，如平均电流螺度的极大值出现在 1991 年晚期，而每月平均黑子数的最大值位于 1989 年 6 月，两者几乎相隔两年；另外，在 1990 年期间平均电流螺度的值是比较低的，这一点很难给予解释，不过有人认为它可能与此间频繁的日冕物质抛射（CMEs）有关，CMEs 会将太阳大气中的磁螺度转移到行星际空间中去。但不管如何，我们认为也许正是这些差异恰恰为人们揭示太阳活动的本质提供了新鲜的证据，像黑子数、日面磁场的总流量、耀斑数、10cm 射电流量以及日面上大尺度纵向磁场的演化等一样，日面上活动区平均电流螺度的演化或许也能作为太阳活动的一个新的标识参数。另外，我们还给出了日面上活动区电流螺度净流量（正负代数和）随时间的变化，发现螺度的负最大值发生在 1989 年和 1991 年且在北半球，而正的最大值大约在 1992 年前后并在南半球。

4．在我们的数据中，大约 20% 的违反螺度符号定则的活动区的出现决不仅仅是由统计涨落或各种误差造成的结果，它们的存在可能反映了太阳内部磁活动的一些信息。通过对这些反号活动区的分析与研究，我们发现它们随卡林顿经度的分布不是随机的，而是倾向于出现在某些特定的卡林顿经度上。另一方面，我们又发现耀斑往往倾向于发生在这些反螺度符号的活动区里，这就意味着反螺度符号的活动区有较强的非势特征或磁不稳定性。此外，这些反螺度符号的活动区在南北半球上的分布也是不对称的。

5．电流螺度和耀斑活动有很好相关性。我们分析了两组不同的活动区，即 5 个多发耀斑活动区(NOAA6233、6891、7321、7590、7773)和 5 个较复杂的但又几乎无耀斑产生的活动区(NOAA5612、5738、7496、7722、7903)，特别是对活动区 6233 进行了详细的分析，结果表明在活动区的某一位置或在其邻域内电流螺度的明显和迅速的变化很可能触发耀斑的爆发，而在电流螺度密度的极大值和耀斑核的位置之间没有因果关系的迹象。事实上，电流螺度的迅速变化就代表着活动区磁场结构的变化，也预示着这个区域的磁不稳定性增强，因而耀斑事件的频率也随之相应地提高。

6．在无力场近似下，我们知道无力因子 α 也可用来作为表征电流螺度的一个量。然而我们发现用 α 来衡量 422 个活动区的螺度符号，其结果是 70%左右的活动区符合通常的螺度符号定则，这与 Pevtsov 等人的结果一致。由此可见，南北半球螺度符号的百分比差异依赖于不同螺度参数的选择。螺度符号的这种南北不对称性究竟是强还是弱对发电机理论的研究有着重要的价值。通过对北京天文台怀柔太阳磁场望远镜观测到的矢量磁图和美国厦威夷 Mees 太阳观测站所观测到的矢量磁图进行比对，我们发现不同磁像仪观测、不同数据处理方法、法拉第旋转效应等都会影响电流螺度的计算，但不可能对电流螺度符号的统计结果有影响。对于比较大的活动区而言，我们估计受磁光效应的影响怀柔矢量磁图的横场方位角平均有大约 10 度 的偏差。

7．我们选择两个不同的电流螺度参数（α_{best} 和 H_c），分别计算了第 23 太阳活动周上升阶段 87 个活动区的螺度符号。我们发现在北半球中大约 59%的活动区有负的 α_{best}，在南半球中有 65%是正的，这个结果与第 22 周的相似。但是电流螺度参数 H_c 却表现出一个弱的相反的半球螺度符号的倾向性。可能的原因在第二篇第二节中被讨论。另外，我们还研究了活动区中光球电流螺度随太阳纬度的分布， 结果表明电流螺度在 15～25 纬度的区间有最大值，在赤道或两极附近变小。

第二篇　主要研究成果

2.1 【研究工作之一】不同磁像仪观测、不同数据处理方法、不同电流螺度参数的选择对半球螺度符号统计结果的影响

（主要完成者，本文已被 Solar Phys. 接受，目前正在印刷）

2.2 【研究工作之二】半球螺度符号规则不依赖于太阳活动周数的变化吗

（主要完成者，本文正在 J. Astrophys. Astr. 受审）

2.3 【研究工作之三】电流螺度变化的快慢与耀斑现象的诊断

（主要完成者，本文已发表在 Astron. Astrophys. Suppl. Ser. **139**, 311-320 (1999)，此文有部分工作是在读博士期间做的）

2.4 【研究工作之四】基于我们对电流螺度计算的结果如何来提取太阳对流区内部 ALPHA-效应的信息

（主要合作者，本文已被 Solar Phys. 接受，目前正在印刷）

2.5 【研究工作之五】太阳活动区光球磁场的扭曲或缠绕性以及描述电流螺度不同参量的分布特征

（主要合作者，本文正在 Solar Phys. 受审）

HELICITY COMPUTATION USING OBSERVATIONS FROM TWO DIFFERENT POLARIMETRIC INSTRUMENTS

S.D. BAO[1], A.A. PEVTSOV[2], T.J. WANG[1], and H.Q. ZHANG[1]
[1] *Beijing Astronomical Observatory/National Astronomical Observatories, Chinese Academy of Sciences, Beijing 100012, China*
[2] *Department of Physics, Montana State University, Bozeman, MT 59717, U.S.A.*

(Received 26 November, 1999; in revised form 21 March, 2000)

Abstract. We compare vector magnetograms of active region NOAA 5747 observed by two very different polarimetric instruments: the imaging vector magnetograph of Huairou Solar Observing Station (HSOS) and the Haleakala Stokes Polarimeter of Mees Solar Observatory (MSO). Unlike previous comparative studies, we concentrate our attention on differences in observations and data reduction techniques that can affect the helicity computation. Overall, we find a qualitative agreement between the HSOS and MSO vector magnetograms. The HSOS data show slightly higher field strength, but the distribution of inclination angles is similar in measurements from the two instruments. There is a systematic difference (up to $\sim 20°$) in the azimuths of transverse fields, which is roughly proportional to the longitudinal field strength. We estimate that Faraday rotation in the HSOS magnetograms contributes $\sim 12°$ in the azimuth difference if possible sources of error are taken into account.

Next, we apply two independent methods to both data sets to resolve 180° azimuth ambiguity and to compute two helicity measures — the force-free field parameter $\alpha_{\rm best}$ and the current helicity fractional imbalance $\rho_{\rm h}$. The methods agree reasonably well in sign and value of the helicity measures, but the HSOS magnetograms show systematically smaller values of $\rho_{\rm h}$ and $\alpha_{\rm best}$ in agreement with an expected contribution of Faraday rotation.

Finally, we discuss the role of Faraday rotation in computation of $\alpha_{\rm best}$ and $\rho_{\rm h}$ and conclude that it does not affect the strength of the hemispheric helicity rule. The strength of the rule appears to be related to a helicity parameter: $\alpha_{\rm best}$ shows weaker hemispheric asymmetry than $\rho_{\rm h}$.

1. Introduction

Recent work on the helicity of magnetic fields observed at the solar surface demonstrated a preferred sign of helicity, or chirality, in each hemisphere. Based on the Mees Solar Observatory (MSO) data Pevtsov, Canfield, and Metcalf (1995) studied the linear force-free field factor α for 69 active regions, and found that 76% of regions in the northern hemisphere had negative α and 69% in the southern hemisphere had positive α. An extended HSP dataset, using 203 active regions, showed that 62% of regions in the northern hemisphere had negative α and 66% in the southern hemisphere had positive α (Longcope, Fisher, and Pevtsov 1998). Using the Huairou Solar Observing Station (HSOS) vector magnetograms, Bao and Zhang (1998) computed the

fractional imbalance of current helicity (ρ_h) for 422 active regions. In their dataset, 84% of the active regions in the northern hemisphere had negative current helicity, and 79% in the southern hemisphere had positive ρ_h.

The strength of the hemispheric helicity rule is important for understanding the origin of helicity on the Sun. Still, two data sets reveal a slightly different tendency. The hemispheric asymmetry in the sign of helicity seems to be stronger in the HSOS data. What causes it? Can the differences in the observations and the data reduction explain it, or it is mostly due to the different helicity parameters used in the two studies?

The HSOS magnetograph is a filter-based polarimeter. It observes simultaneously a large spatial area in a single wavelength band (0.125 Å), selectable within a limited range by tuning the filter. Similar (in principle) filter vector magnetographs operate at Marshall Space Flight Center (MSFC) and Big Bear Solar Observatory (BBSO). The MSO Haleakala Stokes Polarimeter is a spectrograph-type magnetograph, which observes an extended spectral range with high spectral resolution at a single spatial point at a given moment. It scans the solar image to build a magnetogram. Several studies compared these two types of magnetographs and showed qualitative agreement between magnetograms derived from them (e.g., Ronan *et al.* 1992; Wang *et al.* 1992). Recently, Hagyard and Pevtsov (1999) compared the linear force-free field α coefficient for several active regions observed by the MSFC and MSO magnetographs and found no significant difference. They also pointed out potential problems in filter vector magnetograph data that could affect the calculation of helicity. Leka and Skumanich (1999) tested three different methods to calculate the parameter α and discussed the influence of data noise on the results. The value of α was computed (1) using moments of the distribution of $\alpha(x, y)$, (2) as the slope of linear function $J_z(x, y) = \alpha B_z(x, y)$ and (3) as the constant-α force-free field most closely matching the observed horizontal field. All three methods were found to be consistent within the uncertainties.

Thus, in principle, both the observational technique and the data analysis method may contribute to the above-mentioned disagreement between the HSOS and MSO data sets on a strength of the hemispheric helicity rule. In the present paper, we study the relative importance of these factors via direct comparison of magnetograms and the helicity parameters computed from them using different methods. Section 2 describes the instruments and the data sets. Sections 3 and 4 compare magnetic field, electric current and helicity computed using the HSOS and MSO data. Section 5 summarizes the results of our study and the discussion.

2. Polarimetric Observations

2.1. Huairou Vector Magnetograph

The Solar Magnetic Field Telescope at HSOS of Beijing Astronomical Observatory was developed by Ai and Hu (1986) and has made valuable vector magnetic field measurements for more than one decade. The current system consists of a 35 cm vacuum telescope, a 1/8 Å Lyot birefringent filter with three sets of KD*P crystal modulators, a CCD camera with 512×512 pixels, and an image processing system controlled by a computer. It uses the Fe I 5324.191 Å line with a total half-width of 0.334 Å (Landé factor $g_{\rm L} = 1.5$). The spectral line is formed approximately at 180 km in the solar photosphere (e.g., Lin, Zhang, and Zhang 1996). Because the line is strong and broad, magnetic saturation and Doppler shifts are disregarded. The effective field of view is $5.23' \times 3.63'$. The temporal and spatial resolution of the HSOS vector magnetograms depends on the number of video frames that are added to produce them. Each magnetogram used in this paper is the sum of 256 individual frames for both line-of-sight and transverse fields, corresponding to a temporal resolution of about 5 min and a spatial resolution of about 2 arc sec.

A complete vector magnetogram is built up using four narrow-band images (filtergrams) of Stokes I, V, Q and U parameters. I is derived from the sum of two images, either linearly or circularly polarized. V is a difference between the left and right circularly polarized images taken at -0.075 Å from the line center. Q and U are the differences between two orthogonal linearly polarized images in a certain azimuthal direction. When images for determination of Q and U are taken, the filter is normally switched to the spectral line center to achieve maximum sensitivity. Thus, the observed transverse and longitudinal fields correspond to slightly different heights in the solar photosphere with the longitudinal field originating approximately 50 km lower than the transverse field (Wang *et al.* 1996).

The line-of-sight ($B_{\rm l}$) and transverse ($B_{\rm t}$) components of magnetic field are given by

$$B_{\rm l} = C_{\rm l}\frac{V}{I}, \quad B_{\rm t} = C_{\rm t}\left(\frac{Q^2}{I^2} + \frac{U^2}{I^2}\right)^{\frac{1}{4}}, \tag{1}$$

where $C_{\rm l}$ and $C_{\rm t}$ are the calibration coefficients. The azimuthal angle of the transverse field is

$$\phi = \frac{1}{2} tan^{-1}\left(\frac{U}{Q}\right). \tag{2}$$

A more detailed description of the instrument and the observational technique may be found elsewhere (e.g., Wang *et al.* 1996).

2.2. Haleakala Stokes Polarimeter

The Haleakala Stokes Polarimeter of Mees Solar Observatory (Mickey 1985) is a spectrograph-based magnetograph which registers full Stokes I, Q, U, and V profiles of the Fe I 6301.5, 6302.5 Å doublet (g_L=1.67, 2.5) with high spectral resolution (0.025 Å) and constructs a magnetogram by spatially scanning over the active region targeted. A magnetogram is recorded with a 6″ aperture and either 2.8″ or 5.6″ spatial steps. It takes about an hour to complete a typical magnetogram of 60×40 pixels in spatial extent. The MSO magnetograms used in the present study were obtained with 5.6″ spatial steps. The Fe I 6301.5, 6302.5 Å spectral lines are formed at approximately 200 km in the solar photosphere (e.g., Bruls, Lites, and Murphy 1991).

The magnetic field is computed by combining two inversion techniques. When the fractional polarization in a given pixel is above 1% (corresponding to a field strength $\geq$ 100 G), a nonlinear least-squares fitting technique developed by Skumanich and Lites (1987) is used. The method fits the observed Stokes profiles to the analytical Unno-Rachkovsky solution of the radiative transfer equation. The routine takes into account magnetic filling factor, magneto-optical (e.g., Faraday rotation) and scattered light effects, making a first-order correction for unresolved magnetic structures. In areas of polarization below 1% the field values are determined using integrated properties of the Stokes profiles (Ronan, Mickey, and Orrall 1987). The integral method is based on the same weak-field approximation as Equations (1) and (2), so its accuracy decreases for fields above $\approx$ 1000 G (Canfield *et al.* 1993).

2.3. The Data Sets

We use six vector magnetograms of a single active region NOAA 5747. The region is a complex β-δ spot group with strong magnetic fields and high magnetic shear, which helps to study possible effects of Faraday rotation. The region was well observed by both MSO and HSOS from 19 to 22 October 1989, although there were no simultaneous observations. The smallest time difference between the HSOS and MSO magnetograms is about 8 hours. Table I lists the dates of the observations for both instruments. For each magnetogram, we conduct a transformation to the disk center and resolve the 180° azimuth ambiguity using two independent methods (HSOS and MSO methods, thereafter). In the MSO method the azimuth ambiguity is resolved following Canfield *et al.* (1993), starting from a constant-α force-free field and minimizing change between adjacent pixels, minimazing electric currents in a quiet photosphere. In the HSOS method the ambiguity resolution is done following Wang, Xu, and Zhang (1994) by comparison with a potential field. Both methods are used on both data sets.

3. Magnetic Field and Electric Current

First, we compare three pairs of magnetograms on pixel by pixel basis (HSOS — MSO): 20-Oct/01:37 UT — 20-Oct/17:41 UT, 21-Oct/02:15 — 20-Oct/17:41, and 21-Oct/02:15 — 21-Oct/19:20. For each pair we co-register the HSOS and MSO magnetograms and interpolate the HSOS magnetogram to match the coarser $5.6''$ pixel spacing of the MSO data. The interpolation was done by averaging the HSOS magnetograms over the MSO pixel size. All three pairs show similar correlations. Below we demonstate our findings using the second pair of magnetograms.

3.1. Morphological Comparisons

Figures 1–3 show vector magnetic field, vertical electric current density $J_z = (\nabla \times \mathbf{B})_z$ and current helicity density ($\mu_0 J_z B_z$), observed by the two instruments. Despite significant time difference (8 hours) between the two observations one can see close similarities in the distribution of magnetic fields and electric currents. In both cases, the orientation of the transverse field (arrows) exhibits a clockwise rotation in the positive (white) polarity field, and counterclockwise rotation in the negative (dark) polarity (upper part of Figure 1). The sense of rotation implies left-hand twist and, hence, negative current helicity density. Indeed, Figure 3 obviously shows that the current helicity density is negative in most of the active region. From this figure, we also see that the distribution of current helicity density is similar between the HSOS and MSO magnetograms.

3.2. Quantitative Analyses

Figure 4 presents a quantitative comparison of two magnetograms shown on Figures 1–3. The scatter plots confirm the results of the morphological comparison. The longitudinal fields correlate quite well, although the HSOS magnetograms exhibit systematically larger longitudinal field strength. In weak field ($|B_l| < 500$ G) the regression coefficient is near 1., and for stronger fields ($|B_l| > 500$ G) it is 0.61. Such a difference is mainly caused by the calibration procedure employed at HSOS (Ai, Li, and Zhang 1982; Wang, Ai, and Deng 1996). For very strong longitudinal fields, the calibration becomes inaccurate. Similarly, the transverse field (Figure 4b) is also systematically larger in the HSOS magnetograms. It is therefore not surprising that the inclination angles of the two magnetograms are in good agreement. The noise level in transverse field measurements, judging from quiet Sun areas, is comparable in the two data sets (200 G for HSOS and 140 G for MSO). In fact, the disagreement in the transverse field strength between HSOS and MSO was also found in other comparisons, as shown in Figure 3b of Ronan *et al.* (1992).

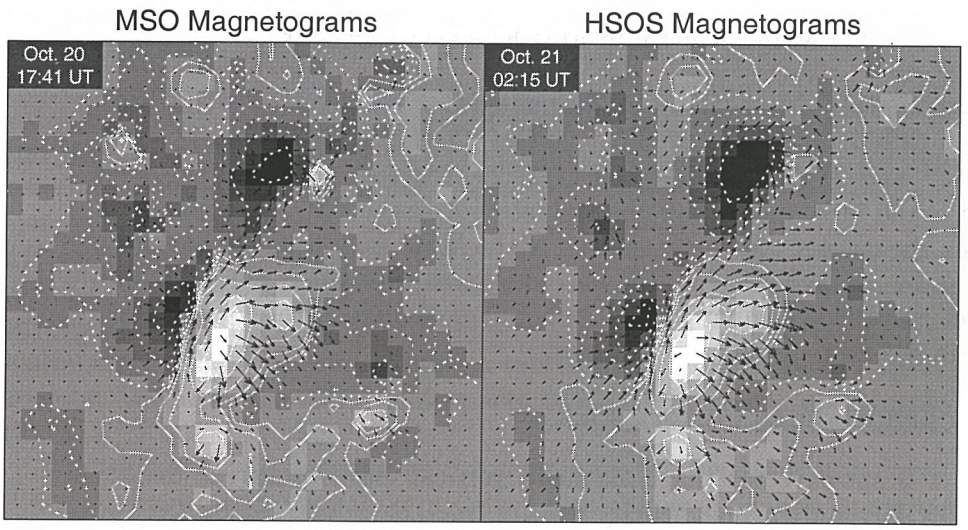

Figure 1. Comparison between a pair of vector magnetograms of AR NOAA 5747 obtained at MSO and HSOS. The MSO magnetogram (left) was recorded with a scan starting at 17:41 UT and ending at 18:37 UT on 20 October 1989. The interpolated HSOS magnetogram (right) was recorded at 02:15 UT on 21 October 1989. The white contours in both maps denote longitudinal field (levels = ±50, 200, 500, 1000, 1800, and 3000 G); solid and dashed lines show positive and negative fields, respectively. The grey-scale continuum image also shows the intensity of the longitudinal field. The black line segments with arrows indicate the strength and direction of transverse field. The pixel spacing is 5.6″.

Figure 4d shows the difference in azimuths of the transverse field as a function of the HSOS longitudinal field strength. The linear fit to the data (*dashed line*) reveals a tendency for the difference in azimuths to be negative for the negative longitudinal field and to be positive for the positive field. This tendency may be related to the Faraday rotation effect. In addition, an *average* offset $\sim 20°$ in azimuths can also be seen in the figure.

The random scatter of the magnetic field parameters may be the result of many factors including atmospheric seeing effects, difference in spatial resolution, non-simultaneous observations, and the inability to co-register the two magnetograms perfectly. However, it is difficult to establish how the scatter is apportioned between all the sources of error. The helicity parameters, averaged over all the active region should not be significantly affected in a systematic manner by these random factors. We speculate that Faraday rotation acts in a systematic way, which might alter the helicity computation.

A difference in line formation between the HSOS and MSO data might result in some discrepancies in the azimuths as well. In the MSO data, magnetic field represents a weighted average over the depths of the spectral line formation with the polarized contribution function as weight. In the HSOS

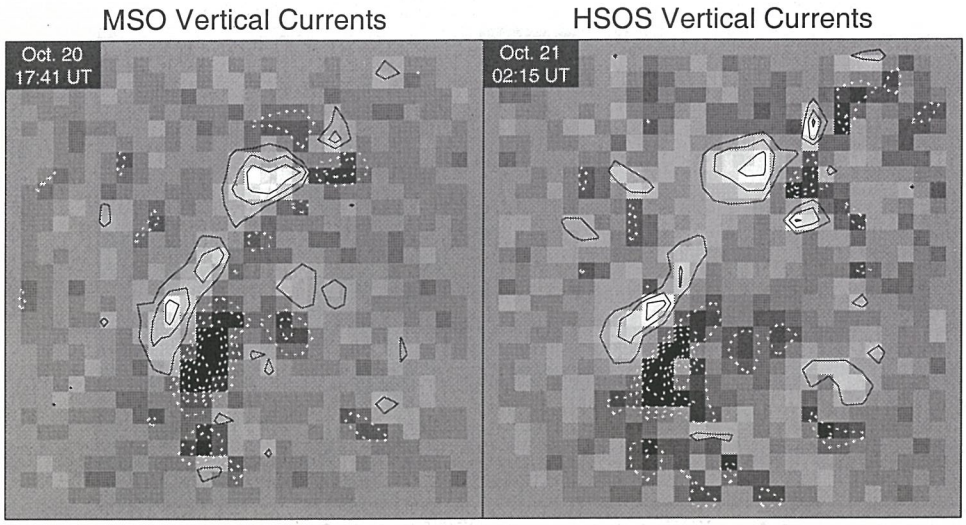

Figure 2. Comparison of vertical current systems derived from two magnetograms of Figure 1. In both maps the vertical currents are contoured at levels of 3, 6, 9, 12, and $15\sigma_j$, where $\sigma_j = 1.60\,\mathrm{mA\,m^{-2}}$ for the MSO magnetogram (left) and $\sigma_j = 1.81\,\mathrm{mA\,m^{-2}}$ for the HSOS magnetogram (right). The grey scale also shows vertical currents (white — positive, black — negative).

data, observed magnetic field is the field averaged over the depths covered by the Lyot filter bandpass (0.125 Å). The typical width of the contribution functions is about 150 km for Fe I 5324.191 Å and Fe I 6301.5, 6302.5 Å and it is much larger than the difference in the effective depths of formation of these lines. Hence, we expect that the discrepancies in azimuths due to the difference in depths of formation of the spectral lines will be small. To estimate this discrepancy we use the HSOS magnetogram (21-Oct-89, 02:15 UT) and compute a constant-α force-free field. For each pixel we calculate a difference in azimuths at two levels (0 km — observed magnetogram and $\sim$ 60 km — extrapolated field). For 98% of all pixels the difference is less than 2° and the average is $0.08° \pm 0.77°$.

3.3. Faraday rotation

To further explore the action of Faraday rotation, we overlay the HSOS and MSO magnetograms on Figure 5a. Careful analysis of Figure 5a rules out a *constant* 20° offset between the two magnetograms, since in many areas the HSOS and MSO azimuths are in a good agreement. On the other hand, one can see a tendency of positive difference in azimuths for positive longitudinal field and negative difference for the negative field — further indicates that Faraday rotation is present in the HSOS magnetograms. However, there is another possible source of the difference in azimuths between these two

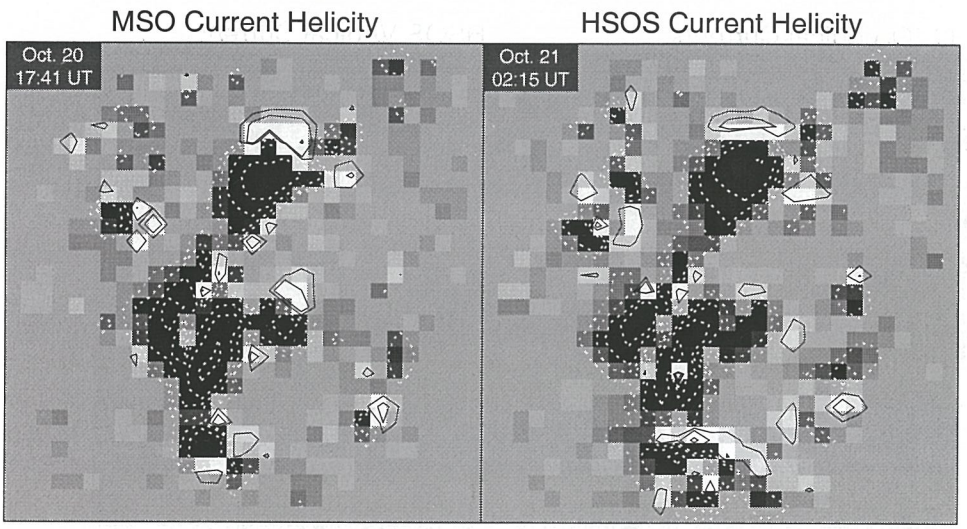

Figure 3. Distribution of the current helicity density $h_c = \mu_0 J_z B_z$ for the magnetograms shown on Figure 1. h_c is shown as the grey-scale image with contours. The contours are drawn at levels of 3, 9, 27, 81, and $243\sigma_h$, where $\sigma_h = 2.32 \times 10^{-3}\,\mathrm{G^2\,m^{-1}}$ for the MSO magnetogram and $\sigma_h = 2.75 \times 10^{-3}\,\mathrm{G^2\,m^{-1}}$ for the HSOS magnetogram.

magnetograms. Figure 5b shows an overlay of two HSOS magnetograms observed about 5 hours apart. The white and black line segments represent the transverse fields recorded at 02:15 and 07:00 UT, respectively. Examining the orientation of transverse field in area of strong positive flux (central part of Figure 5b) one can notice a tendency of counterclockwise rotation. The average rotation of the azimuths between the two magnetograms is about 5° over 5 hours. Assuming that the same rotation rate has been present during a period between the MSO and HSOS observations shown on Figure 5a, one can infer that as much as $\sim 8°$ difference in azimuths might be caused by this type of evolution of the sunspot. Remaining $\sim 12°$ should be the result of Faraday rotation. Indeed, comparison of transverse field observed in the center of the spectral line and its blue wings indicates that about 10° in azimuth difference can be caused by the Faraday rotation effect (e.g., Wang *et al.* 1996). This result is in agreement with those estimated by Wang *et al.* (1992).

4. Helicity Parameters

Our next step is to compare helicity parameters computed using two different methods of the ambiguity resolution. For this study we compute three helicity measures: α_{best}, ρ_h and $\alpha_{Jz/Bz}$. The HSOS magnetograms were interpolated to the MSO grid as described in the previous section

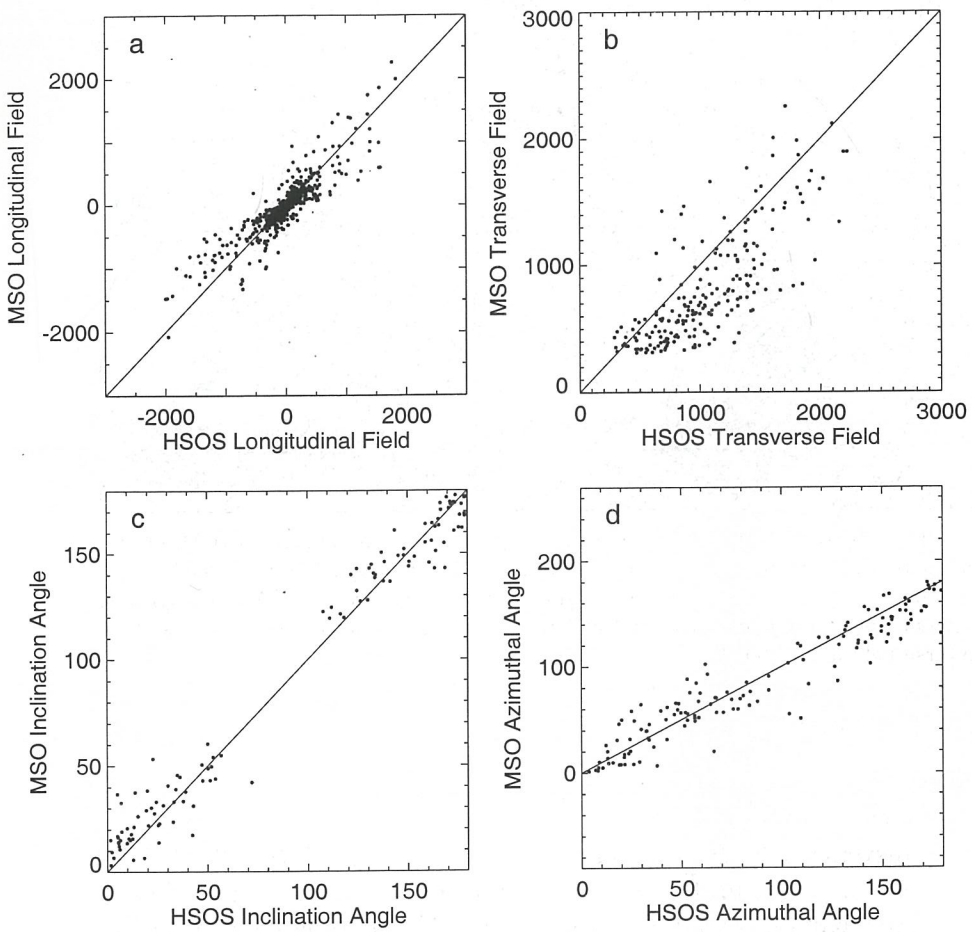

Figure 4. Correlations between magnetic field parameters of the two magnetograms shown on Figure 1. (a) longitudinal field (in G); (b) transverse field (in G); (c) inclination angle (relative to a direction toward observer, degrees); (d) the difference in azimuths as a function of the longitudinal field. Only pixels with transverse field larger than 300 G are included in these correlations. In all the panels, the solid line represents the loci of perfect agreement.

prior to calculating the helicity parameters. $\alpha_{\rm best}$ is computed following Pevtsov, Canfield, and Metcalf (1995), by minimizing the difference between an observed magnetogram and the computed linear force-free field parameterized by $\alpha_{\rm best}$. $\rho_{\rm h}$ is a fractional imbalance of $\mu_0 J_{\rm z} B_{\rm z}$ over an active region (Bao and Zhang 1998). In addition, we define $\alpha_{\rm Jz/Bz}$ as the regression coefficient for the relationship between vertical components of the electric current density ($\mu_0 J_{\rm z}$) and the magnetic induction ($B_{\rm z}$). Pevtsov, Canfield, and McClymont (1997) found a good correlation between $J_{\rm z}$ and $B_{\rm z}$ for this active region, suggesting that the linear force-free field model is a good approximation. All three parameters are computed using only pixels with

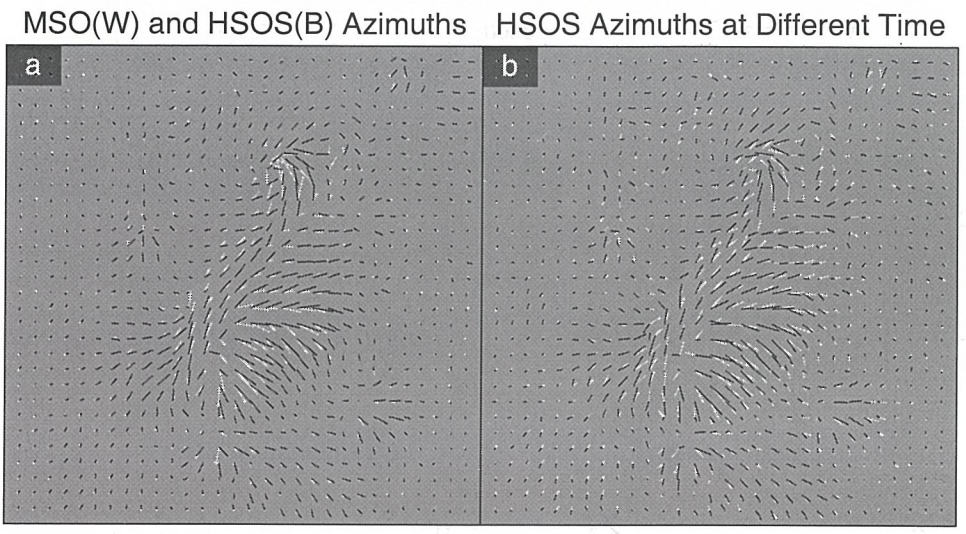

Figure 5. Azimuths of the transverse field of two pairs of magnetograms. (a) MSO and HSOS magnetograms, white segments correspond MSO data (e.g., Figure 1, left), black segments show HSOS magnetogram (e.g., Figure 1, right); (b) two HSOS magnetograms, white segments show the transverse field at 02:15 UT, and the black line segments show the transverse field at 07:00 UT.

value of transverse field $B_t > 300$ G and longitudinal field $B_l > 20$ G. The results are summarized in Table I. α_{best} and ρ_h computed using different methods of the azimuth ambiguity resolution are in good agreement within each set of magnetograms (HSOS or MSO). Thus, for this active region, the results are relatively insensitive to the method of resolution of the 180° azimuth ambiguity. On the other hand, Hagyard and Pevtsov (1999) have shown that for a highly non-potential active region, the azimuth ambiguity resolution method used might affect the value of α_{best}.

In the framework of our present comparison, it is important to note that the MSO data give a more robust result since the data are less affected by Faraday rotation. Hence, we compare the HSOS data with the MSO data assuming that the latter give more "correct" answer.

The helicity parameters computed using the HSOS magnetograms are systematically smaller than those using the MSO data. This is an expected contribution of Faraday rotation. Figure 4d (or Figure 5a) demonstrates that Faraday rotation has a stronger effect in the positive polarity field. The effect of Faraday rotation introduces right-hand twist (positive helicity) in positive flux and, hence, decreases the overall negative current helicity density of this active region.

Table I. α_{best} and ρ_h in AR 5747.

Date	Time (UT)	$\alpha^1{}_{best}$	ρ_h (%)	$\alpha^1{}_{best}$	ρ_h (%)	$\alpha^1{}_{Jz/Bz}$
		HSOS method		MSO method		
HSOS data						
19 Oct., 1989	02:42	−4.16	−58.9	−3.52	−57.9	−3.75
20 Oct., 1989	01:37	−3.25	−66.7	−3.99	−74.8	−4.54
21 Oct., 1989	02:15	−4.46	−71.6	−3.65	−69.0	−3.69
MSO data						
20 Oct., 1989	17:41	−6.29	−82.6	−6.33	−82.3	−5.87
21 Oct., 1989	19:20	−5.64	−79.5	−5.15	−79.2	−5.32
22 Oct., 1989	18:27	−4.97	−69.0	−4.84	−72.3	−4.58

[1] in units 10^{-8} m^{-1}

5. Discussion

In the previous section we have shown that the presence of Faraday rotation reduces the value of the helicity parameters for a given active region. An important question is how it affects the sign of helicity.

Figure 6 demonstrates the effect of Faraday rotation in a bipolar active region represented by a twisted flux tube. The vertical box plotted by the dashed lines encompasses an "active region". The two upper panels represent an active region of positive helicity ($\alpha > 0$, right-hand twist). The two lower panels show an active region of negative helicity ($\alpha < 0$, left-hand twist). The middle column represents a twist introduced by Faraday rotation and the last column depicts the combined effect of the original distribution of azimuths and that resulting from Faraday rotation. From this cartoon, one can see that whether its current helicity is positive ($\alpha > 0$) or negative ($\alpha < 0$) for a bipolar active region, the twist in one polarity (panel a or d) strengthens due to Faraday rotation while that in another opposite polarity (panel b or c) weakens. This means that the effect of Faraday rotation will not change the original sign of current helicity in such a region. Now let us assume that the panels a, b, c, and d respectively represent four unipolar active regions with different twists. In the case of a or d, the current helicity sign is not affected by the Faraday rotation effect, even if their values increase to a great extent. For the panel b or c, however, if the magnetic field is current-free (no original twist) or just slightly twisted, the resulting twist will be determined primarily by the action of Faraday rotation.

On the other hand, Hagyard and Pevtsov (1999) argue that Faraday rotation may affect the helicity computation of even bipolar active regions,

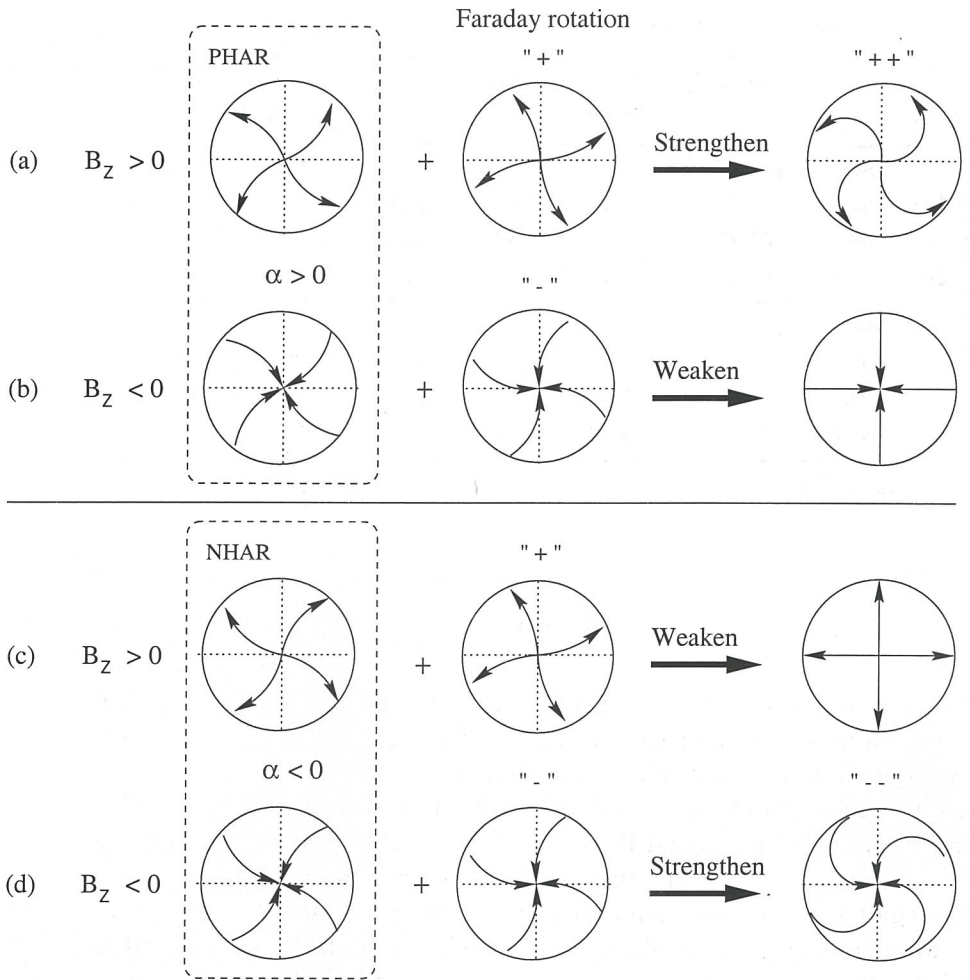

Figure 6. Sketches showing the influence of Faraday rotation action on twisted magnetic flux tubes. The four circles in the first column represent possible configurations of twisted flux tubes. The curves with arrows denote magnetic field lines. The patterns of the second column indicate the sense of the spiral configuration due to Faraday rotation. The sketches of the last column indicate the net effect resulting from the original twist modified by Faraday rotation. The final configuration on panels (b) and (c) depends on the amount of original twist and the Faraday rotation and may be opposite in sign to the original twist.

since the leading polarity sunspot has stronger (and more compact) magnetic field and tends to live longer. Hence, the effect of Faraday rotation will be determined mostly by a leading polarity sunspot. Moreover, because the leading sunspots have opposite polarities in opposite hemispheres (Hale-Nicholson polarity rule) the Faraday rotation may, in fact, influence the hemispheric helicity rule.

Table II. Signs of ρ_h and α_{best} for 422 active regions.

Hemisphere	Total of ARs	ρ_h	α_{best}
		Negative chirality	
Northern	199	168 (84%)	152 (76%)
		Positive chirality	
Southern	223	177 (79%)	159 (71%)

However, it is not that simple. Table I shows that Faraday rotation affects both helicity parameters — α_{best} and ρ_h. Although we studied only one active region, we may speculate that the Faraday rotation has similar effect on both helicity parameters for all active regions. Hence we expect to see the same hemispheric asymmetry in ρ_h and α_{best} for the same data set. Table II shows the sign of those two parameters computed for the data studied by Bao and Zhang (1998). Clearly, the hemispheric asymmetry is weaker in α_{best} and stronger in ρ_h. The strength of the hemispheric helicity rule in MSO and HSOS data sets seems to agree when the same helicity parameter (α_{best}) is used.

Thus, despite that Faraday rotation may affect the hemispheric helicity rule, Table II does not support that. It appears that the strength of the hemispheric helicity rule may be determined by a choice of helicity parameters. Authors could not reach a consensus on either there are physical reasons for that (e.g., relation to the different physical processes on the Sun), or that the reasons are methodological in nature (e.g., one parameter is more susceptible to local variations of azimuths than another). Before the contradiction between α_{best} and ρ_h is solved we think that both parameters should be used in studies of helicity of the photospheric magnetic field on the Sun.

Acknowledgements

We are grateful to the staff of the two observatories for the observations. We wish to thank R.C. Canfield for valuable discussions. The authors also thank the referee for helpful comments and suggestions. This work was carried out under the support of the National Science Foundation of China grants 19791090 and 49990450, and NASA through SR&T grant NAG5-6110.

References

Ai, G.X. and Hu, Y.F.: 1986, *Acta Astron. Sinica* **27**, 173.
Ai, G.X., Li, W., and Zhang, H.Q.: 1982, *Acta Astron. Sinica* **23**, 39.
Bao, S.D. and Zhang, H.Q.: 1998, *Astrophys. J.* **496**, L43.
Bruls, J.H.M.J., Lites, B.W., and Murphy, G.A.: 1991, in L.J. November, editor, *Solar Polarimetry*, NSO/SP, Sunspot, New Mexico, p. 444.
Canfield, R.C., de La Beaujardière, J.-F., Fan, Y. *et al.*: 1993, *Astrophys. J.* **411**, 362.
Hagyard, M. and Pevtsov, A.A.: 1999, *Solar Phys.* **189**, 25.
Leka, K.D. and Skumanich, A.: 1999, *Solar Phys.* **188**, 3.
Lin Y.Z., Zhang, H.Q., and Zhang, W.J.: 1996, *Solar Phys.* **168**, 135.
Longcope, D.W., Fisher, G.H., and Pevtsov, A.A.: 1998, *Astrophys. J.* **507**, 417.
Mickey, D.L.: 1985, *Solar Phys.* **97**, 223.
Pevtsov, A.A., Canfield, R.C., and McClymont, A.N.: 1997, *Astrophys. J.* **481**, 973.
Pevtsov, A.A., Canfield, R.C., and Metcalf, T.R.: 1995, *Astrophys. J.* **440**, L109.
Ronan, R.S., Mickey, D.L., and Orrall, F.Q.: 1987, *Solar Phys.* **113**, 353.
Ronan, R.S., Orrall, F.Q., Mickey, D.L., West, E.A., Hagyard, M.J., and Balasubramaniam, K.S.: 1992, *Solar Phys.* **138**, 49.
Skumanich, A. and Lites, B.W.: 1987, *Astrophys. J.* **322**, 473.
Wang, H.M., Varsik, J., Zirin, H., Canfield, R.C., Leka, K.D., and Wang, J.X.: 1992, *Solar Phys.* **142**, 11.
Wang, J.X., Shi, Z.X., Wang, H.N., and Lü, Y.P.: 1996, *Astrophys. J.* **456**, 861.
Wang, T.J., Ai, G.X., and Deng, Y.Y.: 1996, *Publications of the Beijing Astronomical Observatory* **28**, 31.
Wang, T.J., Xu, A.A., and Zhang H.Q.: 1994, *Solar Phys.* **155**, 99.

J. Astrophys. Astr. (2000) **21**, 000–000

The Hemispheric Sign Rule of Current Helicity During the Rising Phase of Cycle 23

S.D. Bao*, G.X. Ai, and H.Q. Zhang
Beijing Astronomical Observatory/National Astronomical Observatories, Chinese Academy of Sciences, Beijing 100012, China

Received 2000 February 22

Abstract. We choose two different current helicity parameters (i.e., $\alpha_{\rm best}$ and $H_{\rm c}$) to compute their signs for 87 active regions during the rising phase of solar cycle 23, using the vector magnetograms from the Solar Magnetic Field Telescope of Huairou Solar Observing Station of Beijing Astronomical Observatory. We find that 59% of the computed active regions in the northern hemisphere have negative $\alpha_{\rm best}$ and 65% in the southern hemisphere have positive $\alpha_{\rm best}$. This result is consistent with that of the cycle 22. However, the helicity parameter $H_{\rm c}$ shows a weaker opposite hemispheric preference in the current solar cycle. Possible reasons are discussed.

Key words: Sun: activity – magnetic fields – photosphere

1. Introduction

In the last decade observations have revealed that a hemispheric preference of magnetic chirality (handedness) exists throughout the solar atmosphere, such as sunspot whirls (Hale 1927; Richardson 1941), signs of current helicity in active regions (see Table 1), quiescent filaments (Martin *et al.* 1992, 1994; Mackay *et al.* 1998), sigmoid coronal loops (Rust and Kumar 1996; Pevtsov and Canfield 1998; Canfield *et al.* 1999) and interplanetary magnetic clouds (Bieber *et al.* 1987; Rust 1994; Smith 1999). Table 1 shows that the hemispheric asymmetry in sign of current helicity seems to be stronger in the Huairou Solar Observing Station (HSOS) data (Abramenko *et al.* 1996, Bao and Zhang 1998) than in the Mees Solar Observatory (MSO) data (Pevtsov *et al.* 1995, Longcope *et al.* 1998). Bao *et al.* (2000) studied the origin of this phenomenon and concluded that it is mostly due to a choice of two different helicity parameters ($\alpha_{\rm best}$ and $H_{\rm c}$) used in these studies, rather than

*e-mail:bshd@sun10.bao.ac.cn

a disagreement between the two data sets. The interpretation of all these patterns and their possible connection to the dynamo are open to question. In addition, current helicity of magnetic fields also plays an important role in solar flare evolution (Bao *et al.* 1999). However, the purpose of this paper is to examine whether the hemispheric sign rule — most active regions in the northern/southern hemisphere have negative/positive current helicity, does not change with the solar cycle number.

2. Data Analysis and Results

We chose 87 active regions observed with the vector magnetograph at HSOS during the rise of cycle 23 to compute their signs of current helicity. All data used in our study were acquired with favorable weather and seeing conditions during the time in which active regions were located near the central meridian. Considering that the noise level of transverse field measurements is generally higher than that of line-of-sight field measurements by an order of magnitude, we did not transform our data into disk-center heliographic coordinates to avoid dirtying of the vertical components by the projection correction. We therefore take the line-of-sight component of magnetic field $B_{||}$ as B_z. 180° azimuth ambiguity is resolved following Wang *et al.* (1994). A detailed description of the HSOS instruments and observational technique may be found elsewhere (e.g., Wang *et al.* 1996).

Table 1. Signs of photospheric current helicity computed by different groups.

Group	Hemisphere	$\alpha_{\rm best}$		$H_{\rm c}$		Total
		Negative	*Positive*	*Negative*	*Positive*	
Pevtsov et al.	Northern	25(76%)				33
(1995)	Southern		25(69%)			36
Longcope et al.	Northern	58(62%)				93
(1998)	Southern		73(66%)			110
Abramenko et al.	Northern			15(79%)		19
(1996)	Southern				18(86%)	21
Bao and Zhang	Northern			168(84%)		199
(1998)	Southern				177(79%)	223

Table 2 shows the signs of both $\alpha_{\rm best}$ and $H_{\rm c}$ for the selected active regions during the rise of cycle 23. The value of the parameter $\alpha_{\rm best}$ is determined by the best match between the x and y components of the computed constant-α force-free and observed horizontal magnetic field in the sense of a minimum least-squares difference (Pevtsov *et al.* 1995), and the other parameter $H_{\rm c}$ is given by computing $B_z \cdot (\bigtriangledown \times \mathbf{B})_z$ (Bao and Zhang 1998). From this table, we find that 59% of active regions in the northern hemisphere have negative $\alpha_{\rm best}$, and 65% in the southern hemisphere, posi-

tive. This is consistent with those results of cycle 22. However, H_c appears to show a weaker opposite hemispheric preference, in disagreement with this cycle. Moreover, the variation of current helicity with solar latitude for all 87 active regions is displayed in Figure 1. Each plus symbol marks the value of α_{best} or H_c and the latitude (of magnetogram center) for one active region. As a comparison, we give here the variation of α_{best} and H_c with solar latitude for the data of cycle 22, shown in Figure 2. These results further demonstrate that current helicity has a maximum at about 15°–25° latitude and decreases toward both the equator and the poles (Pevtsov *et al.* 1995). On the other hand, we can more clearly see that the consistency of the two dashed lines in Figure 2 is not shown in Figure 1. This means that H_c no longer follows the hemispheric sign rule in the present cycle.

Table 2. Distribution of hemispheric helicity signs for the two cycles.

Cycle	Hemisphere	α_{best}		H_c		Total
		Negative	*Positive*	*Negative*	*Positive*	
22	Northern	152(76%)		168(84%)		199
	Southern		159(71%)		177(79%)	223
23	Northern	26(59%)		14(32%)		44
	Southern		28(65%)		21(49%)	43

3. Discussion

We know that the hemispheric sign rule of photospheric current helicity in active regions was established for the cycle 22 (see Table 1). We expect to see the same hemispheric asymmetry for both α_{best} and H_c in a new solar cycle. However, our observations indicate that the helicity parameter H_c does not obey such a hemispheric rule during the rising phase of cycle 23, unlike α_{best}. How to explain it? Our views are that: (1) Although such a primary result is interesting, it would be premature to make a serious conclusion based on our data. More samples are required to answer this question. (2) Since Faraday rotation will produce a counterclockwise rotation of the azimuth for a line-of-sight field of positive polarity, and during cycle 23 the polarity of leading sunspots is positive in the northern hemisphere, some active regions with negative current helicity in the northern hemisphere due to the effect of Faraday rotation may reverse their original twist configuration to have positive helicity. For all the active regions in which the original twist is right-hand (positive helicity) in the northern hemisphere, their signs will not be influenced by Faraday rotation. On the other hand, H_c may be more susceptible to Faraday rotation than α_{best} because it is mainly related to the areas where the line-of-sight field is strong. H_c, therefore, has a lower

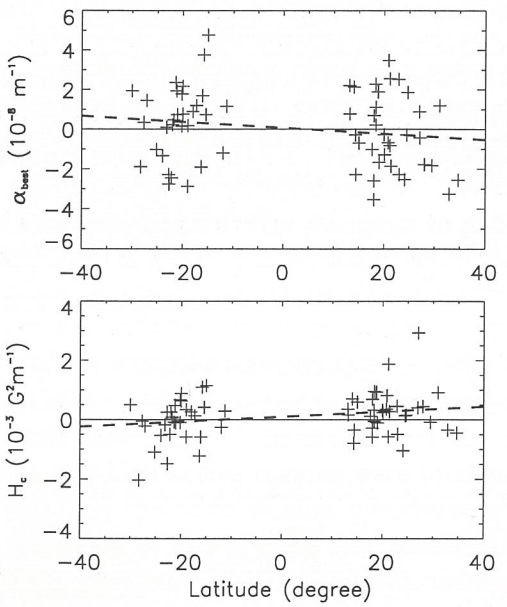

Figure 1. Variation of both $\alpha_{\rm best}$ and $H_{\rm c}$ with solar latitude for 87 active regions observed during the rise of cycle 23. The dashed line shows a linear fit to the data.

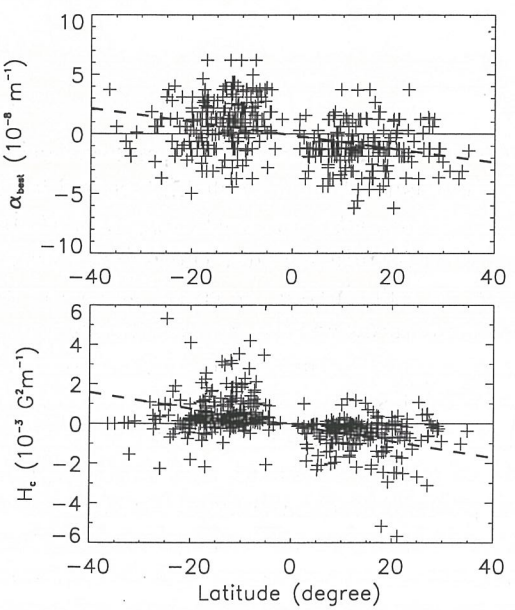

Figure 2. Variation of $\alpha_{\rm best}$ and $H_{\rm c}$ with solar latitude for 422 active regions studied by Bao and Zhang (1998). A linear fit to the data is shown by the dashed line.

percentage of helicity sign in the northern hemisphere during the cycle 23 than $\alpha_{\rm best}$. Since the leading sunspots have negative polarity in the northern hemisphere during 22 cycle, $H_{\rm c}$ should have a higher percentage in sign than $\alpha_{\rm best}$ (see Table 2). (3) The cause of the hemispheric tendency is still uncertain. Perhaps these two parameters reflect different physical nature of subphotospheric origin. (4) A single sign of $\alpha_{\rm best}$ or $H_{\rm c}$ averaged over a whole active region is not appropriate. It ignores the small-scale patterns of oppositely directed twists which are known to exist inside active regions.

Acknowledgements

We thank the staff of Huairou Solar Observing Station for the observations. This work was supported by the National Science Foundation of China under grant 19791090.

References

Abramenko, V. I., Wang, T. J., and Yurchishin, V. B., 1996, *Solar Phys.*, **168**, 75.
Bao, S. D., Pevtsov, A. A., Wang, T. J., and Zhang, H. Q., 2000, *Solar Phys.*, in press.
Bao, S. D. and Zhang, H. Q., 1998, *Astrophys. J.*, **496**, L43.
Bao, S. D., Zhang, H. Q., Ai, G. X., and Zhang M., 1999, *Astron. Astrophys. Suppl. Ser.*, **139**, 311.
Bieber, J. W., Evenson, P., and Matthaeus, W. H., 1987, *Astrophys. J.*, **315**, 700.
Canfield, R. C., Hudson, H. S., and McKenzie, D. E., 1999, *Geophys. Res. Lett.*, **26**, 627.
Hale, G. E., 1927, *Nature*, **119**, 708.
Longcope, D. W., Fisher, G. H., and Pevtsov, A. A., 1998, *Astrophys. J.*, **507**, 417.
Mackay, D. H., Priest, E. R., Gaizauskas, V., and van Ballegooijen, A. A., 1998, *Solar Phys.*, **180**, 299.
Martin, S. F., Bilimoria, R., and Tracadas, P. W., 1994, in Rutten, R. J. and Schrijver, C. J. (eds.), *Solar Surface Magnetisms*, (Dordrecht: Kluwer), 303.
Martin, S. F., Marquette, W. H., and Bilimoria, R., 1992, in Harvey, K. (ed.), *The Solar Cycle*, in ASP Conf. Ser., **27**, 53.
Pevtsov, A. A., Canfield, R. C., 1998, *Eos Trans. AGU*, **79**(17), 273.
Pevtsov, A. A., Canfield, R. C., and Metcalf, T. R., 1995, *Astrophys. J.*, **440**, L109.
Richardson, R. S., 1941, *Astrophys. J.*, **93**, 24.
Rust, D. M., 1994, *Geophys. Res. Lett.*, **21**, 241.
Rust, D. M. and Kumar, A., 1996, *Astrophys. J.*, **464**, L199.
Smith, C. W., 1999, in Brown, M. R., Canfield, R. C., and Pevtsov, A. A. (eds.), *Magnetic Helicity in Space and Laboratory Plasmas*, in Geophysical Monograph **111**, 239.
Wang, J. X., Shi, Z. X., Wang, H. N., and Lü, Y. P., 1996, *Astrophys. J.*, **456**, 861.
Wang, T. J., Xu, A. A., and Zhang H. Q., 1994, *Solar Phys.*, **155**, 99.

Astron. Astrophys. Suppl. Ser. **139**, *311-320 (1999)*

A survey of flares and current helicity in active regions

Shudong Bao, Hongqi Zhang, Guoxiang Ai, and Mei Zhang

Beijing Astronomical Observatory, Chinese Academy of Sciences, Beijing 100080, China
National Astronomical Observatories, Chinese Academy of Sciences, Beijing 100012, China

Received February 9; accepted June 9, 1999

Abstract. We examine the spatial and temporal relationship between chromospheric H_β flares and photospheric current helicities in active regions. All of the data were obtained by the vector magnetograph system at Huairou Solar Observing Station of Beijing Astronomical Observatory. We focus our analysis on NOAA Active Region 6233, which was observed on 30 August 1990. The result shows that rapid and substantial changes of distribution of current helicity in an area or in its vicinity are most likely to trigger flares, but no compelling correlation between peaks of current helicity and flare sites. Furthermore, we study the influence of flares on helicity for several other active regions. We find that the time variations of current helicity in the active regions with highly productive flares are more significant than that of the poorly flare-productive active regions, and that the magnitude of current helicity does not always decrease after flares. Therefore we conclude that the rate of variation of current helicity may be considered as an indicator of flare activity.

In this paper we describe the specifics of the instrumentation and data used, and we describe the methods for computing helicity. The noises and errors in our data are estimated to be at the 2–3 σ level.

Key words: Sun: activity – Sun: flares – Sun: magnetic fields

1. Introduction

The source of energy of solar flares is generally believed to be due to an excess of energy in non-potential magnetic structures. Storage of this energy is perceived as a result of an increasing deformation of magnetic loops initially in a more potential configuration in the upper atmosphere. However, from the observational point of view, how to extract the non-potential component, how to describe the non-potentiality more accurately, are still open questions.

While studying variations of magnetic structures connected with a flare, magnetic shear is of special interest. This concept was firstly recognized from the twisted appearance of H_α fibrils or filaments observed during flare activity (Zirin & Tanaka 1973). A quantitative evaluation of the shear in magnetic fields along the polarity inversion lines was achieved by defining the angular shear, $\triangle\phi$, as the azimuth difference at the photosphere between the potential magnetic fields, which fit the boundary conditions imposed by the observed line-of-sight fields, and the observed transverse fields (Hagyard et al. 1984). The buildup of magnetic shear should be expected to be associated with the overall development of a whole active region, such as different types of photospheric motions and new flux emergence. So it appears desirable to develop a method for describing the overall *regional shear*, not restricting the angular shear analysis to the magnetic inversion lines. A number of papers were devoted to exploring this research field (Gary et al. 1987; Wang 1992; Ambastha et al. 1993; Fontenla et al. 1995; Zhang 1995; Wang et al. 1996), but examples of angular shear increase or decrease after major flares had equal shares.

Moreton & Severny (1968) made pioneer observations of the relationship between H_α emission in flares and active region electric currents. Thirty flares were studied, and it was found that about 80% of the initial brightenings in H_α coincided with the principal sites of vertical currents, to within the 6″ coalignment accuracy of their data sets. With greatly improved observations in quality, vector magnetograms in the photosphere were then used to further examine such a spatial relationship between flares and vertical currents (Lin & Gaizauskas 1987; Canfield et al. 1993; de La Beaujardière et al. 1993; Leka et al. 1993; Metcalf et al. 1994; Wang et al. 1994; Zhang 1995, 1997). Unfortunately, such an attempt failed to give any final conclusions.

Gorbachev & Somov (1988) were the first who studied a quantitative link between observed chromospheric flare kernels and the magnetic topology of the host active region. Since then, there has been a broad interest in the study of magnetic topology in terms of separatrices and separators (Mandrini et al. 1991, 1993, 1995; Démoulin et al. 1993, 1994; van Driel-Gesztelyi et al. 1994; Bagalá et al. 1995; Wang 1997; Wang et al. 1999). In all these studies,

Send offprint requests to: S.D. Bao
Correspondence to: bshd@sun10.bao.ac.cn

flare kernels were found at the intersection of the separatrices with the chromosphere, the kernels being magnetically connected to each other and to a common region around the separator.

We do know that helicity is a topological parameter which describes the complexity of an object and that it is relevant to the effects of twist, writhe and linkage. Magnetic helicity characterizes the topological complexity of a magnetic field. The main advances in magnetic helicity of the solar atmosphere were presented in recent review papers (Ricca & Berger 1996; Low 1996; Canfield & Pevtsov 1998). The most interesting result is the so-called hemispheric handedness rule — various magnetic patterns (e.g., photospheric net helicity in active regions, sunspot whirls, chromospheric filaments, sheared coronal loops, and interplanetary magnetic clouds) in the northern hemisphere show predominantly a left-handed twist while in the southern hemisphere they show a right-handed twist (see Seehafer 1990; Pevtsov et al. 1995; Zirker et al. 1997; and references therein). Bao & Zhang (1998) computed the current helicities in 422 active regions, and found that about 80% of the regions in the northern (southern) hemisphere have negative (positive) helicity. This result confirms the above hemispheric sign asymmetry. The handedness shown in all these large-scale patterns seems to support the solar dynamo operating in the interface between the solar convection and radiation zones. More recently, Zhang & Bao (1998, 1999) also studied the latitudinal variation of current helicity of active regions and the longitudinal distribution of the active regions with a reversed-sign helicity during the solar cycle 22. In the present paper, our primary purpose is to study magnetic activity before and during solar flares from the viewpoint of helicity.

In the next section, the instrumentation and analysis procedures for this study are described. In Sect. 3, we describe the definition of magnetic and current helicity, as well as the methods for computing them from vector magnetograms. In Sect. 4, the spatial and temporal relationship between flare occurrence and current helicity is examined in detail. Finally, the results are discussed in Sect. 5.

2. Observational techniques

The database used in our study was obtained with the Solar Magnetic Field Telescope (SMFT), an imaging vector magnetograph (Ai & Hu 1986) installed at the Huairou Solar Observing Station (HSOS) of Beijing Astronomical Observatory. The SMFT consists of a 35 cm vacuum telescope, a 1/8 Å Lyot birefringent filter with three sets of KD*P crystal modulators, a CCD camera with 512 × 512 pixels, and an image processing system controlled by a computer. It works in either of two spectral lines: Fe I 5324.19 Å (photosphere) and H_β 4861.34 Å (chromosphere). The field of view is about $5.23' \times 3.63'$. The temporal and spatial resolution of the HSOS vector magnetograms depends on the number of video frames that are added to produce them. Each magnetogram used in this paper is the sum of 256 individual frames for both line-of-sight and transverse fields, corresponding to a temporal resolution of about 5 min and a spatial resolution of 2 arc sec.

The inference of vector magnetic fields in the photosphere is on the basis of narrow-band images (filtergrams) of the four Stokes parameters I, V, Q and U. I is always the direct intensity, derived from either the sum of two circularly polarized images used for line-of-sight field measurements, or the sum of two linearly polarized images used for transverse field measurements. V is the difference between the left and right circularly polarized images taken by shifting the bandpass at −0.075 Å from the line center. Q is the difference between two orthogonal linearly polarized images in a certain azimuthal direction. U is the same as Q, but with a 45° change in the azimuthal direction. When Q and U are taken, the filter bandpass is switched to the line center for achieving maximum sensitivity. The line-of-sight component B_l and transverse component B_t of magnetic fields are given by

$$B_l = C_l \frac{V}{I}, \quad B_t = C_t \left(\frac{Q^2}{I^2} + \frac{U^2}{I^2} \right)^{\frac{1}{4}}, \tag{1}$$

where C_l and C_t are calibration coefficients relating the line-of-sight and transverse components of magnetic fields to the circular and linear degree of polarization, respectively. Determining the coefficients is very complicated and difficult. Both theoretical and empirical methods are used to calibrate the HSOS vector magnetograms. Some details have been described by Wang et al. (1996). The azimuthal angle of the transverse field is

$$\varphi = \frac{1}{2} tan^{-1} \left(\frac{U}{Q} \right). \tag{2}$$

It should be mentioned that the magneto-optical effect (Faraday rotation) has been evaluated by theoretical calculations and found to be insignificant (Wang et al. 1996; and references therein). Several tests were made particularly to compare the measured field azimuth for a few sunspots when switching the bandpass from line center to line wings, and the differences in the observed azimuth were less than 10°. The contamination of the relatively weak linear polarization signal by the stronger circular polarization signal (cross-talk) for the HSOS vector magnetograms is not significant. From joint vector magnetograph observations at Big Bear, Huairou, and Mees Solar Observatories, Wang et al. (1992) concluded that the cross-talk in the HSOS magnetograms is only about 2%. In addition, the Fe I 5324.19 Å line used by the SMFT is a broad line with a width of approximately 0.334 Å, and its Landé factor is 1.5. For such a strong and broad line, not only the Zeeman saturation and Doppler shift are not important, but also this line is not very sensitive to

temperature. Numerical simulations show that when B_l is 3000 G, the saturation effect can only cause a 3% relative error for the bandpass location of -0.075 Å to the line center (Ai et al. 1982). For the transverse field measurements, as long as the field strength is less than 2000 G, the linear relation in Equation (1) will hold when the bandpass is less than 0.03 Å from the line center. Although it is impossible to completely eliminate all these errors, some corrections have been made by adjusting the calibration coefficients of magnetic fields.

The 180° azimuthal ambiguity in determining the transverse field direction is an intrinsic defect of Zeeman effect (Harvey 1969). The only way to resolve this problem at present is to introduce an additional constraint on the field azimuth either from independent observations, such as the history of the field evolution and the orientation of chromosphere fibrils, or from other theoretical considerations, such as the potential field approximation. For each magnetogram, we resolved this ambiguity following the method described by Wang et al. (1994).

To reduce the noise, a 3×4 smooth average of V, Q and U parameters was made. The noise level in all the line-of-sight magnetograms shown is 10 G. For the transverse field measurements, the blending of π and σ polarization components over the spectral bandpass used diminishes the linear polarization signal; this limits the sensitivity of B_t to ~ 100 G.

All vector magnetogram data used in this paper were taken with favorable weather and seeing conditions during the time in which active regions were located near the central meridian. The projection effects of high-latitude active regions were removed according to the formulae given by Gary & Hagyard (1990).

3. Magnetic and current helicity

3.1. Helicity definition

The density of magnetic helicity is defined as

$$h_m = \mathbf{A} \cdot \mathbf{B}\,, \tag{3}$$

where $\mathbf{A}$ is a vector potential for magnetic field $\mathbf{B}$ (Moffatt 1978). In general, h_m determines the number of linkages of magnetic field lines. The total magnetic helicity in a domain $\mathcal{D}$ is

$$H_m = \iiint_{\mathcal{D}} h_m \, dV\,. \tag{4}$$

If space is divided into a collection of flux tubes, the helicity integral contains contributions from internal structure within a flux tube, such as twist and writhe, and from external relations between flux tubes, such as knotting and linking. Consider a thin tube T with local $\mathbf{B}(r,\theta,z)$ defined by its axial component $\mathbf{B}_a = (0,0,B_z(r))$ and meridional component $\mathbf{B}_m = (0,B_\theta(r),0)$, Moffatt & Ricca (1992) showed that the total helicity of the thin tube $H_m = \iiint_T \mathbf{A}_a \cdot \mathbf{B}_a \, dV + 2 \iiint_T \mathbf{A}_m \cdot \mathbf{B}_m \, dV$, where first integral represents *writhe* $\mathcal{W}$ and second represents *twist* $\mathcal{T}$. For two untwisted closed flux tubes linked, the total magnetic helicity is given by $H_m = \pm 2 \Phi_1 \Phi_2$, where Φ_1 and Φ_2 measure the magnetic flux of the tubes, and the sign of H_m depends on the sense of linkage (Berger & Field 1984).

For a closed magnetic system ($B_n = \mathbf{B} \cdot \hat{\mathbf{n}}\,|_\sigma = 0$), the variation of magnetic helicity with time is readily derived from the Maxwell equations, and can be written in the final form

$$\frac{dH_m}{dt} = -2 \iiint_{\mathcal{D}} \eta \, \mathbf{J} \cdot \mathbf{B} \, dV\,, \tag{5}$$

here η is the resistivity and $\mathbf{J}$ is the electric current density. Clearly, the total magnetic helicity is conserved in ideal MHD ($\eta = 0$). Equation (5) may be rewritten as

$$\frac{dH_m}{dt} = -\frac{2\eta}{\mu_0} H_c\,, \tag{6}$$

$$H_c = \iiint_{\mathcal{D}} h_c \, dV\,, \quad h_c = \mu_0 \, \mathbf{J} \cdot \mathbf{B} = \mathbf{B} \cdot (\nabla \times \mathbf{B})\,, \tag{7}$$

where μ_0 is the vacuum permeability, h_c is the current helicity density, and H_c is the total current helicity. With analogy to the magnetic helicity, H_c describes the linkages of electric currents.

3.2. Measure of current helicity

The direct computation of magnetic helicity H_m is hindered by the fact that the magnetic vector potential $\mathbf{A}$ is unmeasured. However, under the assumption of a linear force-free field

$$\nabla \times \mathbf{B} = \alpha \, \mathbf{B}\,, \tag{8}$$

the magnetic helicity density will become

$$h_m = \alpha^{-1} B^2\,. \tag{9}$$

Here α is the force-free field parameter, which can be observationally estimated (Seehafer 1990; Pevtsov et al. 1994, 1995). These authors suggest that the parameter α is a plausible helicity proxy to characterize the twist in active region magnetic fields. Similarly, the current helicity density may become also

$$h_c = \alpha B^2\,. \tag{10}$$

There is, indeed, no reason to believe that the magnetic fields at photospheric levels are force-free. In this case we are unable to compute the magnetic helicity, but we can in principle determine the current helicity density according to Equation (7). Unfortunately, our vector magnetograms observed only at a single height allow us to compute only the vertical component of current helicity, i.e., $B_z \cdot (\nabla \times \mathbf{B})_z$. This quantity may be expressed by

$$h_c = \mu_0 B_z J_z\,, \tag{11}$$

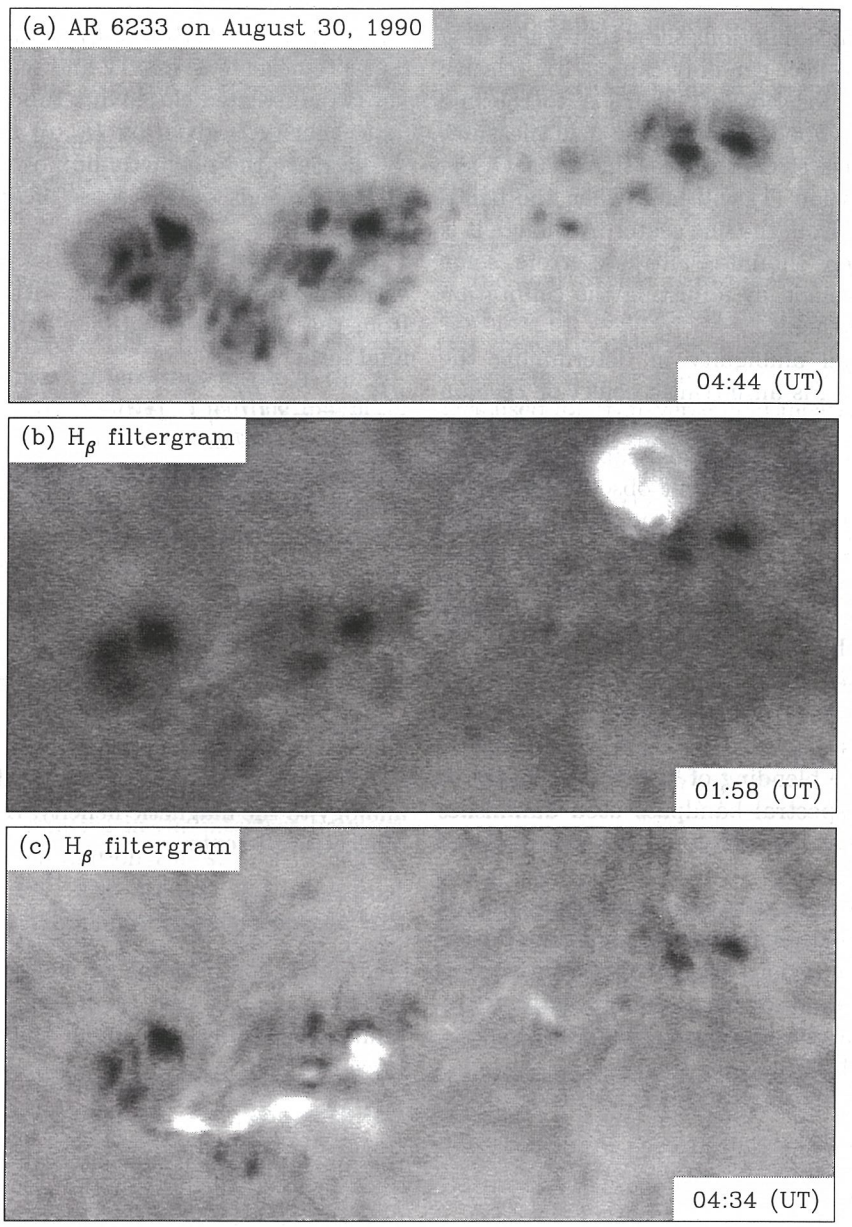

Fig. 1. (a) A photospheric image of NOAA Active Region 6233 on 30 August 1990. (b, c) H_β filtergrams of this region at 01:58 UT and 04:34 UT on the same day. The dark patches are sunspots, while the bright patches are flare kernels. North is at the top, and West is to the right.

Table 1. Characteristics of selected active regions

NOAA/AR	Date	Coordinate	Mag-class	Spot-class	Area(10^{-6} Hemi)
		Flare-productive regions			
6233	30 Aug., 1990	N13 W05	BGD	FKC	700
6891	27 Oct., 1991	S12 E18	BGD	FKC	2100
7321	25 Oct., 1992	S24 E06	BGD	EKC	1200
7773	05 Sep., 1994	S08 E05	B	EKO	470
		Flare-poor regions			
5612	03 Aug., 1989	S17 W01	B	DKI	560
5738	13 Oct., 1989	N11 E05	B	DKO	460
7496	09 May , 1993	N14 E06	BG	DAI	300
7903	30 Aug., 1995	N03 E10	B	CSO	120

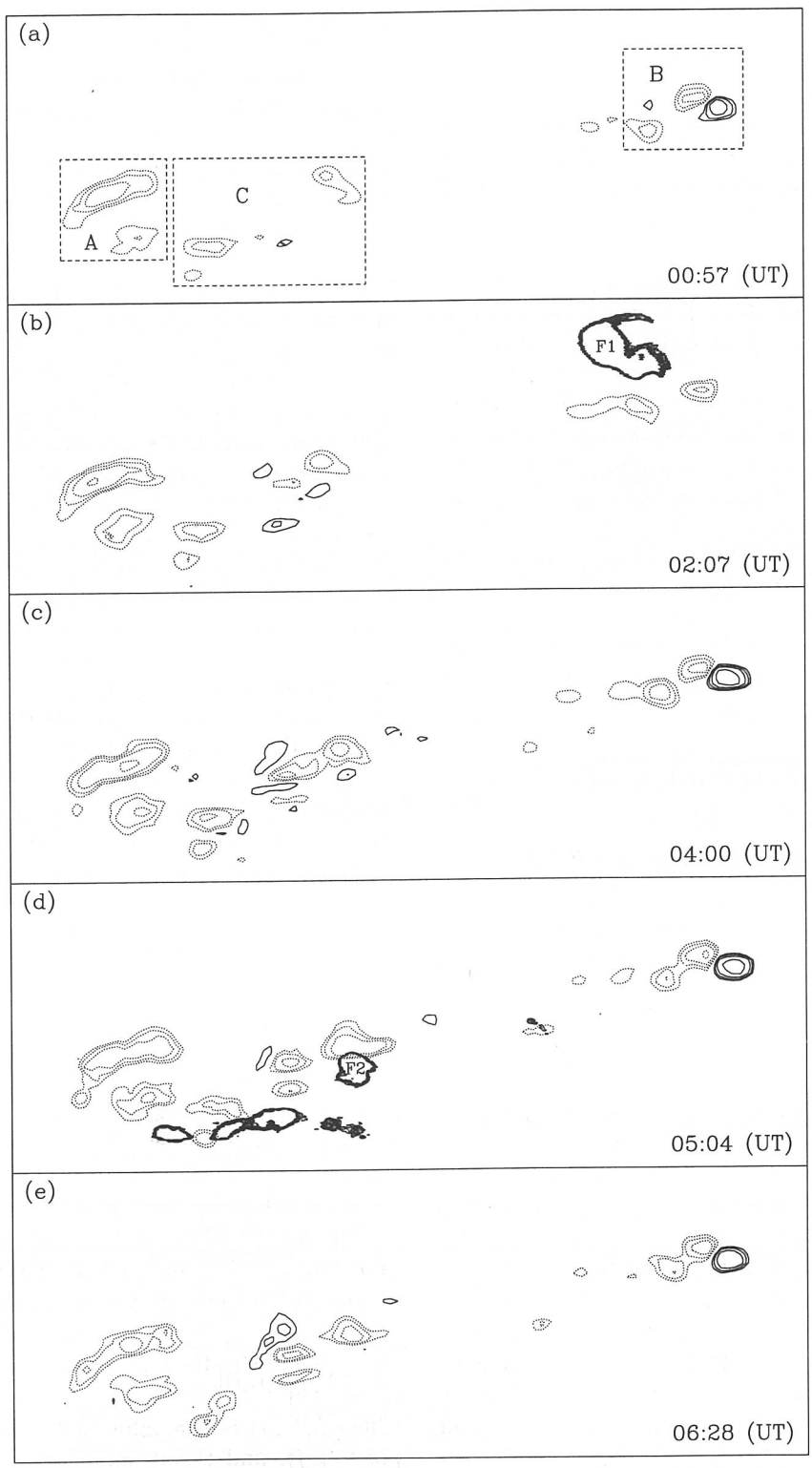

Fig. 2. Time sequence of the distribution of current helicity density in NOAA Active Region 6233 on 30 August 1990. The solid (dotted) contours correspond to positive (negative) current helicity of 0.07, 0.12, 0.20, and 0.40 G^2m^{-1}. The bold contours represent two flares occurred at 01:58 UT and 04:34 UT respectively.

and

$$J_z = \frac{1}{\mu_0}\left(\frac{\partial B_y}{\partial x} - \frac{\partial B_x}{\partial y}\right), \quad (12)$$

where B_z, B_x and B_y are the vertical and horizontal components of magnetic fields in heliographic coordinates, which are derived from both the observed line-of-sight field B_l and transverse field B_t (Venkatakrishnan et al. 1988).

In this paper we choose the formula (11) to compute current helicity, considering that, since only the vertical component of electric currents enters the solar upper atmosphere and determines its helicity, $\mu_0 B_z J_z$ should play a leading role in current helicity (Bao & Zhang 1998). We estimate errors by computing the standard deviation σ_{J_z} of the current values in the set of pixels whose transverse fields are within the estimated uncertainty in B_t; an electric current is considered to be significant only if its magnitude exceeds 3 σ_{J_z}. Note that our analysis, in which we determine a single average value $<h_c>$ for a whole active region, greatly decreases the influence of noise compared to that of a single-pixel measurement of h_c. On the other hand, our choice to use the average value $<h_c>$ has a physical justification because there is often a pronounced overall twist in the active region.

4. Relationship of flare occurrence to current helicity

4.1. Current helicity and flare kernels in AR 6233

Active region 6233 was a flare-productive region which was located near the disk center (N13, W04) on August 30, 1990. Observations of this region, including a study of the morphological relationship between vertical electric currents and chromospheric flare phenomena, can be found in Wang et al. (1996) (also see de La Beaujardière et al. 1993); while the correlation of its magnetic separatrices with flare manifestations has been studied by Mandrini et al. (1995).

In this section we discuss how the distribution of current helicity in AR 6233 changes in the areas where flares occurred. To illustrate its general configuration, a photospheric image of the active region is shown in Fig. 1a; while Fig. 1b and 1c are H_β filtergrams of two flares to be discussed, a SN/M1.2 flare at 01:58 UT and a SN/M1.0 flare at 04:34 UT on August 30. Fig. 2 shows a time sequence of the distribution of current helicity from 00:57 UT to 06:28 UT on the day. Note that only significant current helicity densities ($\geq 10\ \sigma_{h_c}$) are displayed in Fig. 2. Thus, any little changes shown are thought to be due to a true change of current helicity itself rather than from noise or error. The bold contours in Fig. 2b and Fig. 2d represent the brightenings of the flare F_1 and the flare F_2, respectively. The H_β filtergrams of these two flares can be seen in Fig. 1b and 1c. For a convenient description, the active region is partitioned into three parts, panels A, B and C (see Fig. 2a).

From Fig. 2a–2e we see that the distribution of current helicity in panel A hardly varies with time. Panel A is a sunspot region where very strong magnetic fields are observed. Correspondingly, the values of current helicity in panel A are the maximum, but no flare kernel was observed in the panel. This indicates that sites of high current helicity density in active regions do not coincide with flare kernels.

For panel B, the distributions of current helicity in all figures except Fig. 2b are almost the same, as shown in panel A. The only difference among them is that the distribution of positive current helicity (solid contours) in panel B disappears in Fig. 2b. We infer that this phenomenon may be related to the flare (F_1), which occurred near panel B at 01:58 UT. Such a relationship between significant changes of current helicity and flare occurrence is also found in panel C. From Fig. 2a–2d, we can see that the distribution of current helicity in panel C has obvious changes. During the course of the changes there is two flares occurring in panel C. One of them, the flare F_2, is shown in Figure 2d, and it occurred at 04:34 UT. On the other hand, we find that the distribution of current helicity in panel C has almost no changes between Fig. 2d and 2e, while from 05:04 UT to 06:28 UT no flare was observed in panel C. In other words, this panel is quiet in the interval. Therefore, we conclude that rapid and substantial changes of current helicity distribution in an area or in its vicinity seem to be associated with flare eruptions, but in no-flaring regions, such changes are insignificant.

4.2. Changes of current helicity in productive and poor flare regions

In order to have sufficient evidence for the above conclusion, we further analyze some active regions whose characteristics are enumerated in Table 1. These active regions are divided into two groups. One group is flare-productive, and the other shows little flare activity. Note that, compared to typical active regions, the selected flare-poor regions are relatively complicated.

Fig. 3 shows the time series changes of current helicity imbalance, ρ_h, in four flare-productive active regions. The quantity ρ_h is defined by

$$\rho_h = \frac{\sum h_c(i,j)}{\sum |h_c(i,j)|} 100\%, \quad (13)$$

where $h_c(i,j)$ is the value of current helicity at a given pixel (i,j), and the denominator represents the sum of the absolute values of all $h_c(i,j)$ in the active region. ρ_h is actually a measure of imbalance of current helicity sign over a whole active region (Abramenko et al. 1996; Bao & Zhang 1998), and its significant changes undoubtedly reflect that the distribution of current helicity density in an active region does vary with time. Along with the obvious variations of ρ_h in Fig. 3a–3d, some flares occurred in succession (see the arrows in Fig. 5). Similarly, Fig. 4 shows

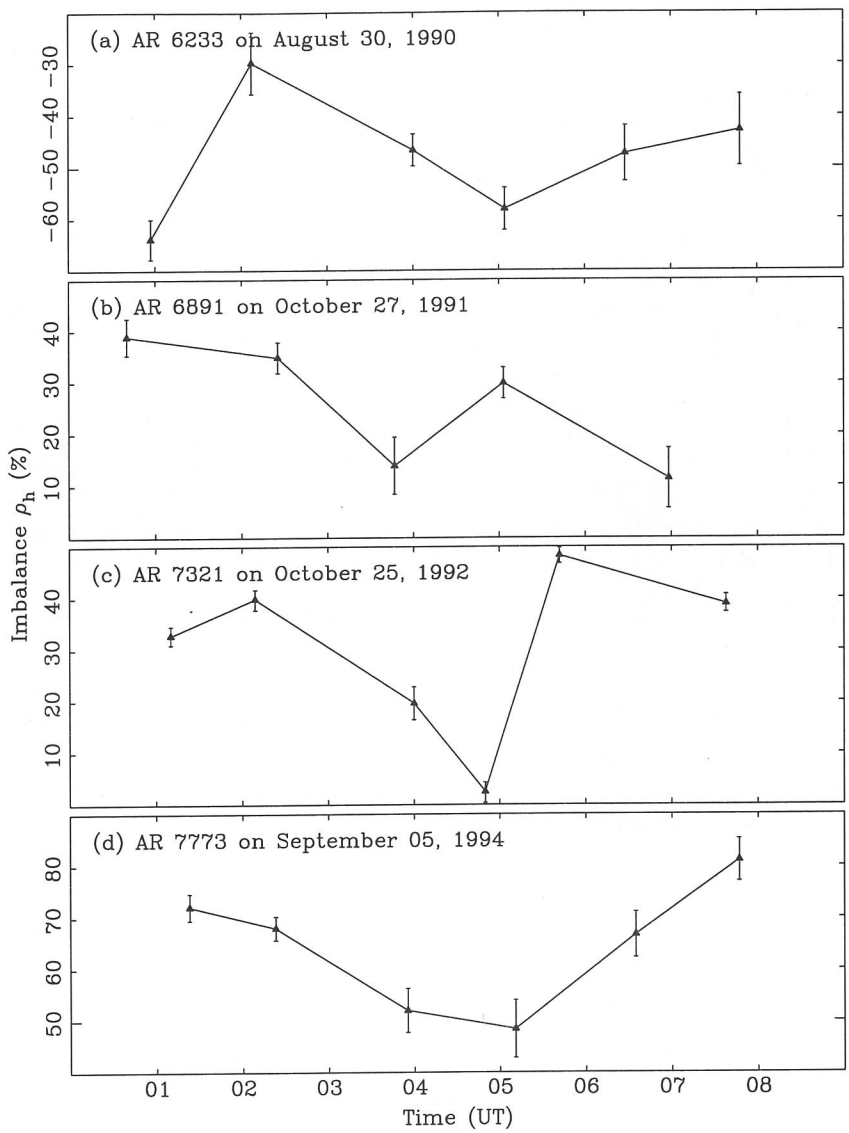

Fig. 3. Maps of the evolution of current helicity imbalance ρ_h in four flare-productive active regions (NOAA 6233, NOAA 6891, NOAA 7321 and NOAA 7773). Solid triangles indicate the times of magnetograms recorded. Obvious variations of current helicity for a whole active region are shown.

the time series changes of ρ_h in poorly flare-productive active regions. By comparing these two figures, We find that the variations of ρ_h are much more significant in Fig. 3 than that in Fig. 4. From this, we may infer that for any active regions, even complicated, if the temporal variations of current helicity are insignificant, the frequency of flaring activity is very low; on the contrary, even if for ordinary active regions, if their ρ_h is changeable, corresponding to the frequency is high.

Note that the average current helicity $< h_c >$ for a whole active region changes as obviously as the current helicity imbalance ρ_h in flare-productive active regions, as shown in Fig. 5. From this figure, we can clearly see that the magnitude of current helicity does not always come down after a flare. Flaring activity seems to be globally associated with the rate of variations in $<h_c>$. However, there is not a one to one relation between flare activity and variation of $<h_c>$. This result does not agree with that of Pevtsov et al. (1995). We argue that the rate of variation of current helicity in active regions is more closely related to solar flares, and it may better characterize the non-potentiality of active regions rather than the values of current helicity.

5. Conclusions and discussion

The above observations and analysis lead us to believe that, (1) rapid and substantial changes of current helicity distribution in an area or in its vicinity probably lead to flare eruptions; (2) active regions in which average cur-

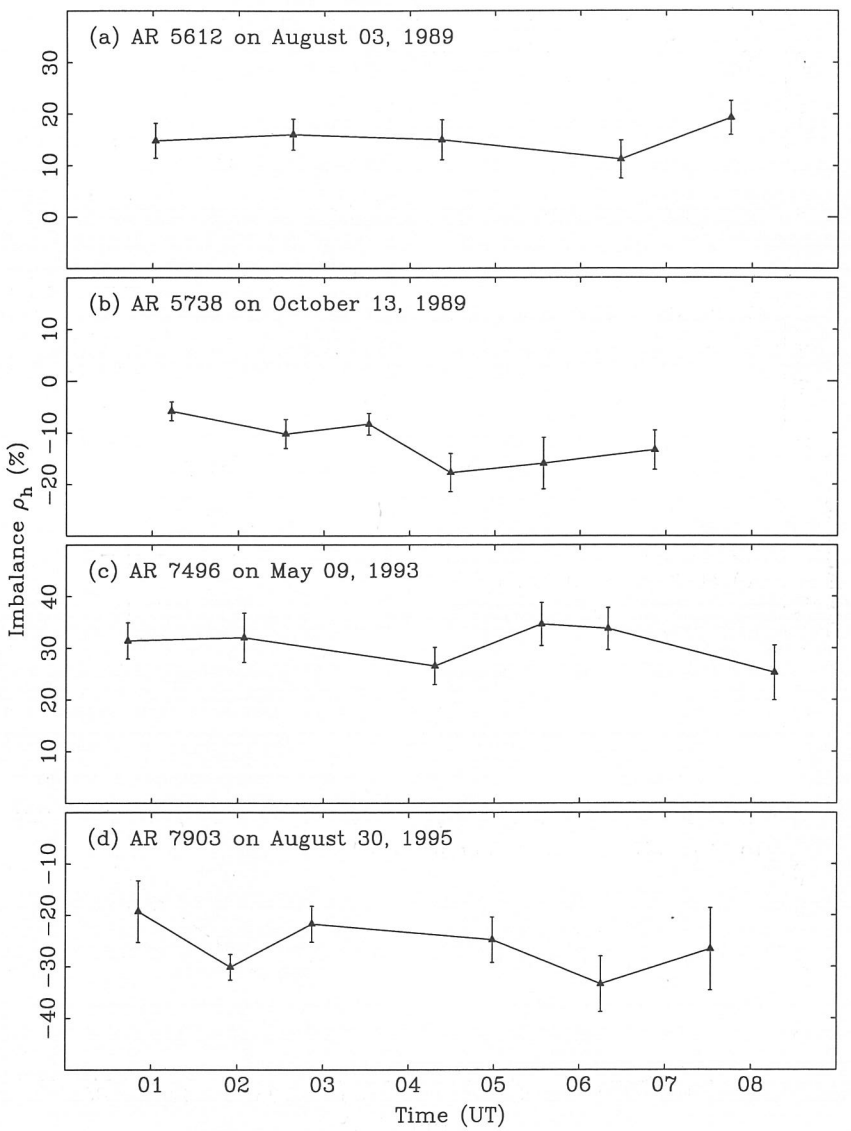

Fig. 4. Maps of the evolution of current helicity imbalance ρ_h in four flare-poor active regions (NOAA 5612, NOAA 5738, NOAA 7496 and NOAA 7903). Solid triangles indicate the times of magnetograms recorded. In these regions, variations of ρ_h are insignificant.

rent helicity has a significant change show more flare activity than typical active regions; (3) no clear correlation between the peak values of current helicity and flare kernels; (4) the rate of variation of current helicity may better characterize the non-potentiality of active region magnetic fields, perhaps it can provide us more information than other parameters, such as angular shear or vertical current.

We know that the magnetic helicity in the solar atmosphere comes mainly from the deeper layers of the Sun, and is accumulated during the course of magnetic activity. The accumulation will increase the magnetic complexity and magnetic free energy in the lower corona, and lead to flare eruptions. Taylor (1974) predicted that as a magnetized plasma relaxes, its magnetic field will evolve toward a force-free state, conserving total magnetic helicity. If Taylor's postulate is applicable for the solar atmosphere, the magnetic energy stored in the solar atmosphere evolves toward small spatial scales and dissipates much faster than magnetic helicity, which cascades toward larger spatial scales. However, this conservation of magnetic helicity is only in a global sense, it may be redistributed locally between magnetic systems as a result of reconnection. Such a helicity exchange may lead to instability in a system with higher helicity. Therefore, solar flares may be understood in the framework of current helicity change processes. Of course, photospheric shear motions besides reconnection may also cause gradual buildup of twist in active regions. Which of these two processes prevails on the Sun? This is beyond the scope of this paper.

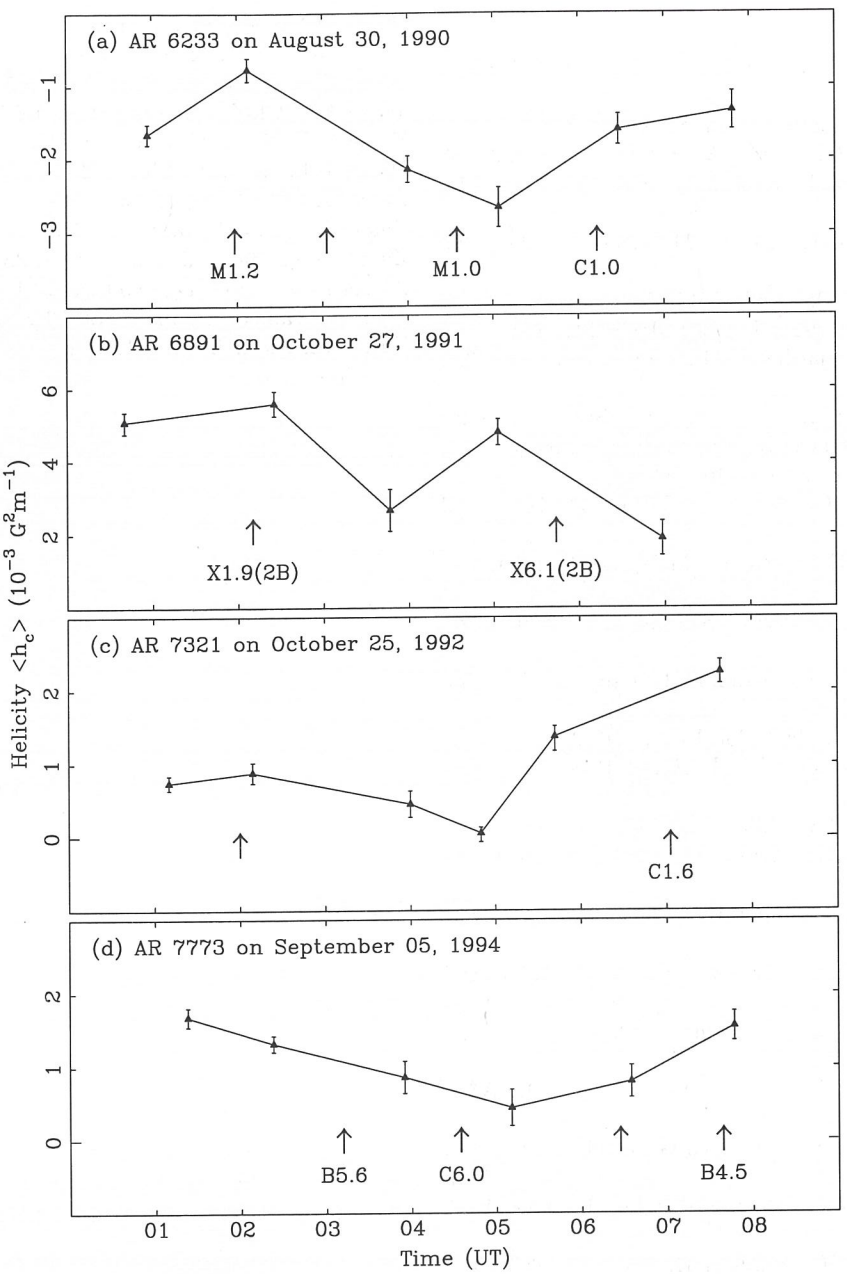

Fig. 5. Variations of the average current helicity $< h_c >$ of the photospheric magnetic fields as a function of time in four flare-productive active regions (NOAA 6233, NOAA 6891, NOAA 7321 and NOAA 7773). Arrows indicate start times of flares.

In fact, many solar observations (e.g., the soft X-ray images and chromospheric filaments) imply that twist is found in magnetic structures that show a tendency to erupt. In the present paper, we try to discuss how the non-potential structures of photospheric magnetic fields in active regions change before and after flares, from the viewpoint of helicity. The results obtained here are preliminary since we do not have 3-dimensional observation data and study changes of current helicity distribution only in the photosphere. Although the helicity approach has not yet been widely applied in the study of flares, we think that the study of the influence of flares on helicity is very important for understanding the magnetic field structure and dynamic processes in the solar atmosphere. One should further research this topic, using a much larger sample.

Acknowledgements. We are indebted to Dr. Tongjiang Wang for helpful software and discussion. We also thank the referee for suggestions for improving the paper. This work was supported by the National Science Foundation of China under grant 19791090.

References

Abramenko V.I., Wang T.J., Yurchishin V.B., 1996, Sol. Phys. 168, 75

Ai G.X., Hu Y.F., 1986, Acta Astron. Sinica 27, 173

Ai G.X., Li W., Zhang H.Q., 1982, Acta Astron. Sinica 23, 39

Ambastha A., Hagyard M.J., West E.A., 1993, Sol. Phys. 148, 277

Bagalá L.G., Mandrini C.H., Rovira M.G., et al., 1995, Sol. Phys. 161, 103

Bao S.D., Zhang H.Q., 1998, ApJ 496, L43

Berger M.A., Field G.B., 1984, J. Fluid Mech. 147, 133

Canfield R.C., de La Beaujardière J.-F., Fan Y.H., et al., 1993, ApJ 411, 362

Canfield R.C., Pevtsov A.A., 1998, in "Synoptic Solar Physics", ed. K.S. Balasubramaniam, J.W. Harvey, D.M. Rabin, ASP conference Series 140, 131

de La Beaujardière J.-F., Canfield R.C., Leka K.D., 1993, ApJ 411, 378

Démoulin P., Mandrini C.H., Rovira, M.G., et al., 1994, Sol. Phys. 150, 221

Démoulin P., Van Driel-Gesztelyi L., Schmieder B., et al., 1993, A&A 271, 292

Fontenla J.M., Ambastha A., Kalman B., Csepura G., 1995, ApJ 440, 894

Gary G.A., Hagyard M.J., 1990, Sol. Phys. 126, 21

Gary G.A., Moore R.L., Hagyard M.J., Haisch B.M., 1987, ApJ 314, 782

Gorbachev V.S., Somov B.V., 1988, Sol. Phys. 117, 77

Hagyard M.J., Smith J.B., Jr. Teuber D., West E.A., 1984, Sol. Phys. 91, 115

Harvey J.W., 1969, NCAR Cooperative Thesis No.17, University of Colorado

Leka K.D., Canfield R.C., McClymont A.N., et al., 1993, ApJ 411, 370

Lin Y.Z., Gaizauskas V., 1987, Sol. Phys. 109, 81

Low B.C., 1996, Sol. Phys. 167, 217

Mandrini C.H., Démoulin P., Hénoux J.C., et al., 1991, A&A 250, 541

Mandrini C.H., Démoulin P., Rovira M.G., et al., 1995, A&A 303, 927

Mandrini C.H., Rovira M.G., Démoulin P., et al., 1993, A&A 272, 609

Metcalf T.R., Canfield R.C., Hudson H.S., et al., 1994, ApJ 428, 860

Moffatt H.K., 1978, Magnetic Field Generation in Electrically Conducting Fluids, Cambridge University Press, p.19

Moffatt H.K., Ricca R.L., 1992, Proc. R. Soc. Lond. A 439, 411

Moreton G.E., Severny A.B., 1968, Sol. Phys. 3, 282

Pevtsov A.A., Canfield R.C., Metcalf T.R., 1994, ApJ 425, L117

Pevtsov A.A., Canfield R.C., Metcalf T.R., 1995, ApJ 440, L109

Ricca R.L., Berger M., 1996, Phys. Today 12, 28

Seehafer N., 1990, Sol. Phys. 125, 219

Taylor J.B., 1974, Phys. Rev. Lett. 33, 1139

van Driel-Gesztelyi L., Hofmann A., Démoulin P., et al., 1994, Sol. Phys. 149, 309

Venkatakrishnan P., Hagyard M.J., Hathaway D.H., 1988, Sol. Phys. 115, 125

Wang H.M., 1992, Sol. Phys. 140, 85

Wang H.M., Varsik J., Zirin H., Canfield R.C., Leka K.D., Wang J.X., 1992, Sol. Phys. 142, 11

Wang H.N., 1997, Sol. Phys. 174, 265

Wang J.X., Shi Z.X., Wang H.N., Lü Y.P., 1996, ApJ 456, 861

Wang T.J., Wang H.N., Qiu J., 1999, A&A 342, 854

Wang T.J., Xu A.A., Zhang H.Q., 1994, Sol. Phys. 155, 99

Zhang H.Q., 1995, A&A 304, 541

Zhang H.Q., 1997, A&A 324, 713

Zhang H.Q., Bao S.D., 1998, A&A 339, 880

Zhang H.Q., Bao S.D., 1999, ApJ 519, 876

Zirin H., Tanaka K., 1973, Sol. Phys. 32, 173

Zirker J.B., Martin S.F., Harvey K, Gaizauskas V., 1997, Sol. Phys. 175, 27

PROBING SIGNATURES OF THE ALPHA-EFFECT IN SOLAR CONVECTION ZONE

K.M. KUZANYAN[1,2], S.D. BAO[1], and H.Q. ZHANG[1]
[1] *Beijing Astronomical Observatory/National Astronomical Observatories, Chinese Academy of Sciences, Beijing 100012, China*
[2] *Heliophysics Lab., IZMIRAN, Russian Academy of sciences, 142092 Troitsk, Russia*

(Received 22 April, 1999; in revised form September 15, 1999)

Abstract. An attempt to extract maximum information on signatures of the alpha-effect from current helicity and twist density calculations in the solar photosphere is carried out. Possible interpretation of the results for developing the dynamo theory is discussed. The analysis shows that the surface magnetic current helicity is mainly negative/positive in the northern/southern hemispheres of the Sun. This indicates the actual alpha-effect at the photospheric level to be positive/negative, respectively. However, at the bottom of the convection zone we may assume this effect to change the sign to negative/positive. We reveal some quantities related to the alpha-effect and discuss its spatial and temporal distribution.

It is also found that there is a minor number of active regions where the the sign of the alpha-effect is indicated opposite to the one in the most of active regions. Such exceptional acive regions with respect to current helicity are seen to localise at certain active longitudes. We compare the determined regularities with theoretical predictions of the alpha-effect distribution in the solar convection zone.

1. Introduction

The role of the alpha-effect is very important for the mean-field dynamo theory. This effect along with the differential rotation provides regeneration of magnetic fields in astrophysical bodies from mechanical turbulent convective motions of cosmic plasmas. For the solar convection zone, the differential rotation is quite well studied by means of helioseismology (e.g., Schou et al. 1998), while knowledge of the alpha-effect is still very little because it cannot be quantitatively observed directly.

The alpha-effect was introduced by Steenbeck, Krause and Rädler (1966) as a quantity linked with the mean kinetic helicity of turbulent motions. Further theoretical advances of Keinings (1983), Seehafer (1994a), and Gruzinov and Diamond (1995) opened an opportunity to gain knowledge on the alpha-effect studying the current helicity of the solar magnetic fields. This became possible with the present level of observational resolution on the basis of recent systematic studies of magnetic fields (Canfield and Pevtsov 1994, 1995), also carried out by Beijing Astronomical Observatory team at Huairou Solar Observing Station (Bao and Zhang 1998; Zhang and Bao 1998, 1999; Bao et al. 1999). Therefore, the studies of strong magnetic fields in the solar

active regions provide very useful information on the magnetic fields at the bottom of the convection zone, and thus they can be used as signatures of the alpha-effect.

The theoretical problem is how to extract such information. The main difficulty is that the values of the magnetic current helicity of small scale fields are highly dispersed over the solar photospheric level in Active Regions (ARs). The dynamo theory interpretation of the data on the alpha-effect in the solar photosphere should take into account the knowledge of convection processes which link the photosphere with the bulk of the Solar Convection Zone (SCZ). The dynamo is believed to operate in the depth of the SCZ, even perhaps at the bottom or beneath (the so-called overshoot layer).

2. Alpha-effect and Turbulent Dynamo Action

2.1. Parker's dynamo. The role of the α- and Ω-effects

In the simplest dynamo models of magnetic field generation there are two main factors which provide positive feedback between the toroidal and poloidal components of the magnetic field: the so-called α- and Ω-effects. They cause regeneration of magnetic fields from mechanical energy of turbulent convective motions of plasma in the SCZ. The magnetic field manifestations calculated in such models appear in the form of a traveling wave which possesses the main properties of the observable magnetic activity of the Sun. The dynamo waves are seen over the butterfly-diagrams of sunspot migration and over other tracers and solar indices.

On the mathematical viewpoint the Parker's dynamo equations (Parker 1955) have the following form:

$$\hat{\mathrm{L}}A = \alpha B \tag{1}$$

$$\hat{\mathrm{L}}B = -D\cos\theta \frac{\partial\Omega}{\partial r}\frac{\partial A}{\partial\theta} \tag{2}$$

where A, B are azimuthal components of the large-scale mean magnetic potential and field, differential operator $\hat{\mathrm{L}} = \partial/\partial t - \partial^2/\partial\theta^2$, α is the alpha-effect (rescaled), Ω the angular velocity, D the dimensionless dynamo number, the regeneration rate, generally large parameter for supercritical oscillatory dynamos. Latitude θ is measured from the equator.

The large-scale mean fields are introduced to represent statistical properties of MHD processes in turbulent media. They are quantities averaged over large enough spatial and temporal scales. The scale should be in accord with our interest for studies of the large scale phenomena. This approach is based on the ideas of mean field dynamo theory (Krause and Rädler 1980).

Unfortunately, as concerned with available observations, there is no distinct scales over the Sun apart of its radius. However, this is often too large for observable temporally-spatial structures of the solar magnetic fields. Therefore, below we consider a few smaller scales regarding to the observable structures of turbulence in the SCZ.

The equations above are significantly one dimensional case which is a rough simplification of a multidimensional one. However, as it was found in many numerical experiments (Moss et al. 1990; Brandenburg 1994), also supported by asymptotic analysis of, e.g., Kuzanyan and Sokoloff (1995, 1996), this simplification does not crucially change the general behavior of the solution. One can see that the solution of eqs. (2) has a form of a traveling dynamo wave (Parker's migratory dynamo). In order to obtain the equatorward waves one can show that quantity $\alpha\,\partial\Omega/\partial r$ should be negative in the Northern and positive in the Southern hemisphere of the Sun.

The Ω-effect is mainly associated with the gradient of angular velocity $G = \partial\Omega/\partial r$ which can be studied from helioseismology data (see, Basu 1997; Kosovichev et al. 1997; Schou et al. 1998) and appears positive in the deep enough convection zone over most of low latitudes in both of the hemispheres. This is perhaps different in the radiative transfer zone or over high latitudes. The dynamo might work in a thin layer at the bottom of the convection zone, where the differential rotation is strong but the alpha-effect is assumed to exist due to turbulent convective motion.

In contrast with the Ω-effect, the α-effect which is responsible for regeneration of the poliodal field from the toroidal one, can be associated with mean kinetic helicity of turbulent motion (e.g., Krause and Rädler 1980) as

$$\alpha_{ef} = -\frac{\tau}{3}\,\langle h_k \rangle\,, \tag{3}$$

where τ is the turbulent correlation time (characteristic convection time), $h_k = \mathbf{v}\cdot\nabla\times\mathbf{v}$ denotes the kinetic helicity, and $\mathbf{v}$ the small scale velocity. Unfortunately, α_{ef} is not available for direct determination. Therefore, various theoretical and numerical attempts have been carried out to estimate this factor.

Krause (1967) gave an estimate of the kinetic alpha-effect in terms of rotation Ω, convection velocity $v_c(r,\theta)$, and density distribution functions $\rho(r,\theta)$ based on the ideas of the mixing length theory with account of Coriolis forces. This reads the following

$$\alpha_{ef} = -\frac{16}{15}\,\tau^2\,v_c^2\;\boldsymbol{\Omega}\cdot\nabla\log(\rho v_c). \tag{4}$$

One can conclude that under quite general assumptions on the convection in the SCZ the α-effect is proportional to the factor $\sin\theta$.

There is no confidence on the sign of the alpha-effect in the SCZ. The observations of the global magnetic activity are not sensible to this sign

but to the sign of the product of the α- and Ω-effects. In order to obtain the observable equatorward migration of the main dynamo wave we should provide the differential rotation and the α-effect to possess opposite signs somewhere in low latitudes of the Northern hemisphere. Two realizations of such condition are possible. In the earlier studies the most or researchers assumed that $G < 0$, and $\alpha > 0$. Later taking into account some results of helioseismology studies of the internal rotation of the Sun they changed their mind to $G > 0$, $\alpha < 0$. There are different ideas on how the alpha-effect is distributed over the depth of the SCZ and how it relates to the domain where the maximum generation takes place. There is an extensive discussion on the thickness of the generation layer in the convection zone (cf., Moss et al. 1990; Brandenburg 1994). This concept of the generation layer is based on the idea of the overshoot layer dynamo (e.g., Skaley and Stix 1991; Rüdiger and Brandenburg 1995). The effective kinetic alpha-effect versus the magnetic field strength was studied in the complete system of the MHD equations by, e.g., Brandenburg and Donner (1997).

Glatzmaier (1985) found numerical evidence that the alpha-effect changes sign with depth. This is linked with that the upward flows diverge in top layers of the convective zone but the downward ones in the bottom. Correspondingly, the upward/downward flows converge in the bottom/top of the SCZ. Although, in a MHD system with extremely high Reynolds numbers like in the SCZ the convection is significantly turbulent, and one can hardly see such prominent divergent/convergent flows at all. Krivodubskij and Schultz (1993) and Krivodubskiy (1998) developed a theory of the alpha-effect distribution over the depth of the SCZ which is large closely below the surface, and zero at the certain level near the bottom of the SCZ. Below this level it changes sign to the opposite one. This is consistent with recent numerical studies of Brummell et al. (1998).

Schlichtenmaier and Stix (1995) considered a phase shift between the toroidal and the poloidal fields in the framework of dynamo models. This quantity can be an independent tracer of particular signs of the α- and Ω-effects. This work needs to be developed to further comparison with available solar indices. The location of the main magnetic field generation in the SCZ and the actual values of signs and magnitudes of the α- and Ω-effects still remain unclear. This puzzle causes serious problems in application of the dynamo theory to the solar case.

In the light of what is said above one can see, that alternative estimates of the alpha-effect would significantly benefit the solution of the dynamo problem. In solar ARs there are strong magnetic fields which arise mainly from the depth of the SCZ. These fields contain information on the MHD flow at the locations where they arise from and through (cf., Melrose 1991). The tilt of sunspots (Longcope et al. 1998; Canfield and Pevtsov 1997; Pevtsov and Canfield 1998; Seehafer 1990) and the magnetic current

helicity (Seehafer 1990; Pevtsov et al. 1994, 1995) could be useful tracers of this factor. This paper is dedicated to analysis of the magnetic current helicity and twist measurements as tracers of the alpha-effect in the SCZ.

2.2. Magnetic and Current helicities. Observations of the solar photosphere.

The helicity of magnetic fields may be characterized by several different parameters. The density of magnetic helicity can be defined as

$$h_m = \mathbf{A} \cdot \mathbf{B}\,, \tag{5}$$

where $\mathbf{A}$ is a vector potential of magnetic field $\mathbf{B}$ (Moffatt 1978). In general, h_m determines the number of linkages of magnetic field lines. The total magnetic helicity in domain $\mathcal{D}$ is

$$H_m = \iiint_{\mathcal{D}} h_m \, dV\,. \tag{6}$$

If space is divided into a number of flux tubes, the helicity integral contains contributions from the internal structure of flux tubes, such as twist and kink, and from external relations between flux tubes, i.e., knotting and linking.

Let us consider an isolated magnetic system ($B_n = \mathbf{B} \cdot \hat{\mathbf{n}}\,|_\sigma = 0$). Then variation of magnetic helicity with time is readily derived from the Maxwell equations, and can be written in the form

$$\frac{dH_m}{dt} = -2 \iiint_{\mathcal{D}} \eta\, \mathbf{J} \cdot \mathbf{B}\, dV\,, \tag{7}$$

here η is the resistivity and $\mathbf{J}$ is the electric current density. For the ideal MHD ($\eta = 0$), the magnetic helicity is apparently conserved. Equation (7) can be rewritten as

$$\frac{dH_m}{dt} = -\frac{2\eta}{\mu_0} H_c\,, \tag{8}$$

$$H_c = \iiint_{\mathcal{D}} h_c \, dV\,, \quad h_c = \mu_0\, \mathbf{J} \cdot \mathbf{B}\,, \tag{9}$$

where μ_0 is the vacuum permeability, H_c is the total current helicity, and h_c is the current helicity density.

Therefore,

$$h_c = \mathbf{B} \cdot \nabla \times \mathbf{B}. \tag{10}$$

Separating h_c into two parts — parallel ($\|$) and perpendicular ($\perp$) to the line of sight — one can write

$$h_c = \mathbf{B}_\| \cdot (\nabla \times \mathbf{B})_\| + \mathbf{B}_\perp \cdot (\nabla \times \mathbf{B})_\perp\,. \tag{11}$$

The both parts of helicity h_c can be linked with each other in the framework of the force-free field theory (see Section 3.1 below).

Unfortunately, because we have magnetic measurements at a single height in the solar atmosphere, we can determine only the first part of current helicity density, i.e., $h_c^{\parallel} = \mathbf{B}_{\parallel} \cdot (\nabla \times \mathbf{B})_{\parallel}$ (see Bao and Zhang 1998). This quantity may be expressed by

$$h_c^{\parallel} = \mu_0 B_z J_z = \mu_0 B_z \cdot (\nabla \times \mathbf{B})_z , \tag{12}$$

where

$$J_z = \frac{1}{\mu_0} \left(\frac{\partial B_y}{\partial x} - \frac{\partial B_x}{\partial y} \right) . \tag{13}$$

Then we may calculate the twist factor

$$\alpha_f = \frac{h_c^{\parallel}}{B_z^2} = \mu_0 \frac{J_z}{B_z} . \tag{14}$$

Here B_z, B_x and B_y are the vertical and horizontal components of magnetic fields in local Cartesian coordinates (with the z-axis upwards), which are derived from both the observed line-of-sight field $\mathbf{B}_{\parallel}$ and transverse field $\mathbf{B}_{\perp}$ (Venkatakrishnan et al. 1988).

We choose formula (12) to calculate the current helicity in our approach, taking into account that only the vertical component of the electric current enters the solar upper atmosphere and determines its helicity. We assume the value $\mu_0 B_z J_z$ to contribute the main impact to the value of the current helicity. The database of active regions used in our study of the current helicity were obtained with the Solar Magnetic Field Telescope (SMFT), a vector video magnetograph system installed at Huairou Solar Observing Station (HSOS) of Beijing Astronomical Observatory. We have considered data for 422 ARs taken within the period of 10 years (1988–1997). They are a quite representative sampling of the total solar surface activity, where there were about 3,000 ARs for the time considered.

Important issues of the studies are criteria of selection of pixels in the magnetograms for calculation of helicity parameters $h_c^{\parallel}$ and α_f. In order to reduce the level of noise which does not normally exceed in determination of the line-of-sight (longitudinal) field $B_{\parallel}$ the level of 20 G, and for the transverse field $B_{\perp}$ 100 G, the pixels where the fields observed is lower such levels were eliminated for calculation of parameters h_c and α_f and further ignored for averaging procedures. Correspondingly, the noise level for J_z was calculated of about 1 mA m^{-2}. Further details of the observational technique and data reduction are described by Bao and Zhang (1998).

3. Magnetic helicity and the alpha-effect

3.1. The force-free field factor

Relatively small domains of the solar atmosphere under certain assumptions can be considered within the framework of the force-free field theory. This theory provides description of magnetic fields for which the following relation is valid (Woltjer 1958)

$$\nabla \times \mathbf{B} = \alpha_f \mathbf{B}, \tag{15}$$

where α_f is a scalar function of position. Assuming that solar ARs are such domains, we can calculate this coefficient from the observational data. Thus we have

$$\alpha_f = \frac{(\nabla \times \mathbf{B})_{||}}{\mathbf{B}_{||}}, \qquad \text{and} \qquad h_c = \frac{B^2}{B_{||}^2} \left(\mathbf{B}_{||} \cdot (\nabla \times \mathbf{B})_{||}\right) = \alpha_f B^2. \tag{16}$$

There is, however, no reason to believe that the magnetic field at photospheric level is force-free. In this case a part of the current helicity density, $h_c^{||} = \mathbf{B}_{||} \cdot (\nabla \times \mathbf{B})_{||}$, can still be calculated, and ratio α_f can also be formally calculated using formula (14).

3.2. Keinings-Seehafer Formula (KSF)

As it was found by Keinings (1983) and Seehafer (1994a, 1994b, 1995, 1996), see also Rädler and Seehafer (1990), Gruzinov and Diamond (1995), that under certain assumptions on the turbulent plasma motion the alpha-effect can be expressed in terms of the magnetic current helicity:

$$\alpha_{ef} = -\eta \frac{\langle \mathbf{b}' \cdot \nabla \times \mathbf{b}' \rangle}{\left(\langle \mathbf{B} \rangle\right)^2} \approx -\eta \frac{\langle h_c \rangle}{\left(\langle \mathbf{B} \rangle\right)^2}. \tag{17}$$

Here we assume $\mathbf{B} = \langle \mathbf{B} \rangle + \mathbf{b}'$, where $\langle \mathbf{B} \rangle$ denotes the mean magnetic field, $\mathbf{b}'$ the small scale one. The main assumption made here is that fluctuations of the magnetic field are considered statistically stationary and homogeneous on the scales of averaging, which are small compared to the scales of the mean field variations. This is a quite natural assumption. Notice, that following Seehafer's papers cited above we do not require this condition in a strict sence on the scales of the entire SCZ, which would not be a correct assumption as there is an anisotropy of turbulence due to rotation.

However, we do not assume that the turbulence is homogeneous and isotropic. Notice that estimates of the α-effect in terms of magnetic and kinetic helicities are considered by e.g., Pouquiet et al. (1976) and Field et al. (1999), as well as by Gruzinov and Diamond (1995).

The both parts of helicity h_c can be linked with each other in the framework of the force-free field theory (see Section 3.1 below).

Unfortunately, because we have magnetic measurements at a single height in the solar atmosphere, we can determine only the first part of current helicity density, i.e., $h_c^{||} = \mathbf{B}_{||} \cdot (\nabla \times \mathbf{B})_{||}$ (see Bao and Zhang 1998). This quantity may be expressed by

$$h_c^{||} = \mu_0 B_z J_z = \mu_0 B_z \cdot (\nabla \times \mathbf{B})_z , \tag{12}$$

where

$$J_z = \frac{1}{\mu_0} \left(\frac{\partial B_y}{\partial x} - \frac{\partial B_x}{\partial y} \right) . \tag{13}$$

Then we may calculate the twist factor

$$\alpha_f = \frac{h_c^{||}}{B_z^2} = \mu_0 \frac{J_z}{B_z} . \tag{14}$$

Here B_z, B_x and B_y are the vertical and horizontal components of magnetic fields in local Cartesian coordinates (with the z-axis upwards), which are derived from both the observed line-of-sight field $\mathbf{B}_{||}$ and transverse field $\mathbf{B}_{\perp}$ (Venkatakrishnan et al. 1988).

We choose formula (12) to calculate the current helicity in our approach, taking into account that only the vertical component of the electric current enters the solar upper atmosphere and determines its helicity. We assume the value $\mu_0 B_z J_z$ to contribute the main impact to the value of the current helicity. The database of active regions used in our study of the current helicity were obtained with the Solar Magnetic Field Telescope (SMFT), a vector video magnetograph system installed at Huairou Solar Observing Station (HSOS) of Beijing Astronomical Observatory. We have considered data for 422 ARs taken within the period of 10 years (1988–1997). They are a quite representative sampling of the total solar surface activity, where there were about 3,000 ARs for the time considered.

Important issues of the studies are criteria of selection of pixels in the magnetograms for calculation of helicity parameters $h_c^{||}$ and α_f. In order to reduce the level of noise which does not normally exceed in determination of the line-of-sight (longitudinal) field $B_{||}$ the level of 20 G, and for the transverse field $B_{\perp}$ 100 G, the pixels where the fields observed is lower such levels were eliminated for calculation of parameters h_c and α_f and further ignored for averaging procedures. Correspondingly, the noise level for J_z was calculated of about 1 mA m^{-2}. Further details of the observational technique and data reduction are described by Bao and Zhang (1998).

3. Magnetic helicity and the alpha-effect

3.1. The force-free field factor

Relatively small domains of the solar atmosphere under certain assumptions can be considered within the framework of the force-free field theory. This theory provides description of magnetic fields for which the following relation is valid (Woltjer 1958)

$$\nabla \times \mathbf{B} = \alpha_f \mathbf{B}, \tag{15}$$

where α_f is a scalar function of position. Assuming that solar ARs are such domains, we can calculate this coefficient from the observational data. Thus we have

$$\alpha_f = \frac{(\nabla \times \mathbf{B})_{||}}{\mathbf{B}_{||}}, \qquad \text{and} \qquad h_c = \frac{B^2}{B_{||}^2}\left(\mathbf{B}_{||} \cdot (\nabla \times \mathbf{B})_{||}\right) = \alpha_f B^2. \tag{16}$$

There is, however, no reason to believe that the magnetic field at photospheric level is force-free. In this case a part of the current helicity density, $h_c^{||} = \mathbf{B}_{||} \cdot (\nabla \times \mathbf{B})_{||}$, can still be calculated, and ratio α_f can also be formally calculated using formula (14).

3.2. Keinings-Seehafer Formula (KSF)

As it was found by Keinings (1983) and Seehafer (1994a, 1994b, 1995, 1996), see also Rädler and Seehafer (1990), Gruzinov and Diamond (1995), that under certain assumptions on the turbulent plasma motion the alpha-effect can be expressed in terms of the magnetic current helicity:

$$\alpha_{ef} = -\eta \frac{\langle \mathbf{b}' \cdot \nabla \times \mathbf{b}' \rangle}{\left(\langle \mathbf{B} \rangle\right)^2} \approx -\eta \frac{\langle h_c \rangle}{\left(\langle \mathbf{B} \rangle\right)^2}. \tag{17}$$

Here we assume $\mathbf{B} = \langle \mathbf{B} \rangle + \mathbf{b}'$, where $\langle \mathbf{B} \rangle$ denotes the mean magnetic field, $\mathbf{b}'$ the small scale one. The main assumption made here is that fluctuations of the magnetic field are considered statistically stationary and homogeneous on the scales of averaging, which are small compared to the scales of the mean field variations. This is a quite natural assumption. Notice, that following Seehafer's papers cited above we do not require this condition in a strict sence on the scales of the entire SCZ, which would not be a correct assumption as there is an anisotropy of turbulence due to rotation.

However, we do not assume that the turbulence is homogeneous and isotropic. Notice that estimates of the α-effect in terms of magnetic and kinetic helicities are considered by e.g., Pouquiet et al. (1976) and Field et al. (1999), as well as by Gruzinov and Diamond (1995).

Another important assumption which we made in formula (17) is that introducing the mean current helicity $\langle h_c \rangle$ we neglect the helicity of the mean field $\langle \mathbf{B} \rangle \cdot \nabla \times \langle \mathbf{B} \rangle$ and treat further the average helicity of the observable magnetic field $\langle h_c \rangle$ as helicity of the small scale fields in formula (17). This assumption is reasonable as the magnitude of large-scale fields in the depth of the Sun is believed to be small compared with the magnitude of small scale fields, and so the impact of helicity of the mean field was estimated small by other studies, e.g., Rädler and Seehafer (1990).

This formulation of the alpha-effect is alternative but complementary to another one which uses terms of kinetic helicity (3). This opens a prospective to use the magnetic current helicity data calculated from observable magnetograms (e.g., Abramenko et al. 1996; Bao and Zhang 1998) for probing the alpha-effect at the solar surface.

In formula (17) η is the molecular magnetic diffusivity. We assume this to be a not very much changing function of position over a given AR. This assumption is definitely crude for the whole SCZ. The value of the alpha-effect used for the dynamo theory is based on estimates in the depth of the SCZ. However, it is believed that the signatures of the alpha-effect at the solar surface can also be useful for revealing the structure of the alpha-effect at the locations further deeper in the solar interior where the dynamo operates. The convection processes cause the active regions to represent a certain fraction of the whole MHD flow and, therefore, the magnetic fields from the deep interior of the SCZ (e.g., Melrose 1991). Thus, we may assume that the α-effect along with current helicity and magnetic helicity are conserved for turbulent convective motions in the SCZ (Berger and Field 1984). Therefore, the surface values of these quantities are likely to be positively correlated with their values in the depth of the SCZ.

The main problem for realization the idea of probing the alpha-effect is quantity $\langle \mathbf{B} \rangle$. Normally in ARs this value is negligible as compared with the current values of B. Perhaps at the present state the observational resolution does not allow one to reveal this quantity reliably.

The analysis of observational data show that the Keinings-Seehafer formula (17) can be used only for observational data taken at large spatial scales, over which the flow is believed to possess some of the mean field properties. This scale should be of order the size of a giant cell. However, the typical time of turbulent motion of such objects is of order one month (Hoyng 1992) while the most of available observations are taken for a few consequent days. One can see from analysis of magnetograms that α_f is highly dispersed over the solar photosphere (e.g., Zhang and Bao 1998). The available data of magnetograms enable us to calculate this factor provided appropriate reliability only over a small fraction of the area of ARs. Therefore, we can hardly use Keinings-Seehafer formula directly, but treat it as an instrument for estimates.

On the contrary with the alpha-effect, the force-free field coefficient α_f can be calculated from available observations over a certain part of area of ARs and is probably the most reliable signature the alpha-effect in the SCZ. Another important signature is twist and, therefore, the current helicity h_c, studied for our collection of magnetograms by, e.g., Bao and Zhang (1998), Zhang and Bao (1998, 1999), and Bao et al. (1999).

Indeed, assuming in the limit of small scale turbulent motion inside a given AR, and that the energy of the mean field $(\langle \mathbf{B} \rangle)^2$ is roughly proportional to the energy of the observable field $\mathbf{B}^2$ (but much smaller in absolute values), the mean force free coefficient α_f is somehow related to the alpha-effect with the opposite sign according to Keinings-Seehafer formula (17), cf., Seehafer (1995):

$$\alpha_{ef} \sim -\left\langle \frac{h_c}{B^2} \right\rangle = -\langle \alpha_f \rangle \,. \tag{18}$$

Notice that if instead of large volumes of the size of a giant cell ($\sim 10^5$ km) we consider smaller volumes of the size of supergranula ($1 - 2 \cdot 10^4$ km) the level of noise and uncertainty caused by the observational resolution does not allow us to reveal any significant spatially-temporal dependence as values of α_f are very highly dispersed for such scales (see, Zhang and Bao 1998, 1999). This quantity is appeared to be very different from one to another location. Due to turbulent fluctuations there is no regularity in its distribution. Furthermore, in this case we are reluctant to consider any temporal evolution as the typical time of turbulent motion of supergranula is of order of one day while the most of available magnetograms of ARs of our collection are taken within just a few consequent days, and very rarely a few magnetograms per day are available.

The further smaller scale is the size of granula ($\sim 10^3$ km) which is at the limit of spatial resolution of observational data. The turnover turbulence time is now of order a few minutes, and neither spatial, nor temporal behavior of α_f over such structures is available for now.

4. Spatially-temporal average of mean $\langle \alpha_f \rangle$

The averaging procedure employed in order to reveal mean-field properties of the observable magnetic fields should operate with large enough structures. They should not exceed the order of giant cell scales: distances of order 10^5 km and times of order one or a few months ($10^6 - 10^7$ s).

Proper spatially-temporal averaging procedure is necessary to reveal the properties of the global alpha-effect. The most of active regions which contain areas with strong magnetic fields contain also weak field domains (e.g., Zhang and Bao 1998, 1999). Considering such small enough regions as well

as some active elements separately from each other would not yield any valuable result due to high dispersion of the quantities. Averaging over the scales smaller than the size of supergranula ($1 - 2 \cdot 10^4$ km) and the times less than at least one Carrington rotation would cause very low spatially-temporal resolution and would not give any regularly changing quantity upon averaging. Therefore, we must use intermediate scales which are consistent with the main actual scales of turbulence in the solar convection zone.

We worked with the data calculated by Bao and Zhang (1998), Zhang and Bao (1998, 1999). First the data on α_f were spatially averaged over a given magnetogram (which is comparable with the size of an AR) of order 10^5 km. Then the data were sorted by time with periods of 27 days (almost Carrington rotations). Spatially they were sorted by latitudinal belts of 5 degrees solar latitude, which corresponds to about $6 \cdot 10^4$ km (comparable with scales of an AR). After that averaging the data became a rather sparse array which still needs to be interpolated and extrapolated in order to reveal a physically consistent function. The results obtained seem to be optimally consistent with available observations.

The properties of the spatial and temporal structure of mean $\langle h_c \rangle$ are described in Bao and Zhang (1998). We can see below that factor $\langle \alpha_f \rangle$ has sometimes similar but still quite different properties from the ones of current helicity density (see Zhang et al. 2000).

5. Properties of the helicity and α_f distribution

There are a few phenomena which are revealed by analysis of observational data by Bao and Zhang (1998), Zhang and Bao(1998, 1999), and Bao et al. (1999). Magnetic, current and kinetic helicities and the alpha-effect contain one inverse length less than magnetic energy. Therefore, they are dissipated slower than the energy during Taylor relaxation. They may be more sensitive to the fine structure of the magnetic fields rather than just energetic level tracers like sunspots. They reveal temporally-spatial properties of the solar magnetic fields like short period oscillations (semi-biennial variations, cf., Benevolenskaya 1998, 1999) likely linked with North-South Asymmetry of the magnetic filed manifestation at the solar surface (e.g., Zhang et al., 2000).

5.1. Latitudinal distribution of mean $\langle \alpha_f \rangle$. Antisymmetry over latitudes

The temporal average of the α_f indicates that this is an antisymmetric function of latitude. Indeed, from Figure 1 you can see that this function

is almost zero at the equator and have almost constantly different signs in different hemispheres (cf., Bao and Zhang 1998; Zhang and Bao 1998). The mean force-free alpha coefficient is mainly negative in the Northern and positive in the Southern hemisphere. Correspondingly, the alpha-effect should be positive/negative in the Northern/Southern hemispheres. Polynomial and running average approximations of this quantity show that this function behaves in a similar way to sine of latitude (Fig. 1). Such behavior is related to ones predicted by theories (Krause 1967; Zeldovich et al. 1983). Indeed, we may expect the alpha-effect to possess such structure as it is influenced by Coriolis forces.

Notice, that the level of antisymmetry of this function may significantly depend on the technique of calculation and inferring of the h_c and α_f data from available magnetograms. The criteria of selection of pixels in the magnetograms refereed in Section 2.2 (see also Bao and Zhang 1998) and the averaging procedure above make the data appropriate to reveal such regularity.

5.2. Longitudinal distribution of mean $\langle\alpha_f\rangle$. Active longitudes and deep interior origin of the ARs. Anomalous sign (reversed sign) average helicity phenomenon

Some longitudes have ARs which persist over long time periods. Some of them often possess the twist (current helicity) opposite to what is seen over the most ARs in a given hemisphere. Such ARs are ARs with anomalous twist (Zhang and Bao 1998, 1999) which is a signature that the alpha-effect in such regions is mainly of opposite sign with respect to the others. The number of such ARs is relatively small, it does not often exceed 30% level for both of parameters $\langle\alpha_f\rangle$ and $\langle h_c\rangle$ for the studied sampling of magnetographic data.

Such ARs often correspond to some specific active longitudes, and they rotate mostly with the radiative transfer interior of the Sun. One can suggest that such ARs capture the flow from very deep layers of the SCZ, where the alpha-effect has probably the sign opposite to the one at the surface (Krivodubskij and Schultz 1993; Krivodubskiy 1998; Brummell et al. 1998). Under this assumption we can interpret the phenomenon of such reversed sign helicity ARs as an evidence of that the alpha effect changes its sign in deep interior of the SCZ. Such depth is normally associated with the so-called overshoot layer (e.g., Glatzmaier 1985) where the solar dynamo is believed to operate.

According to the models the alpha-effect changes sign with the depth. Hence, we can conclude that the alpha-effect in the overshoot layer is negative/positive in the Northern/Southern hemispheres. The acceptance of such explanation would explain at least in part the so-called 'Solar dynamo

dilemma' (Parker 1987) concerning the consistency of the signs of the α- and Ω-effects with the direction of the solar dynamo wave propagation.

5.3. Temporal variations of mean $\langle \alpha_f \rangle$

Temporal dependence of mean $\langle \alpha_f \rangle$ as a signature of the alpha-effect has similarities with the temporal dependence of the current helicity density obtained by Bao and Zhang (1998). Upon smoothing this reveals a short-term period of about 2–3 years (Fig. 2). One could try to interpret this period as the period of exchange of a part of magnetic energy between the Northern and Southern hemispheres of the Sun. Such oscillations may be likely linked with energetic magnetic activity and can be considered in the framework of interaction between odd and even, as well and mixed parity modes of generated magnetic fields (e.g., Sokoloff et al. 1995; Tobias 1997; Knobloch et al. 1998).

The dependence of $\langle \alpha_f \rangle$ on time could be compared with available observations of the solar magnetic activity versus other indices and theoretical predictions. Thus, over the time of one solar magnetic half-cycle (1988–1997) the magnetic current helicity is noticed to be modulated by an oscillation with one remarkable period of about 3 years (Bao and Zhang 1998). The detailed analysis of the latter results and the results presented in Fig. 2 revealed that both quantities $\langle h_c \rangle$ and $\langle \alpha_f \rangle$ oscillate with a short period of about $2 - 3$ years. On the contrary to that of the current helicity, the alpha-factor α_f is not noticed to have remarkable oscillations with longer periods. The dependence of the alpha-effect on the magnetic field is rather complicated. There is a simplified treatment of this problem, considering a simple quenching of the alpha-effect.

Under certain assumptions such properties of the temporal behavior may be in agreement with theoretical studies. Indeed, let us assume that the alpha-effect depends on the magnetic field amplitude as the simplest form of quenching given by series $\alpha(B^2) \simeq \alpha_0 - \alpha_2 B^2 + \alpha_4 B^4 + \ldots$ (α_0, α_2, and α_4 constants). If we imagine the signature of the alpha-effect α_f has such form then $h_c \sim \alpha(B^2)\, B^2$. If the period of oscillation of B is 22 yr., then α would have a period of 11 yr and 5.5 yr, and h_c 5.5 and 2.75 yr etc., correspondingly. This is, however, not clear how such oscillations interact with each other and whether they are reliably to explain a short term oscillation with period of about 2–3 yr. Such treatment is based on some imaginations and should account that the alpha-effect was suggested to be quenched by the small scale rather than large scale fields (e.g., Vainstein and Cataneo 1992; Gruzinov and Diamond 1994). There are different theories concerning the dependence of the alpha-effect on the magnetic fields, e.g., Kleeorin and Ruzmaikin (1982), Kulsrud and Anderson (1992), Rüdiger and Kitchatinov (1993), Cataneo and Hughes (1996).

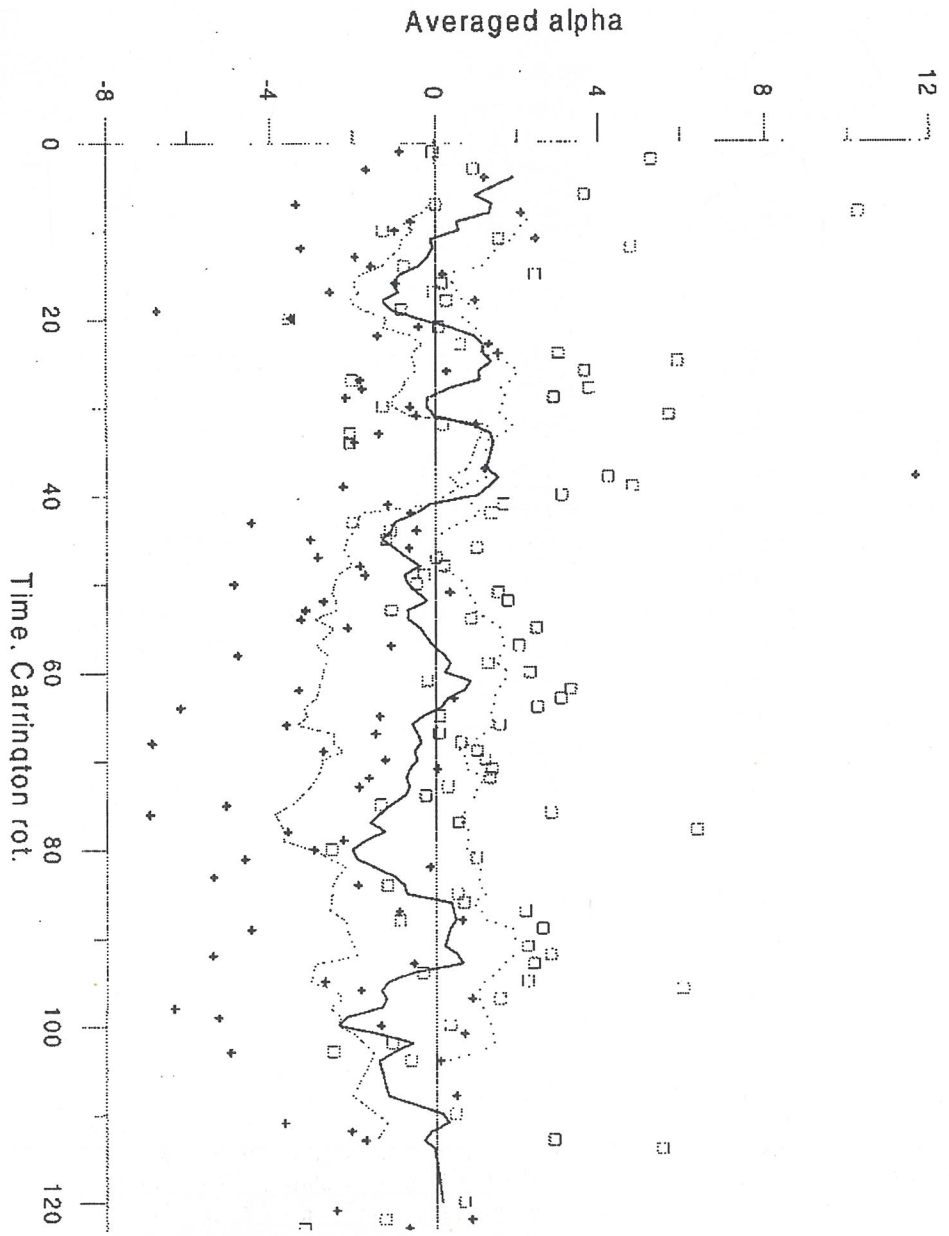

Figure 1. Five point running average interpolation of the mean value $\langle \alpha_f \rangle$ averaged over the total time 1987–1996 versus latitude (dotted line). Averages over ARs sorted by specific 5-degree latitudinal intervals are shown by asterisks. The polynomial interpolation of order 3 is shown as a dash-and-dotted line. This distribution is similar to sine function of latitude.

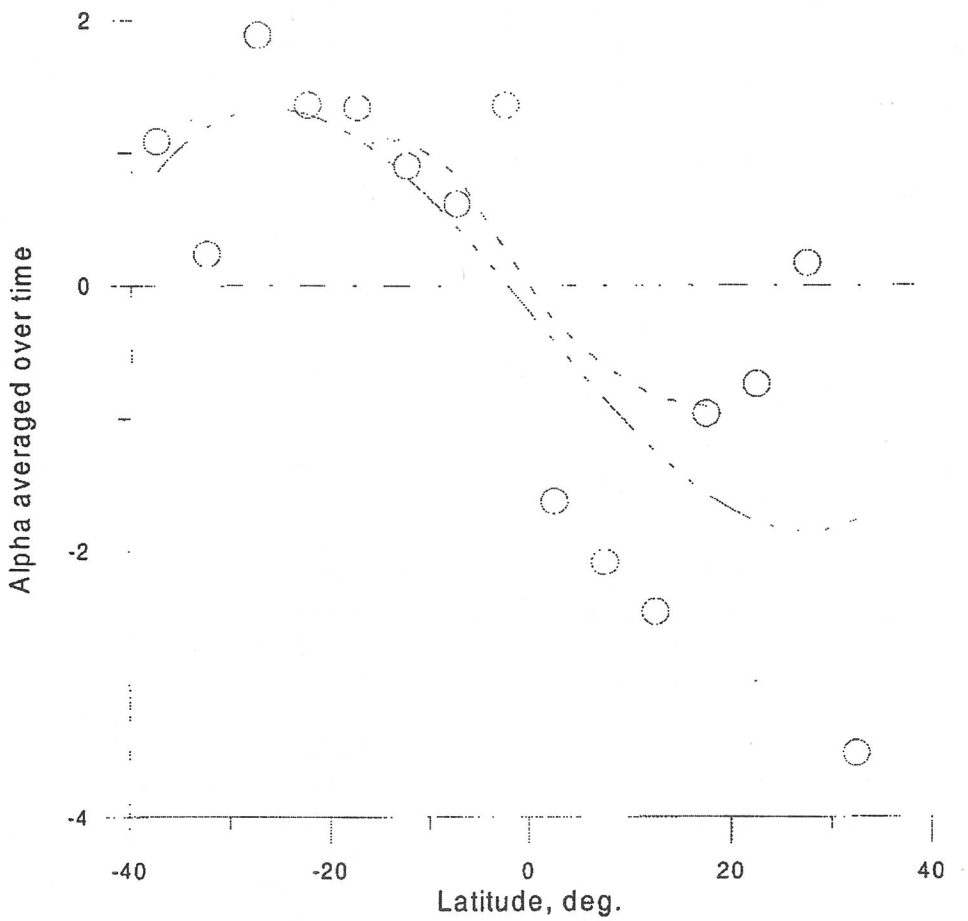

Figure 2. Five point running average interpolation of the mean value $\langle \alpha_f \rangle$ averaged over all latitudes versus time. Crosses indicate averages over individual ARs in the Northern hemisphere, and squares in the Southern. The total sum over the Northern (short dashed line), Southern (dash-and-dotted line) and both the hemispheres (solid line) are shown. Time is given in Carrington rotations numbered starting since rotation 1797 (January 1, 1988).

Thus, we can see here a signature of the so-called semi-biennial cycle. Other signatures of this cycle are also seen by other tracers (Benevolenskaya 1998, 1999; Hoyng 1993; Hoyng et al. 1994; Makarov et al. 1997). Nevertheless, to reveal the global temporal evolution of these quantities one must collect data for the following 11 yr cycle, and so we could carry out such analysis earliest in 2010. We also expect that both of the current helicity and the alpha-factor α_f may be somehow influenced by the main 11 yr cycle (cf., Ruzmaikin 1996).

6. Discussion

Thus, in our analysis we obtained that the force-free alpha-coefficient α_f is negative/positive over the Norther/Southern hemispheres at the photospheric level. Its interpretation as a signature of the α-effect for dynamo mechanism suggests the latter one to have the sign opposite to the first one. Besides that, we found that the values of the α_f slightly vary with time with typical period of 2–3 years irrelatively on the phase of the solar cycle.

We may try to consider a dynamo wave near the surface of the Sun. Although the most of dynamo models assume that the sources of the dynamo mechanism are situated in the depth of the SCZ, we could imagine a surface dynamo as a hypothetical case, which is in accord with recent modelling of the double magnetic cycle with 22 and 2–3 years periods (Benevolenskaya 1999). This hypothetical surface dynamo would require the radial gradient of angular velocity Ω to be negative near the surface of the Sun in order to obtain an equator-ward dynamo wave, which is in agreement with helioseismological studies.

We may suggest that with depth in the SCZ the alpha-effect changes its sign and becomes negative/positive, respectively. This property is in accord with theoretical treatment of, e.g., Glatzmaier (1985), Krivodubskiy (1998), and also recent numerical simulations of Brummell et al. (1998). The phenomenon of the reversed sigh helicity and twist active regions could be considered as an evidence of that.

Indeed, it is also found that there is a minor number of ARS where the the sign of the alpha-effect is indicated opposite to the one in the most of active regions. Such exceptional ARs with respect to current helicity are seen to localise at certain active longitudes, which rotate mostly with the same agnular velocity as the radiative interior of the Sun. One can suggest that such ARs capture the flow from very deep layers of the SCZ, where the alpha-effect has presumably the sign opposite to the one at the surface.

Then we must suggest that $\partial\Omega/\partial r$ is positive in the depth of the SCZ for the case of an equator-ward wave. This conclusion is in agreement with recent helioseismology results (e.g., Kosovichev 1997; Schou et al. 1998) at

least in low latitudes. Therefore, we must conclude that the dynamo generation of magnetic fields may take place in the depth of the convection zone but not necessarily in the overshoot layer. This conclusion means that the direction of propagation of the hypothetical surface dynamo wave coincides with the one at the bottom of the SCZ.

We must stress that numerous assumptions made for interpretation of the mean value $\langle \alpha_f \rangle$ as a signature of the α-effect are crude and should be understood as a first theoretical outlook on the available observational data on the twist and helicity in the solar photosphere. Further progress in observational technique and new theoretical treatment of the fine structure of the magnetic field would open new perspectives for understanding the mechanism of the solar magnetic activity.

Acknowledgements

We wish to thank T.J. Wang and L.R. Tian for the discussion and kind help with computer programs. This research was supported by the Chinese Academy of Sciences and National Science Foundation of China. One of the authors (K.K.) would like to thank the Chinese Academy of Sciences and National Research Council of China for supporting his visit to Beijing Astronomical Observatory, and his thanks go to the staff of Huairou Solar Observing Station for providing good conditions of his stay in China. He also would like to acknowledge financial support from Russian Fund for Basic Research under grants numbers 99-02-18346a and 96-02-10013, and Young Researchers' grant of Russian Academy of Sciences No. 41. Our thanks also go to the referee Prof. N. Seehafer whose comments enabled us to seriously improve the paper.

References

Abramenko, V.I., Wang, T.J., and Yurchishin, V.B.: 1996, *Solar Phys.* **168**, 75.
Bao, S.D. and Zhang, H.Q.: 1998, *Astrophys. J.* **496**, L43.
Bao, S.D., Zhang, H.Q., Ai, G.X., and Zhang, M.: 1999, *Astron. Astrophys. Suppl. Ser.* **139**, 311.
Bassom, A.P., Kuzanyan, K.M., and Soward, A.M.: 1999, *Proc. Roy. Soc. Lond. A* **455**, 1443.
Basu, S., Christensen-Dalsgaard, J., and Thompson, M.J.: 1997, *Astron. Astrophys.* **321**, 634.
Benevolenskaya, E.E.: 1998, *Solar Phys.* **181**, 479.
Benevolenskaya, E.E.: 1999, *Astrophys. J.* **509**, L49.
Berger, M. and Field, G.: 1984, *J. Fluid Mech.* **147**, 133.
Brandenburg, A.: 1993, *The Cosmic Dynamo*, IAU-157, Potsdam, 111.

Brandenburg, A.: 1994, in M.R.E. Proctor and A.D. Gilbert (eds.), *Lectures on Solar and Planetary Dynamos*, Cambridge University Press, 117.
Brandenburg, A. and Donner K.J.: 1997, *Mon. Not. R. Astr. Soc.* **288**, L29.
Brummell, N.H., Hurlburt, N.E., and Toomre, J.: 1998, *Astrophys. J.* **493**, 955.
Canfield, R.C. and Pevtsov, A.A.: 1997, *American Astronomical Society, SPD meeting* **29**, 1705.
Canfield, R.C. and Pevtsov, A.A.: 1998, in K.S. Balasubramaniam, J. Harvey, and D. Rabin (eds.), *ASP Conference Series* **140**, 131.
Cataneo, F. and Hughes, D.W.: 1992, *Phys. Rev. E* **54**, 4532.
Field, G.B, Blackman, E.G., and Chou, H.: 1999, *Astrophys. J.*, in press.
Glatzmaier, G.: 1985, *Astrophys. J.* **291**, 330.
Gruzinov, A.V. and Diamond, P.H.: 1994, *Phys. Rev. Lett.* **72**, 1651.
Gruzinov, A.V. and Diamond, P.H.: 1995, *Phys. Plasma* **2**, 1941.
Hoyng, P.: 1992, in Schmelz, J.T. and Brown, J.C. (eds.), *The Sun, A Laboratory for Astrophysics*, 99.
Hoyng, P.: 1993, *Astron. Astrophys.* **272**, 321.
Hoyng, P., Schmitt, D., and Teuben, L.J.W.: 1994, *Astron. Astrophys.* **289**, 265.
Keinings, R.K.: 1985, *Phys. Fluids* **26**, 2558.
Kleeorin, N. and Ruzmaikin, A.: 1982, *Magnitnaia Gidrodynamika* **2** 17.
Knobloch, E., Tobias, S.M., and Weiss, N.O.: 1998, *Mon. Not. R. astr. Soc.* **297**, 1123.
Kosovichev, A.G.: 1996, *Astrophys. J.* **469**, L61.
Kosovichev, A.G., Schou, J., Scherrer, P.H., et al.: 1997, *Solar Phys.* **170**, 43.
Krause, F.: 1967, *The Turbulent Dynamo*, NCAR Technical Note TN/IA-60.
Krause, F. and Rädler, K.H.: 1980, *Mean Field Magnetohydrodynamics and Dynamo Theory*, Pergamon, Oxford.
Krivodubskiy, V.N.: 1998, *Astron. Rep.* **42**, 122.
Krivodubskij, V.N. and Schultz, M.: 1993, *The Cosmic Dynamo*, IAU-157, Potsdam, 25.
Kulsrud, R.M. and Anderson, S.W.: 1992, *Astrophys. J.* **396**, 606.
Kuzanyan, K.M. and Sokoloff, D.D.: 1995, *Geophys. Astrophys. Fluid Dynamo.* **81**, 113.
Kuzanyan, K.M. and Sokoloff, D.D.: 1996, *Astron. Rep.* **40**, 425.
Kuzanyan, K.M. and Sokoloff, D.D.: 1997, *Solar Phys.* **173**, 1.
Longcope, D.W., Fisher, G.H., and Pevtsov, A.A.: 1998, *Astrophys. J.* **507**, 417.
Makarov, V.I., Tlatov, A.G., and Callebaut, D.K.: 1997, *Solar Phys.* **170**, 373.
Melrose, D.B.: 1991, *Astrophys. J.* **381**, 306.
Meunier, N., Proctor, M.R.E., Sokoloff, D.D., Soward, A.M., and Tobias, S.M.: 1997, *Geophys. Astrophys. Fluid Dynamo.* **86**, 249.
Moffatt H.K.: 1978, *Magnetic Field Generation in Electrically Conducting Fluids*, Cambridge University Press.
Moss, D., Tuominen, I., and Brandenburg, A.: 1990, *Astron. Astrophys.* **240**, 142.
Parker, E.N.: 1955, *Astrophys. J.* **122**, 293.
Parker, E.N.: 1987, *Solar Physics* **110**, 11.
Pevtsov, A.A., and Canfield, R.C.: 1998, in T. Watanabe et al. (eds.), *Observation Plasma Astrophysics: Five Years of Yokhoh and Beyond*, 85.
Pevtsov, A.A., Canfield, R.C., and Metchalf, T.R.: 1994, *Astrophys. J.* **425**, L117.
Pevtsov, A.A., Canfield, R.C., and Metchalf, T.R.: 1995, *Astrophys. J.* **440**, L109.
Pouquet, A., Frisch, U., and Leorat, J.: 1976, *J. Fluid Mech.* **77**, 321.
Rädler, K.H. and Seehafer, N.: 1990, in H.K. Moffat and A. Tsinober (eds.), *Topological Fluid Mechanics*, Cambridge University Press, 157.
Rüdiger, G. and Brandenburg, A.: 1995, *Astron. Astrophys.* **297**, 557.
Rüdiger, G. and Kitchatinov, L.L.: 1993, *Astron. Astrophys.* **269**, 581.
Ruzmaikin, A.A.: 1996, *Geophys. Res. Lett.* **23**, 2649.

Schlichtenmaier, R. and Stix, M.: 1995, *Astron. Astrophys.* **302**, 264.
Schou J., Antia H.M., Basu S., et al.: 1998, *Astrophys. J.* **505**, 390.
Seehafer, N.: 1990, *Solar Phys.* **125**, 219.
Seehafer, N.: 1994a, *Astron. Astrophys.* **284**, 593.
Seehafer, N.: 1994b, *Europhys. Lett.* **27** 353.
Seehafer, N.: 1995, *Astron. Astrophys.* **301**, 290.
Seehafer, N.: 1996, *Phys. Rev. E* **53**, 1283.
Skaley, D. and Stix, M.: 1997, *Astron. Astrophys.* **241**, 227.
Sokoloff, D.D., Fioc, M., and Nesme-Ribes, E.: 1995, *Magnitnaya Gidrodynamika* **31**, 19.
Steenbeck, M., Krause, F., and Rädler, K.-H.: 1966, *Z. Naturforsch.* **A21**, 369.
Tobias, S.M.: 1997, *Astron. Astrophys.* **322**, 1007.
Vainstein, S.I. and Cataneo, F.: 1992, *Astrophys. J.* **393**, 165.
Venkatakrishnan, P., Hagyard, M.J., and Hathaway, D.H.: 1988, *Solar Phys.* **115**, 88.
Woltjer, L.: 1958, *Proc. Nat. Acad. Sci. USA* **44**, 489.
Zeldovich, Y., Ruzmaikin, A., and Sokoloff, D.: 1983, *Magnetic Fields in Astrophysics*, Gordon and Breach, N.-Y.
Zhang, H.Q. and Bao, S.D. 1998, *Astron. Astrophys.* **339**, 880.
Zhang, H.Q. and Bao, S.D. 1999, *Astrophys. J.* **519**, 876.
Zhang, H.Q., Bao, S.D., and Kuzanyan, K.M.: 2000, *Solar Phys.*, submitted.

TWIST OF MAGNETIC FIELDS IN SOLAR ACTIVE REGIONS

H.Q. ZHANG[1], S.D. BAO[1], and K.M. KUZANYAN[1,2]
[1] *Beijing Astronomical Observatory/National Astronomical Observatories, Chinese Academy of Sciences, Beijing 100012, China*
[2] *Heliophysics Lab., IZMIRAN, Russian Academy of sciences, 142092 Troitsk, Russia*

(Received 8 March, 2000)

Abstract. In this paper we study the twist properties of photospheric magnetic fields in solar active regions, using the magnetographic data from Huairou Solar Observing Station of Beijing Astronomical Observatory. We calculate the average force-free field factor α_f of active regions and compare it with the average current helicity density $h_c = \mathbf{B}_{\parallel} \cdot (\nabla \times \mathbf{B})_{\parallel}$ of same active regions. The results demonstrate that, as a whole effect, the average twist of the magnetic field α_f in active regions does not significantly vary with the solar cycle. The distributions of both α_f and h_c show the hemispheric tendency — negative/positive sign in the northern/southern hemisphere, although such a asymmetry is stronger for the helicity parameter h_c. In some active regions the average α_f and h_c disobey this trans-equatorial sign rule. We found that the active regions which disobey this rule with respect to α_f have no obvious tendency to cluster at certain longitudes, on the contrary to those of h_c.

1. Introduction

The configuration of solar magnetic fields and their evolution in the solar surface are important problems. It is believed that the magnetic field is generated by the dynamo operating near the base of the convection zone and emerges into the solar surface. The strong twist of the photospheric magnetic field normally occurs in the solar active regions and may contain information about the mechanism of the solar dynamo. Recently, the concept of magnetic helicity was employed to describe the twist of magnetic field in solar active regions. Several previous investigations of the trans-equatorial change of the sign of the magnetic helicity have been carried out (Seehafer 1990; Pevtsov et al. 1995; Abramenko et al. 1996; Bao and Zhang 1998; Kuzanyan et al. 2000). The longitudinal distribution of magnetic helicity in active regions was analyzed by Canfield and Pevtsov (1998) and Zhang and Bao (1999). Bao and Zhang (1998) found a correlation between the monthly averaged sunspot numbers and the current helicity during solar cycle 22. Temporal dependence of the averaged force-free coefficient was studied also (Kuzanyan et al. 2000).

The magnetic twist can also be indirectly inferred from the chromospheric Hα structures around sunspots (Hale 1927; Richardson 1941), the distribution of quiescent filaments (Martin et al. 1994) and a pattern of soft X-ray images (Rust and Kumar 1996). These observations provide information on

the twist of the magnetic field above the solar photosphere. The question is what twists the magnetic field in the solar surface. The α-effect, introduced in dynamo theory (e.g., Krause and Rädler 1980), is an important quantity to characterize the properties of turbulent convection in the solar convective zone. This effect is believed to enable regeneration of the magnetic field according to the dynamo mechanism. Its original estimate is

$$\alpha_{ef} = -\frac{\tau}{3}\langle \mathbf{v} \cdot \bigtriangledown \times \mathbf{v} \rangle, \tag{1}$$

where τ is the turbulent correlation time and $\mathbf{v}$ is the velocity of turbulent fluctuations. There is no reliable estimates of this effect based on observations. Therefore, the α-effect was extensively studied theoretically. Some authors suggest that the dynamo α_{ef} quantity increases with magnetic field strength (e.g., Brandenburg and Donner 1997; Brandenburg, Saar and Turpin 1998). An expression for α_{ef} in terms of the current helicity [see formula (9) below] was derived by Keinigs (1985), who used the first order smoothing approximation, and rederived without this approximation by Seehafer (1994). Using this (or similar) relationship, some properties of the solar dynamo mechanism can probably be traced by photospheric vector magnetograms.

2. Helicity on the Solar Surface

2.1. Expressions for the helicity and twist

With $\mathbf{B}$ denoting the magnetic induction, the density of current helicity is defined as

$$h_c = \mathbf{B} \cdot \bigtriangledown \times \mathbf{B}. \tag{2}$$

Separating h_c into two parts, which are determined by parallel ($\|$) and perpendicular ($\perp$) to the line-of-sight component of magnetic fields, one can write

$$h_c = \mathbf{B}_{\|} \cdot (\bigtriangledown \times \mathbf{B})_{\|} + \mathbf{B}_{\perp} \cdot (\bigtriangledown \times \mathbf{B})_{\perp}. \tag{3}$$

Within the limits of one active region we can impose the assumption of the force-free field (e.g., Woltjer 1958). For the force-free field we have

$$\bigtriangledown \times \mathbf{B} = \alpha_f \mathbf{B}, \tag{4}$$

where the constant α_f can be calculated as

$$\alpha_f = \frac{\mathbf{B}_{\|} \cdot (\bigtriangledown \times \mathbf{B})_{\|}}{B_{\|}^2}. \tag{5}$$

Then

$$h_c = \alpha_f B^2 = \left(\frac{B^2}{B_{\|}^2}\right) \mathbf{B}_{\|} \cdot (\nabla \times \mathbf{B})_{\|}, \tag{6}$$

where B is the absolute value of the magnetic field. Note that α_f has only dimensions of inverse length but not of magnetic field strength explicitly.

2.2. Observational determination of current helicity

The presently existing solar vector magnetographs enable us to measure three components of the photospheric magnetic field $\mathbf{B} = \{B_x, B_y, B_z\}$. Let B_z be the component of the magnetic field along the line-of-sight, and B_x and B_y are vertical (transverse) ones of the magnetic field relative to the line-of-sight direction. As the active regions are not located near the center of the solar disk, the projection effect of the magnetic field in active regions probably becomes a notable but not a crucial problem for analyzing configuration of the magnetic field at relatively high latitudes.

The current helicity parameters h_z (a part of the current helicity h_c) and α_f can be calculated from observational photospheric vector magnetograms as follows

$$h_z = \mathbf{B}_{\|} \cdot (\nabla \times \mathbf{B})_{\|} = B_z \left(\frac{\partial B_y}{\partial x} - \frac{\partial B_x}{\partial y}\right), \tag{7}$$

and

$$\alpha_f = \frac{\mathbf{B}_{\|} \cdot (\nabla \times \mathbf{B})_{\|}}{B_{\|}^2} = \left(\frac{\partial B_y}{\partial x} - \frac{\partial B_x}{\partial y}\right) / B_z. \tag{8}$$

We can find that the two parameters also do not provide any real information on the horizontal component of the electric current in the current helicity calculations. The horizontal component of the electric current may sometimes contribute an important impact to the total helicity in the photosphere, because the approximation of force-free field is unsuitable in the entire domain of an active region.

The observational data reduction technique was discussed in the previous papers (e.g., Wang et al. 1994; Bao and Zhang 1998). To calculate the helicity parameters we used only selected domains of active regions which are far beyond the magnetic neutral lines (e.g., Abramenko et al., 1996). For this we applied some selection criteria to the values of the magnetic field components and the current (Bao and Zhang 1998). In order to reduce the level of noise which does not normally exceed in determination of the line-of-sight field $B_{\|}$ the level of 20 G, and for the transverse field $B_{\perp}$ 100 G, the pixels where the fields observed is lower than such levels were eliminated for calculation of parameters h_c and α_f and further ignored for averaging procedures. Correspondingly, the noise level for J_z was calculated of about

1 mA m^{-2}. Thus we keep accuracy of determniation of values of α_f and h_c of order 20–25%.

It is interesting to notice that intensity distributions of both parameters h_z and α_f are different, but these parameters have same signs in same areas of active regions (Zhang and Bao 1999). For understanding the basic properties of the current helicity parameters h_z and α_f, we show a vector magnetogram of an active region (NOAA 6659 on June 9, 1991) and corresponding values of h_z and α_f which are calculated by the magnetogram (Figure 1). We can find that the distribution of current helicity parameters h_z and α_f is much the same as that obtained in another time in the previous paper by Zhang and Bao (1999). This means that the distributions of the both current helicity parameters of the active region is relatively similar to each other, even if the intensity values of the current helicity parameters in an active region are normally spread over a relatively wide range, such as in the active region 6659 in Figure 2.

2.3. Statistical reduction of the current helicity data

For understanding the statistical properties of the current helicity, we calculate the mean helicity parameters of active regions. Under the assumption of the force-free field by the formula (8), we can obtain the mean $\langle \alpha_f \rangle$ of active regions, where brackets $\langle\ \rangle$ indicate spatial average. Neglecting the contribution of the transverse component of the electric current, taking into account formula (7), we calculate mean density of the current helicity $\langle h_c \rangle$ in the photosphere.

Both quantities $\langle \alpha_f \rangle$ and $\langle h_c \rangle$ have been previously used to study the helicity properties of active regions, although they were analyzed separately from each other. In the present study we compute both $\langle \alpha_f \rangle$ and $\langle h_c \rangle$ using the same dataset and compare their spatial and temporal structure.

We use photospheric vector magnetograms of solar active regions observed by the Vector Magnetograph at Huairou Solar Observing Station. The dataset covers the period 1988–1997 and includes most of large active regions in the past decade. For 422 active regions (one magnetogram per region), we computed both $\langle \alpha_f \rangle$ and $\langle h_c \rangle$ as described above (Abramenko et al. 1996; Bao and Zhang 1998). For the sake of simplicity we omitted $\langle\ \rangle$ in further description. Figure 3 shows the latitudinal distribution of α_f and h_c. Although the definitions of the two helicity parameters are different, both show similar hemispheric tendency — the magnetic fields in opposite hemispheres are mainly twisted in opposite directions. The dotted-dashed lines in the figure show the average values of helicity computed by averaging over the scale 0.05 in the sine of a latitude. Figure 4 shows histograms of the mean current helicity parameters α_f and h_c.

For $h_c = \mathbf{B}_{||} \cdot (\bigtriangledown \times \mathbf{B})_{||}$ 84% of active regions in the northern hemisphere have negative mean current helicity density, and 79% of active regions in the southern hemisphere have the positive one. For α_f the percentage of active regions following the rule is lower. Only 74%/62% of active regions in the northern/southern hemisphere obey the rule. This is consistent with the result of Pevtsov et al. (1995), although our definition of the α_f is different from that used by Pevtsov et al. The most of active regions were observed within the belt $\pm 30°$, with a few exceptions. Maxima of the average current helicity density occur near the belt $\sin\theta = \pm 0.25$, where θ (solar latitude) is about $\pm 15°$, in agreement with Zirker et al. (1997). Although, one can see that these figures are consequence of the specific samlpling of the active regions under consideration and the fact, that the current helicity parameters are visualisated over regions of strong magnetic fields which normally appear in such latitudes.

Figure 5 shows relation between h_c and α_f. There are about 40% of active regions where the mean current helicity parameters h_c and α_f have opposite signs. The current helicity density h_c is influenced by the magnitude of the magnetic field as a weight factor when averaging over a given active region. This can explain the difference between the properties of h_c and α_f. In Figure 5b we show the latitudinal dependence of correlation of h_c and α_f upon averaging over latitude. The correlation decreases with increase of the heliocentric distance, e.g., the correlation is about 70% near the heliocenter and about 50% near the latitude $\pm 25°$. It is also found a slight difference in the two hemispheres.

3. Evolution of the Mean Helicity Density

Figure 6 shows temporal variation of h_c. The data show significant scatter during 1989–1993, and much lower values between 1994–1997. Accordingly, the solar activity was much higher during 1988–1993 and lower during 1994–1997. The link between the averaged current helicity density and the number of sunspots was briefly analyzed by Bao and Zhang (1998). Comparing our Figure 6 with Figure 3 of Bao and Zhang (1998), one can find that the amplitude of $\mathbf{B}_{||} \cdot (\bigtriangledown \times \mathbf{B})_{||}$ changes with time. This implies that the current helicity density of active regions depends on the phase of the solar magnetic cycle. It is perhaps due to the fact that the magnetic field strength varies with the solar cycle and h_c is the function of magnetic field.

Figure 7 shows the evolution of α_f factor during the same period. It shows no significant difference between the solar maximum and minimum years. This implies that the mean twist density of active regions does not significantly depend on the solar activity. Moreover, it is noticed that α_f factor in active regions looses information on the magnetic field strength,

even if the convection flow in the solar subatmosphere has probably stronger influence on weak magnetic fields rather than on strong fields. From statistical point of view, over a studied sampling of active regions, it is difficult to find a distinct dependence of mean α_f on the phase of the solar cycle.

4. Longitudinal Evolution of α_f and h_c

Figure 8 shows longitudinal distribution of the factor α_f versus time measured in solar rotation cycles in both the hemispheres. We found that the regions, where the sign of factor α_f disobeys the trans-equatorial rule, are distributed over longitudes quite uniformly. On the other hand, Zhang and Bao (1999) found a tendency for the active regions with reversed signs of h_c to cluster in some longitudes.

We should, however, notice that Canfield and Pevtsov (1998) also analyzed the longitudinal distribution of α_f and found a tendency for active regions for which the helicity distribution disobeys the trans-equatorial rule to cluster at certain longitudes for many rotations.

5. Discussion and Conclusions

The alpha-effect in the solar dynamo theory was suggested to be connected with the current helicity of the fluctuating magnetic field, as indicated by Keinigs (1985) and Seehafer (1994). Under certain assumptions we have

$$\alpha_{ef} = -\frac{\eta}{\langle \mathbf{B} \rangle^2} \langle \mathbf{B}' \cdot \bigtriangledown \times \mathbf{B}' \rangle, \tag{9}$$

where η is the molecular magnetic diffusivity, $\langle \mathbf{B} \rangle$ is the mean field and $\mathbf{B}'$ is the fluctuating field. The magnetic field in active regions is assumed to be mainly the fluctuating field, and one can suggest the magnetic fluctuations to be statistically stationary. Other assumptions are discussed in the above cited papers. We may expect that the functions of helicity density and twist have positive correlations with the α-effect. Thus, the statistical distribution of current helicity density actually provides some qualitative information on the alpha-effect. Moreover, there is no explicit criterion whether the observed active-region fields are mean or fluctuation ones in the sense of the mean-field dynamo theory (Seehafer 1998), but in any case the statistical distribution of current helicity can provide information on the α-effect in dynamo theory (although if the relationship between the current helicity and the dynamo α-effect is a complex problem). We also notice that other opinions are proposed by some authors, such as an important alternative study on the generation

of the magnetic helicity the solar turbulent convection made by Longcope, Fisher and Pevtsov (1998).

One can find from the equation (4) that α_f describes degree of twist of the magnetic field. It is normally believed that the twist of magnetic lines of force is caused by the action of the Coriolis force, the differential rotation etc., as magnetic lines of force arise up from the bottom of the convection zone and form active regions at the solar surface. If the magnetic field is generated by the solar dynamo action and the magnitude of the photospheric large-scale magnetic field depends on the phase of the solar activity cycle, the mean intensity of the current helicity density should contain information on both the twist and strength of the magnetic field. However, the α_f factor is related to the twist of the magnetic field of active regions and does not depend on the intensity of the magnetic field, so that the calculated α_f factor probably contains mainly information on the Coriolis force and differential rotation, which do not significantly change with the phase of the solar cycle. On the other hand, in each hemisphere there are about 30% of the total number of active regions, for which the sign of factor α_f is opposite to that of the majority of active regions over a given hemisphere. This probably reflects some statistical means of the generation of solar magnetic fields. In such active regions, the mean twist of the magnetic field is different from the one caused by the Coriolis force.

Various properties of twist of the photospheric magnetic field can be found from magnetograms of active regions. The twist of the magnetic field is linked with the magnetic (current) helicity. Because the total helicity $\mathbf{B} \cdot (\bigtriangledown \times \mathbf{B})$ can not be obtained by the photospheric magnetographs until now, the study of the $\mathbf{B}_{\|} \cdot (\bigtriangledown \times \mathbf{B})_{\|}$ and $\mathbf{B}_{\|} \cdot (\bigtriangledown \times \mathbf{B})_{\|}/B_{\|}^2$ (i.e., α_f factor) becomes important and necessary. By analysis of the helicity parameters in detail, we can find that they not only obey the trans-equatorial rule (i.e., in the northern/southern hemisphere the average current helicity and twist density of active regions mainly have negative/positive sign), but also contain slightly different information on the twist properties of the magnetic field.

The results of this study show that two different helicity quantities α_f and h_c have different properties. The trans-equatorial rule is stronger for the h_c distribution and weaker for the α_f one. The h_c distribution shows clear dependence on the level of the solar activity (phase of the solar cycle), while α_f does not. The active regions with 'reversed' sign of h_c disobeying the trans-equatorial rule cluster at some specific longitudes. We can see the indication of such 'reverse sign longitudes' for h_c and do not see it for α_f significantly. One possibility is that the α_f lost information on the magnetic field strength and contains mainly information on the magnetic shear near the magnetic neutral lines, which was discussed by Zhang and Bao (1998, 1999), and where the influence of the projection effect of the magnetic field

is significant due to the difference of inclination angles of the field to the solar surface in the active regions, because the active regions are normally located at non-zero latitude.

Although some properties of helicity in solar active regions were discussed above, we also need to point out that some difference between the distributions for α_f and h_c is influenced by the observational and data reduction technique and other factors, for instance, the projection effect of the vector magnetic field in the solar surface and measurement errors of the transverse magnetic field. However, this can not probably cause that much as about 40% of active regions have opposite signs of the mean helicity parameters h_c and α_f.

The basic agreement between the transverse magnetic field in the Huairou magnetograms and the fine structures of the Hα and Hβ filtergrams is confirmed by a series of papers, such as Zhang et al. (1991) and Zhang (1994). The influence of the measurement errors of the transverse field to the difference in calculation of the current helicity between the Huairou and Mees datasets was recently analyzed by Bao et al. (2000). It is found that such a influence is insignificant in the most areas of active regions. While, we also notice that the resolution of the 180° ambiguity of the highly sheared transverse magnetic field is often difficult in areas near the magnetic neutral line in active regions. The mean α_f factor is probably more influenced by calculation errors near the magnetic neutral lines in active regions rather than h_c. To overcome such difficulties we have taken into account only the pixels of magnetograms which are far from magnetic neutral lines.

After the analysis, the main results are as follows:

(1) The average α_f and $h_c = \mathbf{B}_{||} \cdot (\nabla \times \mathbf{B})_{||}$ both provide information on a twist of the magnetic field lines. The difference is that α_f does not contain information on the magnetic field strength, but h_c does.

(2) α_f and h_c show similar longitudinal distributions. The current helicity density h_c distribution in active regions shows stronger trans-equatorial regularity rather than α_f.

(3) About 40% of active regions have α_f and h_c of opposite signs. This may be explained by the fact that the magnetic field strength enters the expression for h_c as a weight factor.

Acknowledgements

We wish to thank Dr. T.J. Wang for the discussion and kind help with computer programs. This research was supported by the Chinese Academy of Sciences and National Science Foundation of China. K.K. would like to thank the Chinese Academy of Sciences and National Science Foundation

of China for supporting his visit to Beijing Astronomical Observatory, and also thank the staff of Huairou Solar Observing Station for providing good conditions of his stay in China. He would like to acknowledge partial financial support from Russian Fund for Basic Research under grants numbers 96-02-10013, 99-02-18346, and 00-02-17854 and Young Researchers' grant of Russian Academy of Sciences. We wish to thank Dr. V. Obridko for helpful comments and suggestions.

References

Abramenko, V.I., Wang, T.J., and Yurchishin, V.B.: 1996, *Solar Phys.* **168**, 75.
Ai, G.X. and Hu, Y.F.: 1986, *Publ. Beijing Astron. Obs.* **8**, 1.
Bao, S.D., Pevtsov, A.A., Wang, T.J., and Zhang, H.Q.: 2000, *Solar Phys.*, in press.
Bao, S.D. and Zhang, H.Q.: 1998, *Astrophys. J.* **496**, L43.
Brandenburg, A. and Donner K.J.: 1997, *MNRAS* **288**, L29.
Brandenburg, A., Saar, S.H., and Turpin, C.R.: 1998, *Astrophys. J.* **498**, L51.
Canfield, R.C. and Pevtsov, A.A.: 1998, in K.S. Balasubramaniamn, J.W. Harvey, and D.M. Rabin (eds.), *Synoptic Solar Physics, ASP Conf. Ser.* **140**, 131.
Hale, G.E.: 1927, *Nature* **119**, 708.
Keinigs, R.K.: 1985, *Phys. Fluids* **26**, 2558.
Krause, F., Rädler, K.H.: 1980, *Mean-Field Magnetohydrodynamics and Dynamo Theory*, Academic-Verlag, Berlin; Pergamon Press, Oxford.
Kuzanyan, K.M., Zhang H.Q., and Bao, S.D.: 2000, *Solar Phys.*, in press.
Landolfi, M. and Landi Degl'Innocenti, E.: 1982, *Solar Phys.* **78**, 355.
Longcope, D.W., Fisher, G.H., and Pevtsov, A.A.: 1998, *Astrophys. J.* **507**, 417.
Martin, S.F., Bilimoria, R., and Tracada, P.W.: 1994, in Rutten, C.J. and Schrijver, C.J. (eds.), *Solar Surface Magnetism*, p.303, Kluwer Academeic Publishers.
Pevtsov, A.A., Canfield, R.C., and Metchalf, T.R.: 1995, *Astrophys. J.* **440**, L109.
Richardson, R.S.: 1941, *Astrophys. J.* **93**, 24.
Rust, D.M. and Kumar, A.: 1996, *Astrophys. J.* **404**, L119.
Seehafer, N.: 1990, *Solar Phys.* **125**, 219.
Seehafer, N.: 1994, *Europhys. Lett.* **27**, 353.
Seehafer, N.: 1998, in D. Webb, D. Rust and B. Schmieder (eds.), *New Perspectives on Solar Prominences, ASP. Conf. Ser.* **150**, 407.
Stenflo, J.O.: 1994, *Solar Magnetic Field, Polarized Radiation Diagnostics*, Kluwer Academic Publishers, Dordrecht.
Wang, H.M., Varsik, J., Zirin, H., Canfield, R.C., Leka, K., and Wang, J.X.: 1992, *Solar Phys.* **142**, 11.
Wang, T,J., Xu, A.A., and Zhang, H.Q.: 1994, *Solar Phys.* **155**, 99.
West, E.A. and Hagyard, M.J.: 1983, *Solar Phys.* **88**, 51.
Woltjer, L.: 1958, *Proc. Nat. Acad. Sci. USA* **44**, 489.
Zhang, H.Q.: 1994, *Solar Phys.* **154**, 207.
Zhang, H.Q.: 1995a, *Astron. Astrophys. Suppl. Ser.* **111**, 27.
Zhang, H.Q.: 1995b, *Astron. Astrophys.* **297**, 869.
Zhang, H.Q.: 1996, *Astrophys. J.* **471**, 1049.
Zhang, H.Q., Ai, G.X., Sakurai, T., and Kurokawa, H.: 1991, *Solar Phys.* **136**, 269.
Zhang, H.Q. and Bao, S.D.: 1998, *Astron. Astrophys.* **339**, 880.
Zhang, H.Q. and Bao, S.D.; 1999, *Astrophys. J.* **519**, 876.

Zirker, J.B., Martin, S.F., Harvey, K., and Gaizauskas, V.: 1997, *Solar Phys.* **175**, 27.
Zirin, H.: 1988, *Astrophysics of the Sun*, Cambridge University Press

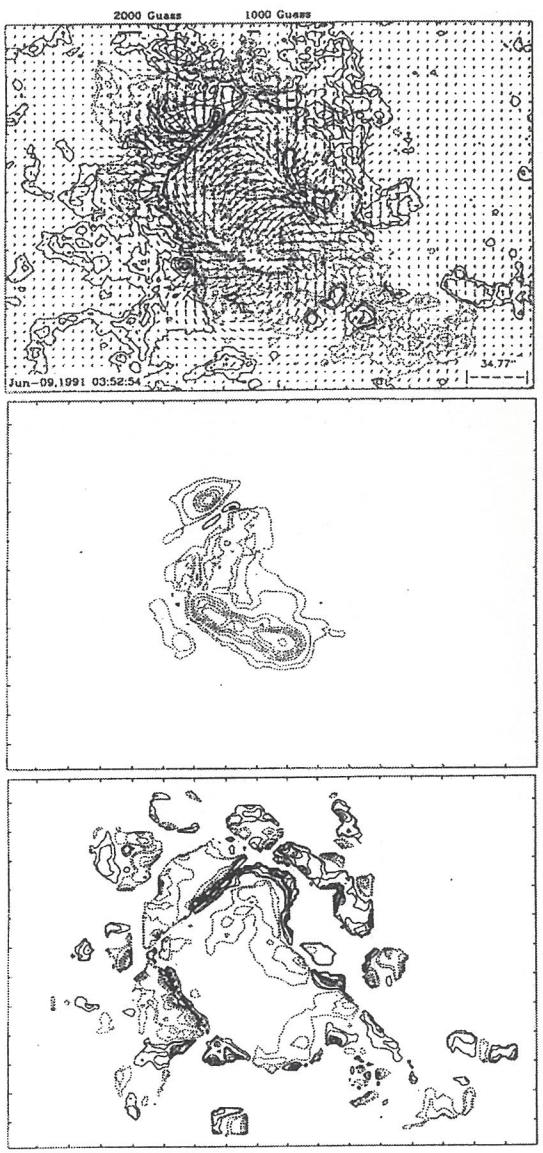

Figure 1. (a) A vector magnetogram of active region (NOAA 6659) at 05:29 UT on June 9, 1991. The solid (dashed) contours indicate the positive (negative) longitudinal magnetic field distribution of ±20, 160, 640, 1280, 1920, 2240, 2560 and 2880 Gauss. (b) The current helicity parameter $\mathbf{B}_{\parallel} \cdot (\nabla \times \mathbf{B})_{\parallel}$. The solid (dashed) contours indicate the positive (negative) regions of the current helicity distribution of ±0.25, 0.5, 1.0, 1.25, 1.5, 1.75, 2.0, $2.5(\times 10^{-1} G^2 M^{-1})$. (c) The α factor of force-free field in the areas where the longitudinal field is larger than 100G. The solid (dashed) contours indicate the positive (negative) α factor distribution of ±0.5, 1.0, 2, 2.5, 3.0, 3.5, 4.0, $5.0(\times 10^{-7} M^{-1})$. The north is top and the east is at left.

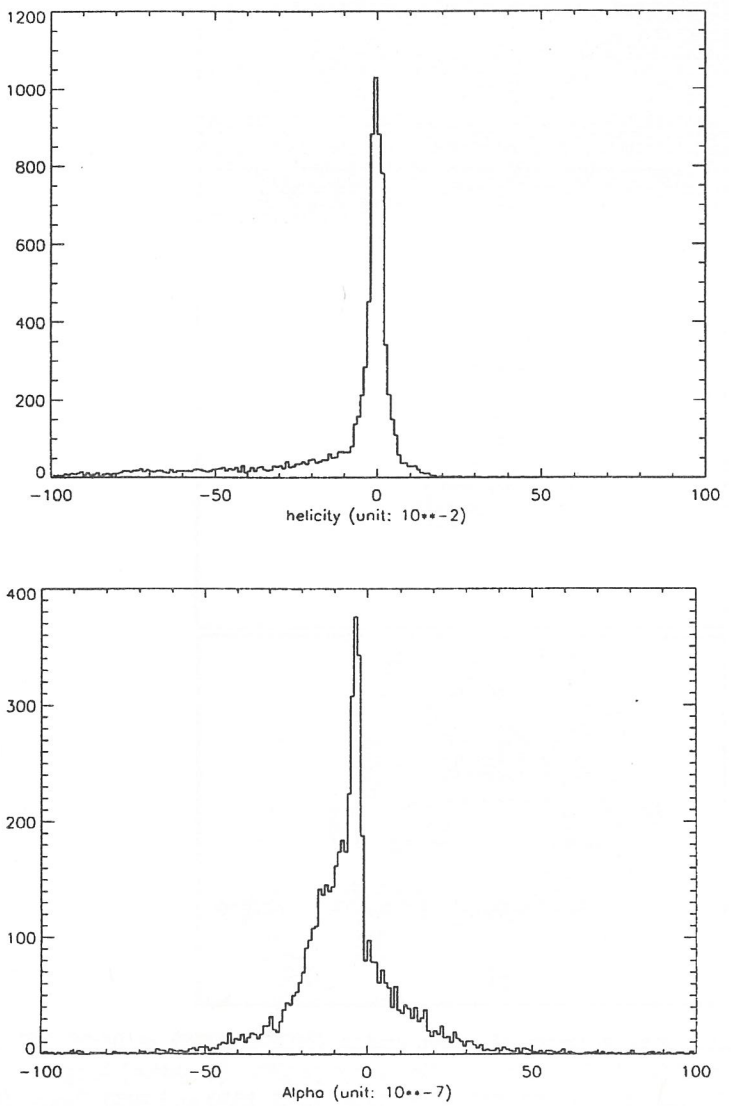

Figure 2. Histograms of current helicity parameters h_c (unit: $10^{-2}G^2M^{-1}$) and α (unit: $10^{-7}M^{-1}$) of the active region (NOAA 6659) at 05:29 UT on June 9, 1991.

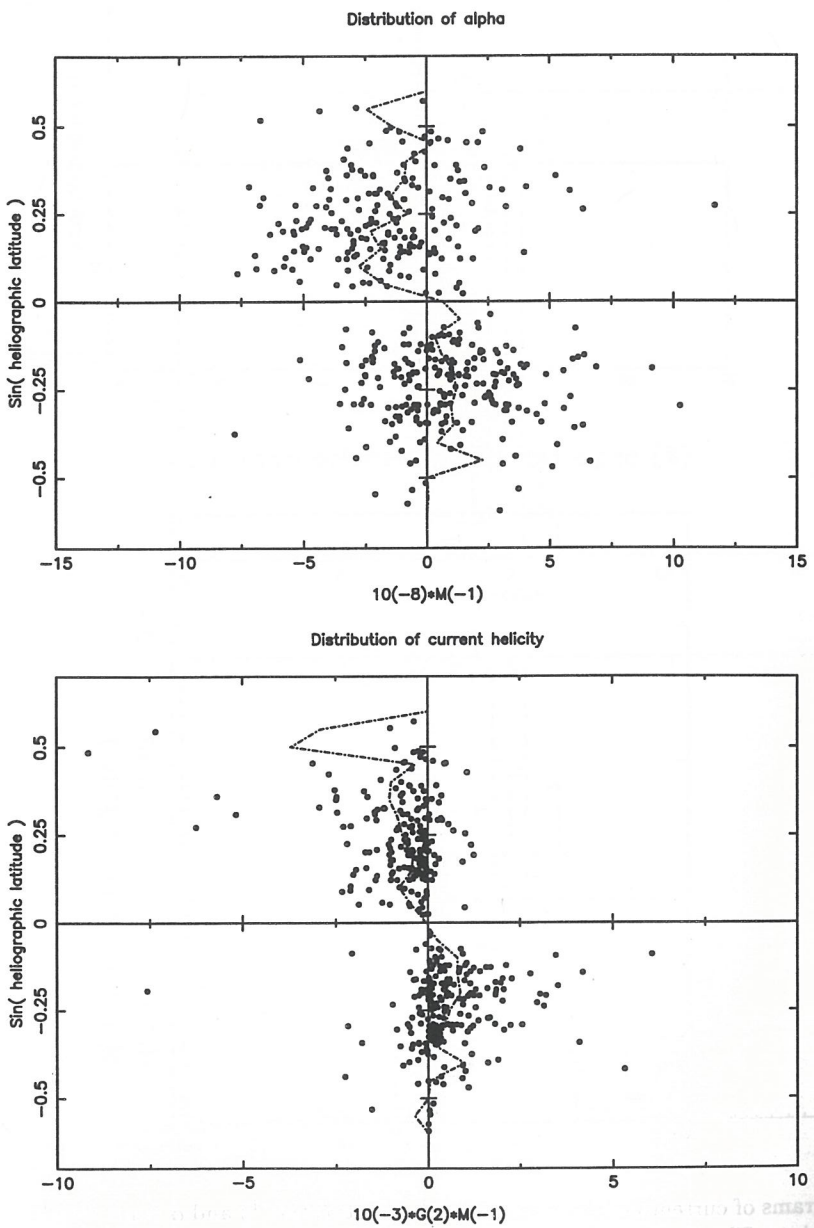

Figure 3. Latitudinal distribution of the mean current helicity and twist density parameters $\langle \alpha_f \rangle$ (a) and $\langle \mathbf{B}_{\|} \cdot (\nabla \times \mathbf{B})_{\|} \rangle$ (b) for 422 active regions. Each point represents a single active region. The dotted-dashed lines show the average values.

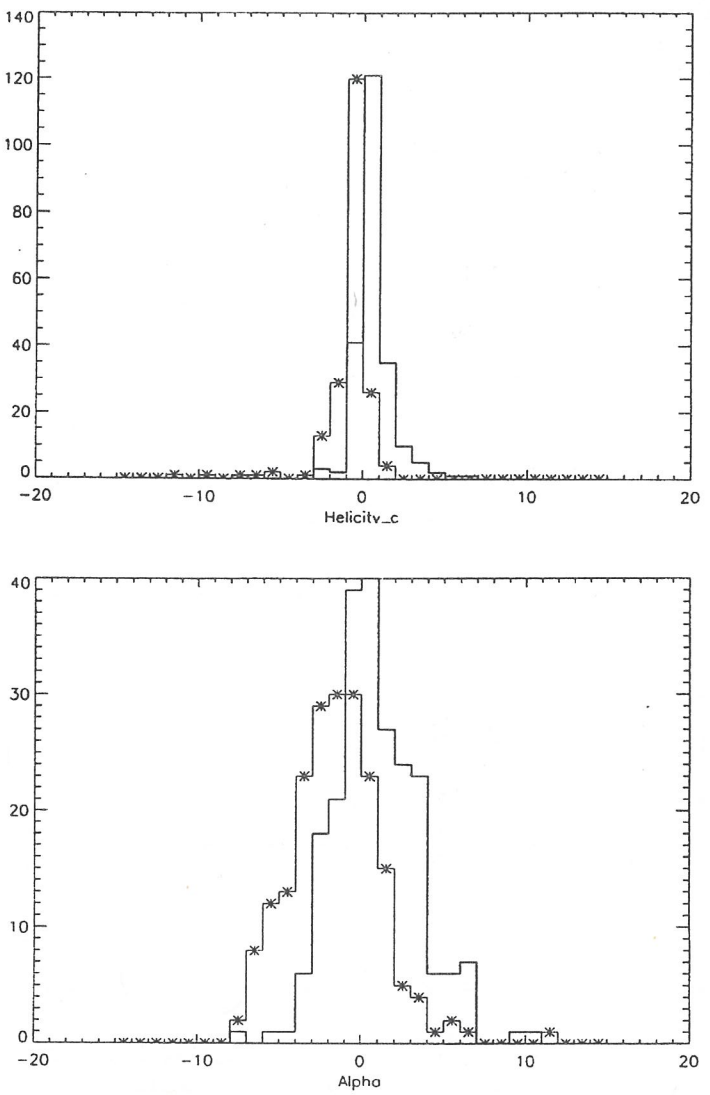

Figure 4. Histograms of current helicity parameters h_c (unit: G^2M^{-1}) and α (unit: M^{-1}) for 422 active regions. The histograms with (without) snowflakes show the current helicity parameters in the northern (southern) hemisphere.

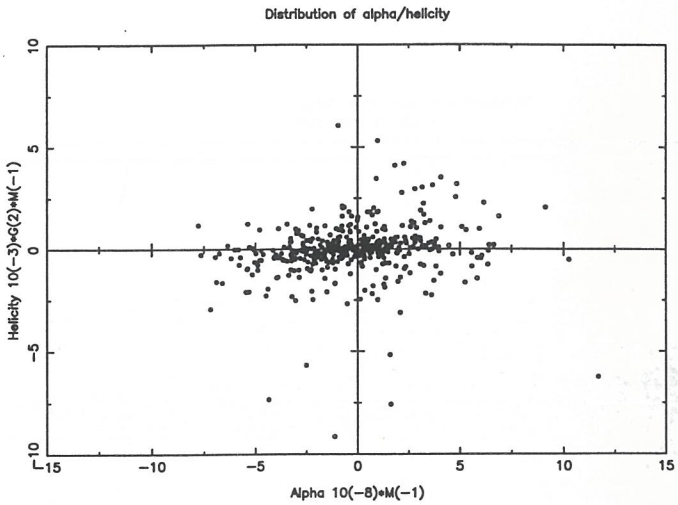

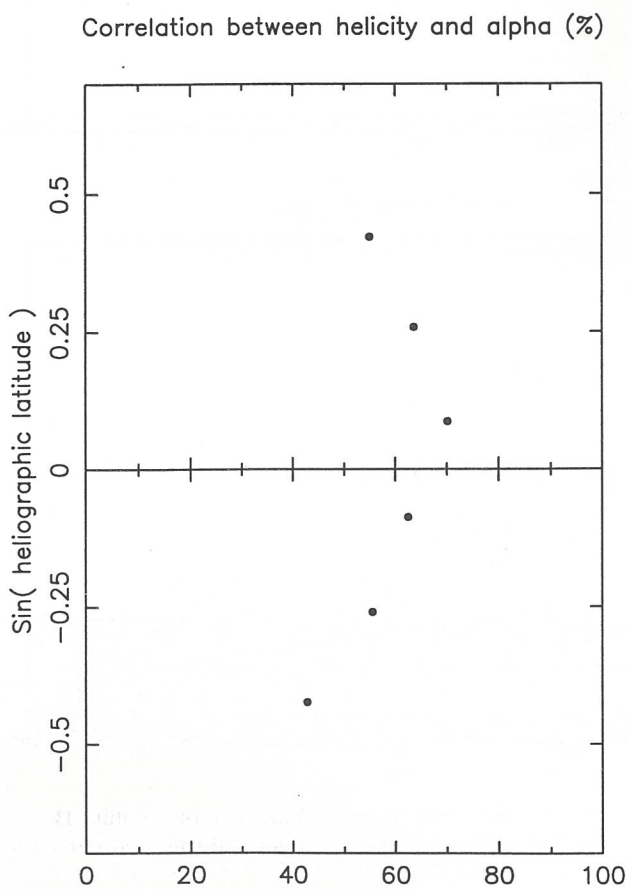

Figure 5. The relationship between the mean current helicity parameters α_f (alpha) and $\mathbf{B}_{\|} \cdot (\nabla \times \mathbf{B})_{\|}$ (helicity) for 422 active regions. (b) The correlation between current helicity parameters h_c and α over latitudes after averaging of the data.

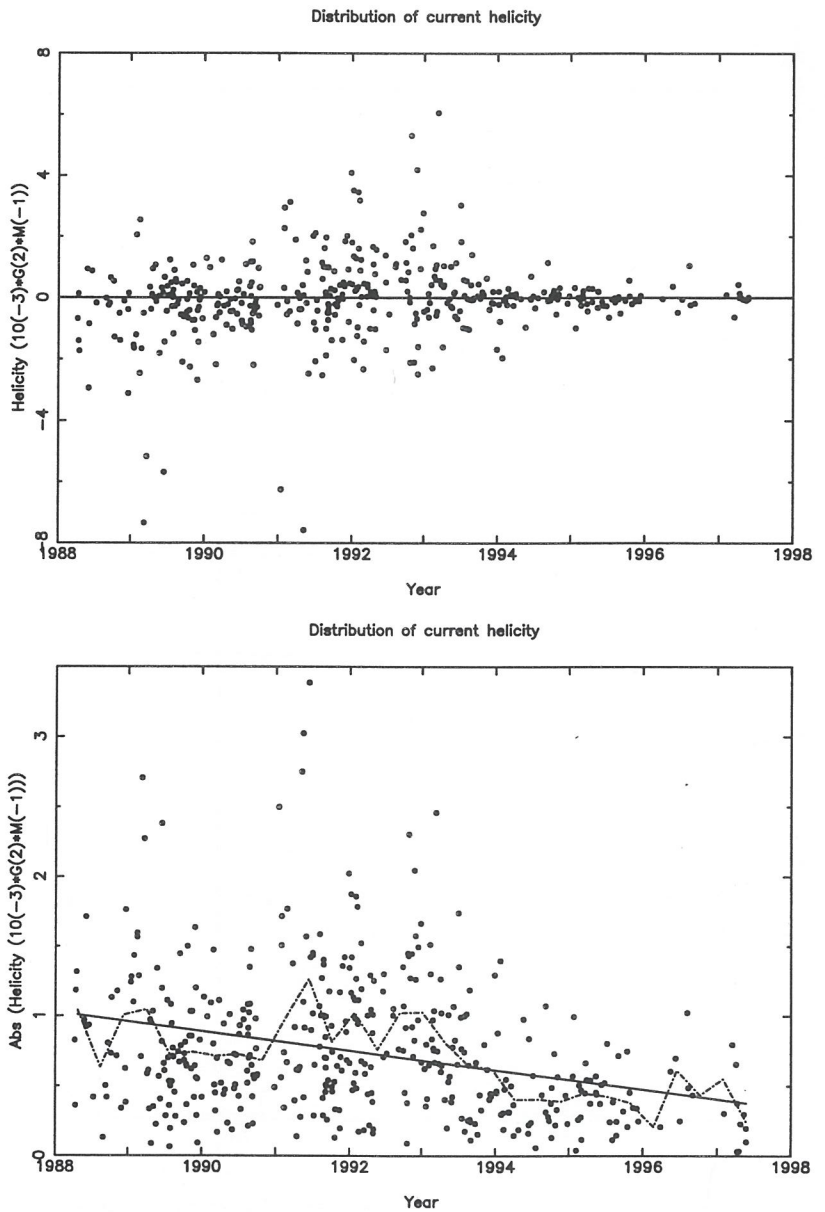

Figure 6. (a) Variation of $\mathbf{B}_{\|} \cdot (\nabla \times \mathbf{B})_{\|}$ with time. (b) Variation of absolute $\mathbf{B}_{\|} \cdot (\nabla \times \mathbf{B})_{\|}$ with time. The dotted-dashed lines show the average values and the solid line is the linear fit.

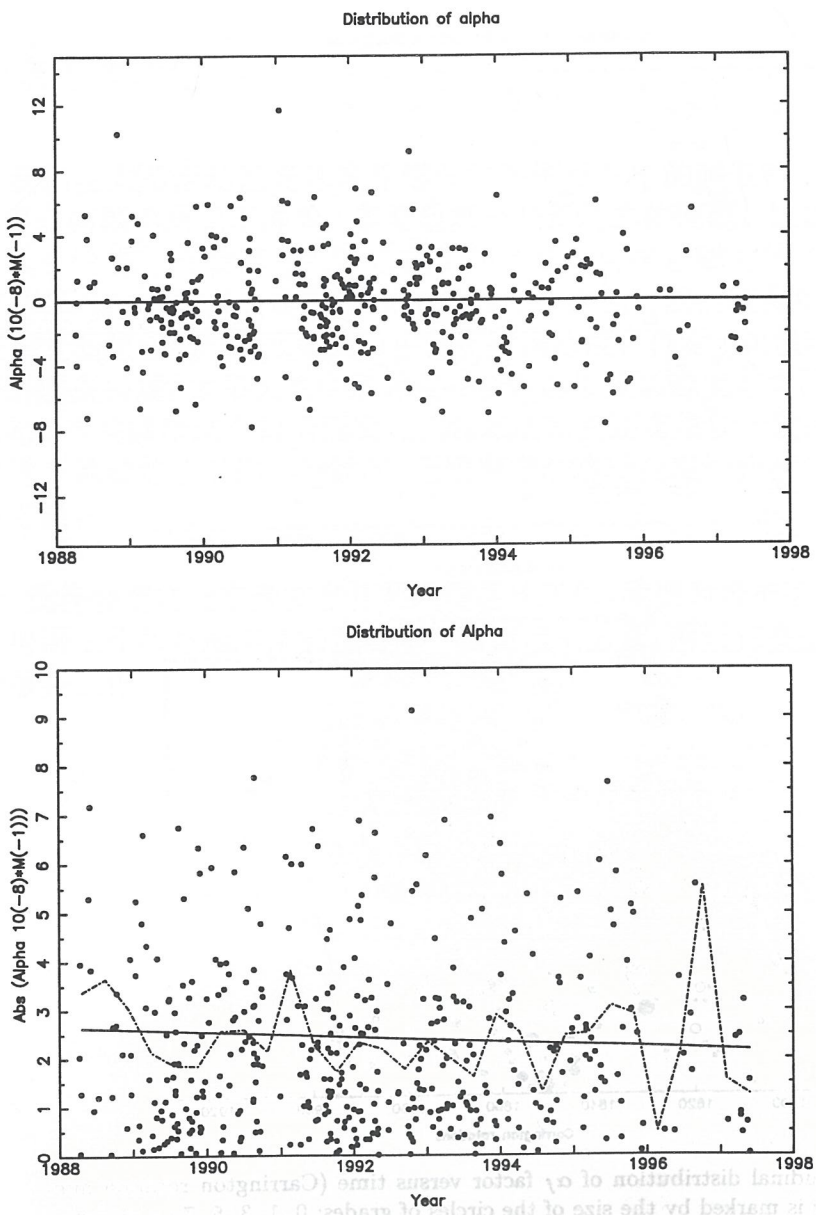

Figure 7. (a) Variation of α_f with time. (b) Variation of absolute α_f with time. The dotted-dashed lines show the average values and the solid line is the linear fit.

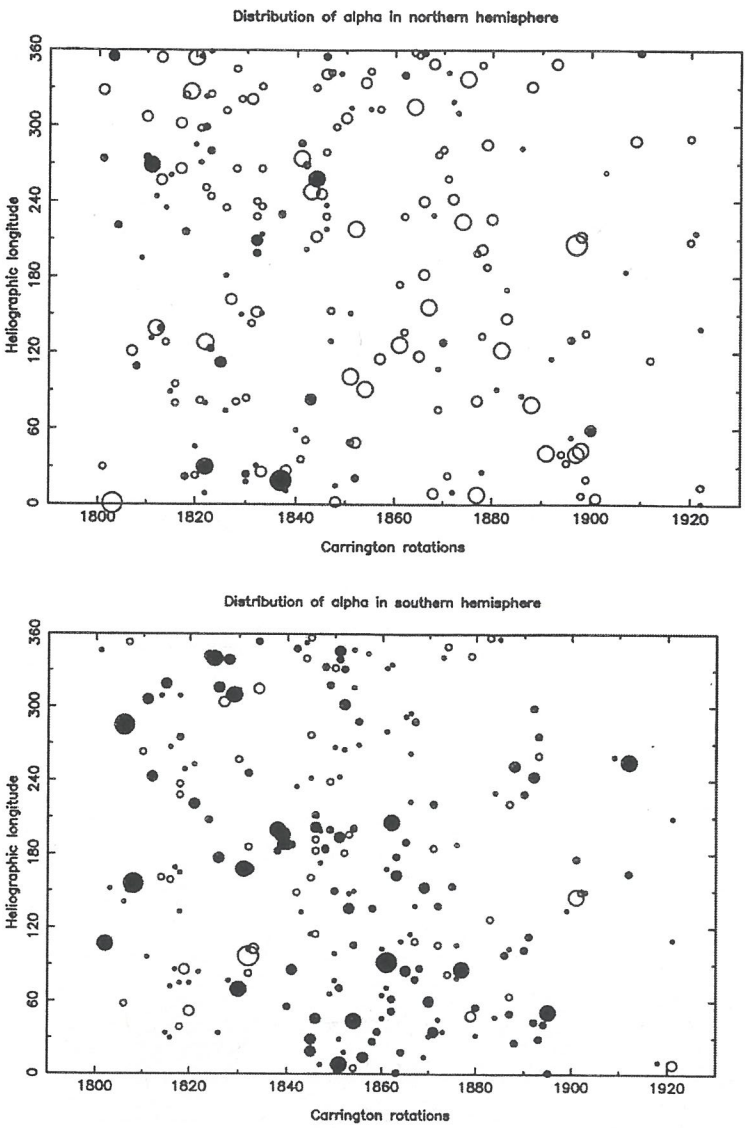

Figure 8. Longitudinal distribution of α_f factor versus time (Carrington rotation number). The density is marked by the size of the circles of grades: 0, 1, 3, 5, 7 ($\times 10^{-8} m^{-1}$) in the northern (a) and the southern (b) hemispheres. The black (white) circles denote positive (negative) sign.

第三篇　其 他

3.1 未来工作计划

总之，我们在太阳活动区光球电流螺度的观测研究中的确取得了一些有趣的结果，但很多问题仍然说不清楚，甚至包括一些最基本的问题。比如，磁螺度的起源是什么？它有什么物理意义？它在拓扑上是如何描述磁力线的空间结构？电流螺度的符号在太阳发电机的理论中扮演什么角色？我们获得的这种所谓观测螺度在多大程度上代表着太阳大气中的实际磁螺度？再者，如色球层、日冕和太阳风中的螺度问题，太阳大气中磁螺度守恒问题以及磁螺度与太阳活动周问题等等。因此，有关螺度这个前沿而又热门领域的研究还有很长一段路要走，我想我还会在这个领域继续工作一段时间，但研究方法将转向理论分析及三维空间的数值模拟方面。

出站后，我将会留在北京天文台怀柔观测基地工作。我要为维护基地的正常运转、基地的科研工作和基地未来的发展尽一份自己的力量；同时也要努力做好基地各方面的服务工作。

3.2 博士后期间参与的学术和社会活动

1. 1998.7.24—1998.8.5 去美国参加 the AGU Chapman Conference on Magnetic Helicity in Laboratory and Space Plasmas (获 800 美金的资助)，并提供一篇学术论文。
2. 1999.12.11—1999.12.24 去印度参加 the IAU Colloquim No.179 on Cyclical Evolution of Solar Magnetic Fields: Advances in Theory and Observations (获 1350 瑞士法朗的资助)，并被安排一个 15 分钟的口头报告，题目为“The Hemispheric Sign Rule of Current Helicity During the Rising Phase of Cycle 23”。
3. 参加第 23 周太阳活动峰年观测与研究选题学术会议（1998.10.9—1998.10.14 在青岛市举行）。
4. 参加第六届太阳磁场和速度场学术研讨会（1998.8.10—1998.8.17 在北京天文台怀柔基地和泰安市举行）。
5. 第七届太阳磁场和速度场学术研讨会（1999.8.10—1999.8.16 在北京天文台怀柔基地和大连市举行）的主要组织者，并负责出版这次会议的会议文集。
6. 首届国内太阳物理暑期讲习班（1999.7.26—1999.8.10 在北京天文台怀柔基地举行）的主要发起和组织者，本期开设的课程为《天体物理中的辐射机制》和《恒星大气理论与太阳光谱》。
7. 和张枚博士共同主持北京天文台怀柔观测基地两周一次的太阳物理讨论班。
8. 参加北京天文台怀柔基地的值班与常规观测。

3.3 近两年来发表文章的目录

3.3.1 在 SCI 杂志上

1. 题目：Patterns of Current Helicity for Solar Cycle 22
   作者：**Bao Shudong** and Zhang Hongqi
   刊物：1998, *Astrophys. J.* 496, L43.
2. 题目：A Survey of Flares and Current Helicity in Active Regions
   作者：**Bao Shudong**, Zhang Hongqi, Ai Guoxiang, and Zhang Mei
   刊物：1999, *Astron. Astrophys. Suppl. Ser.* 139, 311.
3. 题目：Helicity Computation Using the HSOS and MSO Data
   作者：**Bao Shudong**, Pevtsov Alexei, Wang Tongjiang, and Zhang Hongqi
   刊物：2000, *Solar Phys.*, in press.
4. 题目：Hemispheric Sign Rule of Current Helicity in Solar Cycle 23
   作者：**Bao Shudong**, Ai Guoxiang, and Zhang Hongqi
   刊物：2000, *J. Astrophys. Astr.*, submitted.
5. 题目：Latitudinal Distribution of Photospheric Current Helicity
   作者：Zhang Hongqi and **Bao Shudong**
   刊物：1998, *Astron. Astrophys.* 339, 880.
6. 题目：Longitudinal Distribution of Current Helicity and Solar Activities
   作者：Zhang Hongqi and **Bao Shudong**
   刊物：1999, *Astrophys. J.* 519, 876.
7. 题目：Probing Signatures of the Alpha-Effect in the Solar Convection Zone
   作者：Kuzanyan Kirill, **Bao Shudong**, and Zhang Hongqi
   刊物：2000, *Solar Phys.*, in press.
8. 题目：Twist of Magnetic Fields in Solar Active Regions
   作者：Zhang Hongqi, **Bao Shudong**, and Kuzanyan Kirill
   刊物：2000, *Solar Phys.*, submitted.
9. 题目：Relationship Between Tilt and Current Helicity in Active Regions
   作者：Tian Lirong, **Bao Shudong**, Zhang Hongqi, and Tong Yi
   刊物：2000, *Astron. Astrophys.*, accepted.

3.3.2 在其他杂志或会议文集上

1. 题目：Investigation of Helicity Signs in Active Regions During the Cycle 22
   作者：**Bao Shudong** and Zhang Hongqi
   刊物：1998, *JOSO Annual Report'97*, 132.
2. 题目：Recent Progress in Solar Magnetic Fields
   作者：**Bao Shudong** and Ai Guoxiang
   刊物：1998, *Publ. Beijing Astron. Obs.* Special Issue, 76.
3. 题目：A Comparison of Vector Magnetograms in the two Different Instruments
   作者：**Bao Shudong**, Wang Tongjiang, and Zhang Hongqi
   刊物：1999, *Publ. Beijing Astron. Obs.* 34, 8.
4. 题目：Averaging the Force-Free Coefficient in the Solar Photosphere
   作者：**Bao Shudong**, Kuzanyan Kirill, and Zhang Hongqi
   刊物：1999, in *Solar-Terrestrial Physics*, Proc. of 7th Symposium in Russia, 293.
5. 题目：太阳光球磁场的螺度
   作者：**包曙东** 张洪起
   刊物：1999, *紫金山天文台台刊*, vol.18，No. 2, 117.
6. 题目：A Comparison of Hemispheric Helicity Signs between the Cycle 22 and 23
   作者：**Bao Shudong**
   刊物：2000, *Publ. Beijing Astron. Obs.*, in press.
7. 题目：Studies of Intranetwork Elements and Current Helicity
   作者：Ai Guoxiang and **Bao Shudong**
   刊物：1998, *Publ. Beijing Astron. Obs.* Special Issue, 1.
8. 题目：Distribution of Photospheric Current Helicity
   作者：Zhang Hongqi and **Bao Shudong**
   刊物：1999, *Proceedings of Nobeyama Symposium*, in press.
9. 题目：Semi-biennial Variations of Helicity Parameters in the Solar Atmosphere
   作者：Kuzanyan Kirill, Zhang Hongqi, and **Bao Shudong**
   刊物：1999, *Astron. Zh.* [translated into English: *Astronomy Reports*], in press.
10. 题目：1997 年 3 月 9 日漠河日全食期间的太阳磁场观测
    作者：张洪起 张 枚 **包曙东** 等人
    刊物：1999，*《日全食与近地环境》*, 87.
11. 题目：太阳磁场研究的前沿与展望
    作者：刘煜 张洪起 **包曙东**
    刊物：2000，*河北师范大学学报*, in press.

3.4 致谢

在此研究工作报告即将完成之际，我首先要衷心地感谢北京天文台台长艾国祥院士所给予的工作指导和支持，这使得我在近两年的博士后学习和工作中各方面都有了长足的进步。

非常感谢北京天文台的张洪起研究员、李威研究员、邓元勇研究员、颜毅华研究员、王华宁研究员、王同江副研究员等在本课题的研究过程中给予的支持、帮助和指导，尤其指出的是张洪起研究员在课题选择方面给予了特别的关注和深入的讨论。感谢北京天文台怀柔观测基地的全体同仁在各方面的关心、帮助与合作。

我也要感谢北京师范大学天文系李宗伟教授和孙锦教授曾对我以前科研工作及其学术水平、科研工作能力等作出正确的评价，并积极推荐我来北京天文台做博士后研究工作。在博士后工作阶段，李老师仍给予我许多的关怀与鼓励。为此，我再次向他表示深深的谢意。感谢北京天文台人事处杜红荣女士在各方面的帮助。

感谢我的爱妻葛正红女士的所有理解与支持。感谢她分担大部分的家务和照料我们可爱的小女儿包宇。

感谢中国国家自然科学基金（19791090）的大力支持，可以说本报告中涉及到的所有工作都是在此基金支持下完成的。

谨以此文献给所有关心、爱护和帮助过我的师长、亲人、朋友和同事们！

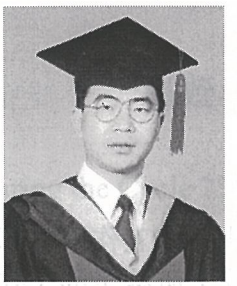

3.5 个人学习和工作经历

包曙东 男 1964年12月出生于安徽省肥东县，汉族。

1981.9－1985.7 在安徽省阜阳师范学院物理系学习，获理学学士学位。在阜阳师范学院物理系学习期间，成绩优秀，年年被评为三好学生。

1985.9－1988.7 在河北师范大学物理系攻读理论物理专业硕士研究生，硕士学位论文的题目为“特殊Ⅰ型超新星爆发的一种新的物理模型”，指导老师为葛蕴藻教授。

1988.7－1995.8 在河北师范大学物理系工作。其中1988.9－1989.7在河北省井陉县第一中学高中部教《物理》（边远地区支教计划）；1994.9－1995.6 在北京师范大学天文系做访问学者。自1989年9月起，主要讲授硕士研究生课程《高等量子力学》。此外，还曾讲授过或辅导过本科生课程《电动力学》、《线性代数》和《广义相对论简介》等。1991年3月被聘为讲师。

1995.9－1998.6 在北京师范大学天文系攻读博士学位，博士论文的题目为“太阳活动区光球电流螺度的观测研究”，指导老师为李宗伟教授和张洪起研究员。其中1996－1997年度被评为北京师范大学优秀博士研究生；1998年6月被评为北京师范大学优秀毕业博士生，且获得北京师范大学励耘奖学金三等奖。

1998.7－至今 在中国科学院北京天文台做博士后研究工作，指导老师为北京天文台台长艾国祥院士。1998.7.24－1998.8.5 去美国参加 the AGU Chapman Conference on Magnetic Helicity in Laboratory and Space Plasmas（获800美金的资助），并提供一篇学术论文。1999.12.11－1999.12.24 去印度参加 the IAU Colloquim No.179 on Cyclical Evolution of Solar Magnetic Fields: Advances in Theory and Observations（获1350瑞士法朗的资助），并被安排一个15分钟的口头报告，题目为杯“The Hemispheric Sign Rule of Current Helicity During the Rising Phase of Cycle 23”。2000年2月获一九九九年度“纪念成中杰奖”。

3.6 通讯地址

姓名： **包曙东**
工作单位：中国科学院北京天文台
地址：北京市朝阳区大屯路甲 20 号　　邮政编码：100012
电话：64888764（办公室） 64850171（住宅）
传真：64888716
电子邮件：bshd@sun10.bao.ac.cn
主页：http://www-hsos.bao.ac.cn/staff/bshd/bshd.html

Name：**Shudong Bao**
Institute：Beijing Astronomical Observatory, Chinese Academy of Sciences
Address：A20 Datun Road, Chaoyang District, Beijing 100012, China
Telephone：+86-10-64888764 (O);　+86-10-64850171 (H)
Fax：+86-10-64888716
E-mail：bshd@sun10.bao.ac.cn
Homepage：http://www-hsos.bao.ac.cn/staff/bshd/bshd.html

3.7 博士生研究工作已发表文章的全文

为了便于读者完整地了解我近年来在太阳磁场螺度方面所做的研究工作，这里附上三篇以前发表文章的全文。应该提及的是这些工作主要是在博士生期间在张洪起研究员指导下完成的。

THE ASTROPHYSICAL JOURNAL, 496:L43–L46, 1998 March 20

PATTERNS OF CURRENT HELICITY FOR SOLAR CYCLE 22

SHUDONG BAO[1,2] AND HONGQI ZHANG[1]

Received 1997 August 4; accepted 1998 January 15; published 1998 March 6

ABSTRACT

Using a 1988–1997 data set of original photospheric vector magnetograms from the Solar Magnetic Field Telescope (SMFT) of the Huairou Solar Observing Station of Beijing Astronomical Observatory, we computed the local current helicity $B_z \cdot (\nabla \times \boldsymbol{B})_z$ for 422 active regions. We found that any given active region contained mixed signs of current helicity, but in most cases current helicity with a particular sign was dominant over a whole region area. In our data set, 84% of the active regions in the northern hemisphere have negative helicity, and 81% in the southern hemisphere have positive helicity. It is estimated that the noise and error in our calculation are at the 2 σ level.

In addition, we have studied the evolution of the large-scale surface current helicity during the cycle 22, which is a running mean of absolute current helicity of the active regions observed over a Carrington rotation period. By comparing with monthly mean sunspot number, we found that the average current helicity has a good correlation with solar activity.

Subject headings: Sun: activity — Sun: magnetic fields — Sun: photosphere

1. INTRODUCTION

In surveys of magnetic activity on the solar surface, vortex, magnetic, and current helicities have played an important role. With $\boldsymbol{V}$, $\boldsymbol{A}$, and $\boldsymbol{B}$ denoting fluid velocity, magnetic vector potential, and magnetic induction, the densities (per unit volume) of vortex, magnetic, and current helicity are defined by

$$H_v = \boldsymbol{V} \cdot (\nabla \times \boldsymbol{V}),$$
$$H_m = \boldsymbol{A} \cdot (\nabla \times \boldsymbol{A}),$$
$$H_c = \boldsymbol{B} \cdot (\nabla \times \boldsymbol{B}). \quad (1)$$

Topologically, they are a measure of the structural complexity of the corresponding fields (Berger & Field 1984). For instance, if the magnetic field consists of an ensemble of flux tubes, then H_m determines the number of linkages of the magnetic field lines, and the total magnetic helicity (volume-integrated) contains contributions from the internal structures of the tubes, such as twisting, and from the external intertwining of the tubes.

It is also interesting to study the solar dynamo from the viewpoint of helicity. Over the last two decades, two representative models of solar dynamo have been developed (De Luca & Gilman 1991). The kinematic mean-field dynamo theory in the bulk of the convection zone argues that the helicity should be negative in the northern hemisphere and positive in the southern. To accomplish the migration of toroidal and poloidal field patterns toward the equator requires that the radial differential rotation rate increase significantly with depth in the convection zone, namely, $\partial\omega/\partial r < 0$ (ω is the angular velocity of the solar rotation, and r is the radial variable of the Sun). On the contrary, the global convection theory, in which the dynamo operates in the thin overshoot region at the base of the convection zone, predicts the opposite sign of helicity in the two hemispheres compared with the bulk of the zone above so that the magnetic field migrations should be toward the equator in low latitudes, and toward the poles in higher latitudes, and correspondingly, $\partial\omega/\partial r > 0$. Though the analysis of the global oscillations of the Sun provides information on the internal rotation, a clear decision from observations whether the angular velocity increases or decreases with depth is presently not possible. Therefore, attention should be given to other observations related to helicity on the solar surface.

Seehafer (1990) studied signs of current helicity of active regions by comparing a variety of images with magnetograms extrapolated assuming constant-α force-free field. For all but two of the 16 active regions, he found negative helicity in the northern hemisphere and positive in the southern. Martin et al. (Martin, Marquette, & Bilimoria 1992; Martin, Bilimoria, & Tracada 1993) found that the vortex structures of 72 quiescent filaments tended to have an opposite sense across the equator, but the 80 filaments in active regions did not. In a study of the helicity of 16 interplanetary magnetic clouds associated with filament eruptions and solar flares, Rust (1994) found that 13 showed helicity whose sign agreed with Seehafer. Adopting the linear force-free field parameter α taken as the ratio between the vertical current and the vertical magnetic field, Pevtsov, Canfield, & Metcalf (1995) studied the local helicity of 69 active regions and obtained the result that 75% of active regions in the northern hemisphere have negative helicity, and 69% in the southern hemisphere have positive helicity. Abramenko, Wang, & Yurchishin (1996) calculated current helicity $B_z \cdot (\nabla \times \boldsymbol{B})_z$ of 40 active regions and found that in 82% of cases the helicity in the northern (southern) hemisphere was negative (positive). However, the results are not conclusive.

Observations are needed to establish firmly the conclusion that the sign of the helicity is dependent on hemisphere. This is the main motivation for our work.

2. OBSERVATIONS AND DATA REDUCTION

We have chosen to study 422 active regions observed from 1988 to 1997, spanning about a sunspot cycle. All vector magnetic field data included in our study were acquired with favorable weather and seeing conditions during the time in which active regions were located near the central meridian. The projection effects of high-latitude active regions were removed according to the formulae given by Gary & Hagyard (1990). Although the number of 422 active regions is much less than

[1] Beijing Astronomical Observatory, Chinese Academy of Sciences, Beijing 100080, China.
[2] Department of Astronomy, Beijing Normal University, Beijing 100875, China; bshd@sun10.bao.ac.cn, zhq@sun10.bao.ac.cn.

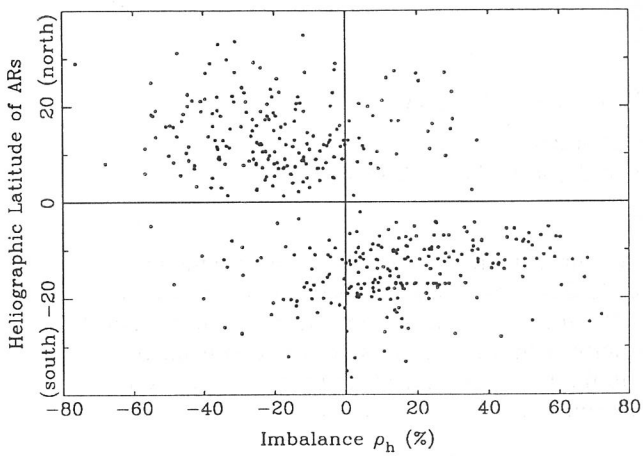

FIG. 1.—Distribution of the imbalance ρ_h of current helicity over an active region area against heliographic latitude for 422 active regions. Each dot represents an active region.

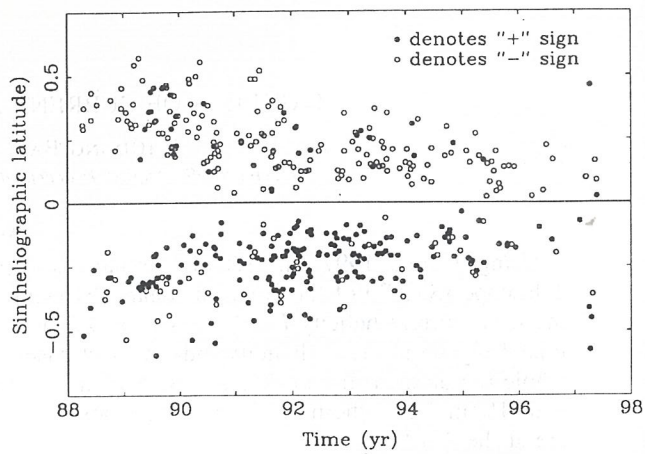

FIG. 2.—Two-dimensional distribution (time and latitude) of the sign of current helicity in the two hemispheres during the cycle 22. There are 199 active regions in the northern hemisphere, and 31 of them have positive helicity. There are 223 active regions in the southern, and 46 of them are negative.

the sum of all active regions in the cycle 22, our study still reflects some important information on current helicity because our data contain the large active regions during the period.

The vector magnetic fields in the photosphere were obtained on the basis of measurements of four Stokes parameters *I*, *Q*, *U*, and *V*. The longitudinal component of magnetic field (parameter *V*) was measured at 0.075 Å from the line center of Fe I λ5324.19, and the transverse components (*Q* and *U*) were measured at the line center. The field of view of the SMFT is about 4′ × 6′. The pixel resolution on the CCD is about 0″.4 × 0″.7. The spatial resolution of our data is actually 2″ × 2″ after a smoothing average of 3 × 4 pixels to the Stokes parameters *Q*, *U*, and *V*. The magnetic field calibration and more details have been described by Wang et al. (1996) and Zhang et al. (1994).

The direct calculation of magnetic helicity has been hindered by the fact that the magnetic vector potential $\boldsymbol{A}$ is not measured, but practical observations of current helicity may be characterized by the force-free field parameter α (Pevtsov et al. 1995) or the measure $B_z \cdot (\nabla \times \boldsymbol{B})_z$ (Abramenko et al. 1996). We chose to calculate the latter. The measure may also be written as

$$h_c = \mu_0 B_z J_z, \tag{2}$$

where $\mu_0 = 4\pi \times 10^{-3}$ G m A^{-1}, and the vertical current density J_z can be expressed by

$$J_z = \frac{1}{\mu_0}\left(\frac{\partial B_y}{\partial x} - \frac{\partial B_x}{\partial y}\right). \tag{3}$$

We resolved the 180° ambiguity of the transverse field and computed J_z using the techniques described by Wang, Xu, & Zhang (1994) (see also Abramenko et al. 1996).

It is important to understand the influence of noise in these data. The noise level in the original magnetograms is usually less than 20 G for the longitudinal field and about 100 G for the transverse field. The noise level of J_z in our calculations was about 0.001 A m^{-2}. To minimize the influence of noise, we calculated the current helicity $h_c(i, j)$ only for pixels for which $B_z > 20$ G, $B_{\rm trans} > 100$ G, and $J_z > 0.001$ A m^{-2}. Eventually, we determined an average of current helicity for each active region, and it showed a sign difference at the 2 σ level in the opposite hemispheres.

3. PATTERNS OF CURRENT HELICITY

3.1. *Distribution of Current Helicity Sign*

In our calculation, the average current helicity of per active region always contained a mixture of positive and negative helicity. To reveal whether there exists a predominant sign, we calculated the quantity ρ_h defined by

$$\rho_h = \frac{\sum h_c(i, j)}{\sum |h_c(i, j)|} 100\%, \tag{4}$$

where $\sum$ represents the sum for a whole active region. The quantity ρ_h is called the imbalance of current helicity over an active region (Abramenko et al. 1996).

The distribution of the imbalance ρ_h of 422 active regions is shown in Figure 1. It can be seen that in most cases the absolute values of ρ_h are much more than zero. In other words, a significant excess of current helicity of a certain sign within an active region is indeed an universal phenomenon. We found that 84% of active regions in the northern hemisphere have negative helicity (the points located in the second quadrant), and 81% in the southern hemisphere have positive helicity (the fourth quadrant); the active regions located in the first and third quadrants break the sign rule, and their values of ρ_h are comparatively smaller. We think that the presence of these active regions (less than 20%) is not entirely due to systematic and random errors, and the true cause remains to be studied.

Figure 2 shows the two-dimensional (time and latitude) distribution of signs of current helicity. From this pattern, we may more clearly see that the sign of helicity is dependent on hemisphere. Again, the "reversed-sign" regions do not show any particular tendency to form at high or low latitude or at any particular time. The diagram contains more information than the butterfly diagram of sunspot.

Hale (1927) found that active regions in each hemisphere retain the same sense of vorticity from one cycle to the next. The observations related to current helicity now span three solar cycles (20–22). Some observations (Seehafer 1990; Pevtsov et

al. 1995) corroborate this result on the hemispheric preference for a fixed sign of the helicity independent of solar cycle (see also review of Low 1996). Similarly, at the beginning of cycle 23 the current helicities of several active regions were calculated, and we found that the helicity signs in the new cycle do not break the above sign rule (see Fig. 2).

3.2. *Evolution of Average Current Helicity*

Solar activity is usually associated with an 11 yr sunspot cycle and other surface phenomena, such as the variations in the flare count, the total magnetic flux, the strength of Ca II emission, the 10 cm radio flux, and even the evolution of the large-scale fields patterns. Each of these quantities exhibits a slightly different pattern of variation, and the investigation of the various time series can provide insights into the nature of the solar cyclic activity. Considering that the strong twisted magnetic fields and large-flare activity normally occur in the years around sunspot maximum, and their relationship to the current helicity, the evolution of the large-scale surface current helicity in active regions offers the possibility of a new indicator of activity.

This large-scale evolutionary pattern of average current helicity during cycle 22 is shown in Figure 3, where 1 σ error bars are indicated for our calculation of the average of absolute values of current helicity of the active regions observed during a complete Carrington rotation. The resolution of the plot is one Carrington rotation. For comparison, we also give the variation of monthly mean sunspot number in the cycle (Fig. 3, *dotted line*). The figure shows a high correlation between them, such as the general trend of variation and two peaks during the first half of this cycle. A slightly different pattern of variation, however, can be seen in Figure 3: the maximum of the average current helicity occurs in late 1991, almost 2 yr following sunspot maximum in 1989 June. Again, the values of average current helicity in 1990 are much less than expected. Although only 422 active regions were selected during the period 1988–1997 and some uncertainties exist in our approach, we believe that the basic result can not be changed.

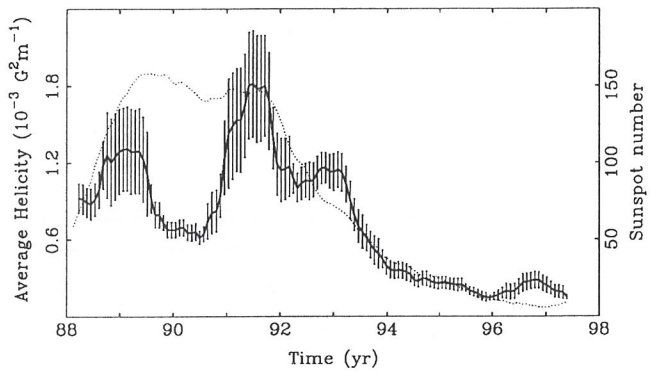

FIG. 3.—Solid curve represents the evolution of the large-scale surface current helicity in active regions for Carrington rotations 1801–1922. The monthly mean sunspot number during the cycle 22 provided by SGD is also shown (*dotted line*). Note the similarities and differences between two curves.

4. CONCLUSIONS

On the basis of vector magnetic field measurements we calculated the current helicity $B_z \cdot (\nabla \times B)_z$ in the photosphere for 422 active regions and obtained the following results:

1. 84% of active regions in the northern hemisphere have negative helicity, and 81% in the southern hemisphere have positive helicity. The point is consistent with other observations. It provides favorable evidence for the kinematic α-ω dynamo theory in the bulk of the convection zone. Hence, this result excludes the possibility that the helicities on the solar surface contain contributions from the large-scale shearing motions in the photosphere due to the differential rotation of the Sun and from the interface dynamo operating in the thin overshoot region at the base of the convection zone, since they both generate positive helicity in the northern and negative helicity in the southern hemisphere. They do not play a leading role in contributing to the surface current helicity of the Sun.

2. Each active region contains a mixed sign of current helicity, but in most cases the so-called imbalance ρ_h of current helicity over a whole region is extreme; namely, most active regions show a predominant sign. This indicates that a predominant twisting (left-handed or right-handed) of magnetic flux tubes in an active region may be general. In other words, there occurs a predominant twisting of magnetic structures not only for unipolar spots with obvious vortex structure (Richardson 1941) but also for active regions of different types.

3. We found that the evolution of the surface current helicity in active regions has a good correlation with monthly mean sunspot number during the cycle 22. The trend of their variations with time is consistent, and they all show two peaks around 1990. This indicates that the current helicities of active regions on the solar surface also reach the maximum near sunspot maximum, as do other activities (such as the flare counts and the total magnetic flux). We think that their differences (see § 3.2) are probably caused by two quantities involved in the current helicity, the longitudinal component B_z of magnetic field and the vertical electric current J_z. When the longitudinal magnetic field is strong over a given area, the vertical electric current of this area need not be big simultaneously. Therefore, we suggest that the current helicity may be a better indication of the magnetic nonpotentiality of solar active regions. To uncover the relation between current helicity and the magnetic activities (the magnetic energy storage, transport and release), we must study the current helicity on a small scale with high temporal resolution.

The author (S. D. B.) is most grateful to Professors Guoxiang Ai, Zongwei Li, and Jingxiu Wang for their instruction and encouragement. We are indebted to Professor Wei Li, Tongjiang Wang, and Huaning Wang for their helpful discussions. Finally, we also wish to thank the referee for some valuable suggestions. This work is supported by National Nature Science Foundation of China under grant 19791090 and Doctoral Foundation of Chinese Educational Committee under grant 9502716.

REFERENCES

Abramenko, V. I., Wang, T. J., & Yurchishin, V. B. 1996, Solar Phys., 168, 75
Berger, M. A., & Field, G. B. 1984, J. Fluid Mech., 147, 133
De Luca, E. E., & Gilman, P. A. 1991, in Solar Interior and Atmosphere, ed. A. N. Cox, W. C. Livingston, & M. S. Matthews (Tucson: Univ. Arizona Press), 275
Gary, G. A., & Hagyard, M. J. 1990, Solar Phys., 126, 21
Hale, G. E. 1927, Nature, 119, 708
Low, B. C. 1996, Solar Phys., 167, 217
Martin, S. F., Bilimoria, R., & Tracada, P. W. 1993, BAAS, 25(3), 1217
Martin, S. F., Marquette, W. H., & Bilimoria, R. 1992, in ASP Conf. Ser. 27, The Solar Cycle, ed. K. L. Harvey (San Francisco: ASP), 53
Pevtsov, A. A., Canfield, R. C., & Metcalf, T. R. 1995, ApJ, 440, L109
Richardson, R. S. 1941, ApJ, 93, 24
Rust, D. M. 1994, Geophys. Res. Lett., 21, 241
Seehafer, N. 1990, Solar Phys., 125, 219
Wang, J. X., Shi, Z. X., Wang, H. N., & Lü, Y. P. 1996, ApJ, 456, 861
Wang, T. J., Xu, A. A., & Zhang, H. Q. 1994, Solar Phys., 155, 99
Zhang, H. Q., Ai, G. X., Yan, X., Li, W., & Liu, Y. 1994, ApJ, 423, 828

THE ASTROPHYSICAL JOURNAL, 519:876–883, 1999, July 10

DISTRIBUTION OF PHOTOSPHERIC ELECTRIC CURRENT HELICITY AND SOLAR ACTIVITIES

HONGQI ZHANG[1] AND SHUDONG BAO[1,2]
Received 1998 April 6; accepted 1998 May 19

ABSTRACT

In this paper, we describe the distribution of photospheric current helicity of active regions in the solar surface. The sign of helicity is mainly negative in the northern hemisphere of the Sun and positive in the southern hemisphere. We also discuss the relationship between the current helicity parameter $B_{\|} \cdot (\nabla \times B)_{\|}$ and the α-factor of the force-free field. Our observations show that active regions with current helicity signs opposite to most others in the same hemispheres occur normally at some heliographic longitudes and persist over long periods.In addition, we analyze a possible mechanism of the sign rule of current helicity that shows opposite signs in both hemispheres.

Subject headings: MHD — Sun: activity — Sun: magnetic fields — Sun: photosphere

1. INTRODUCTION

Our observations demonstrate that strong magnetic fields in the solar atmosphere are normally concentrated in the active regions. This provides information on magnetic helicity in the solar atmosphere that has been transported from the solar interior. Solar dynamo theories have been around for a long time. The two major factors in cyclic dynamo models (Parker 1955) are differential rotation, which generates toroidal magnetic fields from poloidal magnetic fields, and the helicity of convective motion, which generates poloidal fields from toroidal fields. Helioseismic data have shown that the Sun's deep interior may rotate much more rapidly than the surface (Goode, Frohlich, & Toutain 1992). It is generally believed that magnetic fields are generated by a dynamo operating at or beneath the bottom of the convection zone and that magnetic flux rises through the convection zone to the solar surface and forms active regions. Photospheric vector magnetograms of active regions provide such information only for the solar surface. The magnetic helicity of active regions can provide information on twisted magnetic lines of force in the subatmosphere. Several previous investigations have implied that there is a transequatorial change in the sign of magnetic helicity in the photosphere (Seehafer 1990; Pevtsov, Canfield, & Metcalf 1995; Abramenko, Wang, & Yurchishin 1996). The distribution of current helicity in solar cycle 22 was preliminarily demonstrated by Bao & Zhang (1998), who have calculated 422 active regions in last 10 years and have provided a "butterfly diagram" of the electric current helicity of active regions.

In this paper, we present some properties of the magnetic helicity of active regions. In § 2, we discuss the relationship between different observational parameters of magnetic helicity, such as the current helicity parameter $B_{\|} \cdot (\nabla \times B)_{\|}$ and the α-factor of the force-free field. In § 3, we discuss the longitudinal distribution of current helicity. In § 4, we discuss our results.

2. THE RELATIONSHIP BETWEEN DIFFERENT PARAMETERS OF THE ELECTRIC CURRENT HELICITY

The linkage of the magnetic field can be represented in several ways using magnetic helicity (Moffatt 1978; Berger & Field 1984). The electric current helicity can be written in the form

$$H_c = \boldsymbol{B} \cdot \nabla \times \boldsymbol{B} = \boldsymbol{B}_{\perp} \cdot (\nabla \times \boldsymbol{B})_{\perp} + \boldsymbol{B}_{\|} \cdot (\nabla \times \boldsymbol{B})_{\|} . \quad (1)$$

The second term in equation (1) is observable and can be inferred by the photospheric vector magnetogram (Abramenko et al. 1996). In the approximation of the force-free magnetic field, the electric current helicity can also be written as

$$H_c = \alpha B^2 = (B/B_{\|})^2 \boldsymbol{B}_{\|} \cdot (\nabla \times \boldsymbol{B})_{\|} , \quad (2)$$

and we set $\boldsymbol{B} = B\boldsymbol{b}$, where $\boldsymbol{b}$ is the unit vector along the magnetic field, then

$$\alpha = \boldsymbol{b} \cdot \nabla \times \boldsymbol{b} . \quad (3)$$

This means that α is a factor reflecting the twist of the unit force lines along themselves. We can find that the α-factor is the helicity of the unit magnetic field. The α-factor was introduced by Pevtsov et al. (1995) to define magnetic helicity. In the case of strong magnetic fields in active regions, the approximation of the force-free field is normally correct.

Figure 1 shows the distribution of the current helicity parameter $B_{\|} \cdot (\nabla \times B)_{\|}$ and the α-factor of the force-free field in active region NOAA 6659. The 180° ambiguity of the transverse component of the field is normally resolved by the approach of the potential field, and the continuity of the transverse field sometimes is used in the vicinity of highly sheared magnetically neutral lines. We find that the α-factor shows the same sign distribution in the active region as does the observational parameter $B_{\|} \cdot (\nabla \times B)_{\|}$ of current helicity and that the difference between the current helicity and α-factor can be found easily. The maximum values of the current helicity parameter $B_{\|} \cdot (\nabla \times B)_{\|}$ normally occur near the peaks of the longitudinal magnetic field, but those of the α-factor occur near the magnetically neutral lines of the active regions, where the photospheric transverse magnetic field shears significantly. Analyzing the helical properties of the whole active region, we conclude that these two parameters probably contain different means. The highly sheared transverse magnetic field normally connects with newly emerging magnetic flux near the magnetically neutral line in the solar active regions and also probably provides information about the interaction of magnetic main poles of opposite polarities near their interface in the photosphere. The twist of the transverse magnetic component of the field near high-intensity areas of the longitudinal field mainly reflects a property of the whole

[1] Beijing Astronomical Observatory, Chinese Academy of Sciences, Beijing 100080, China.
[2] Department of Astronomy, Beijing Normal University, Beijing 100875, China.

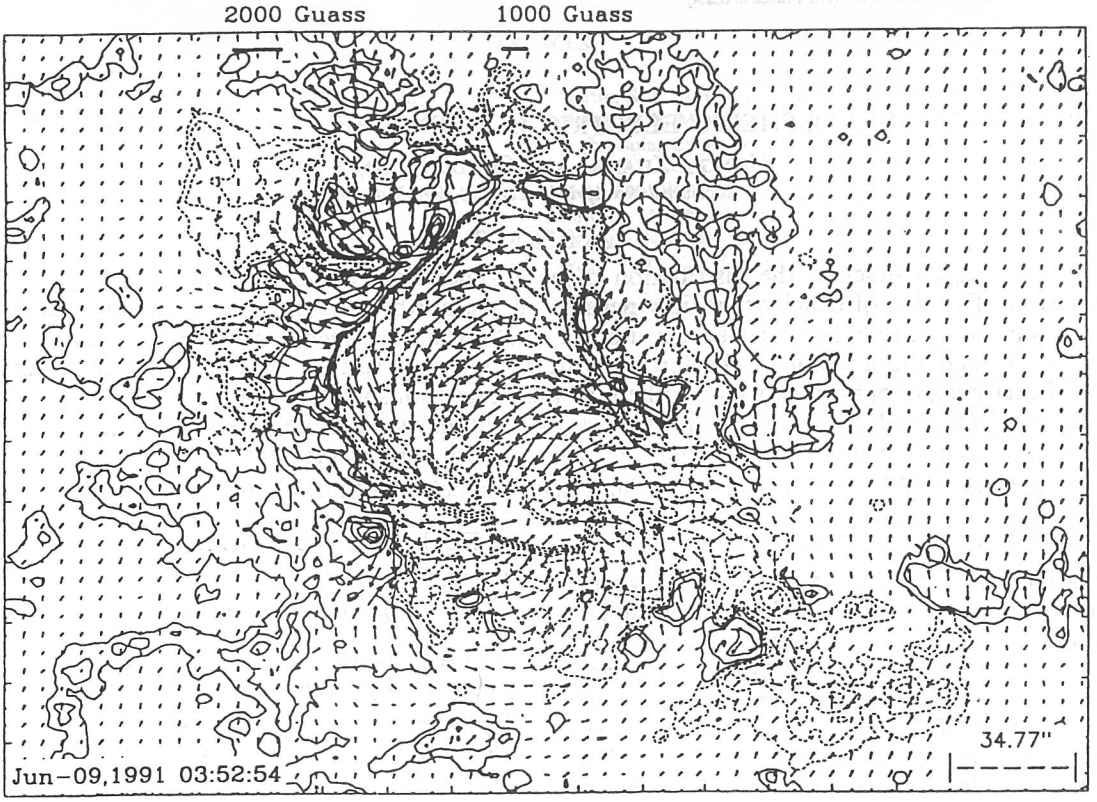

FIG. 1*a*

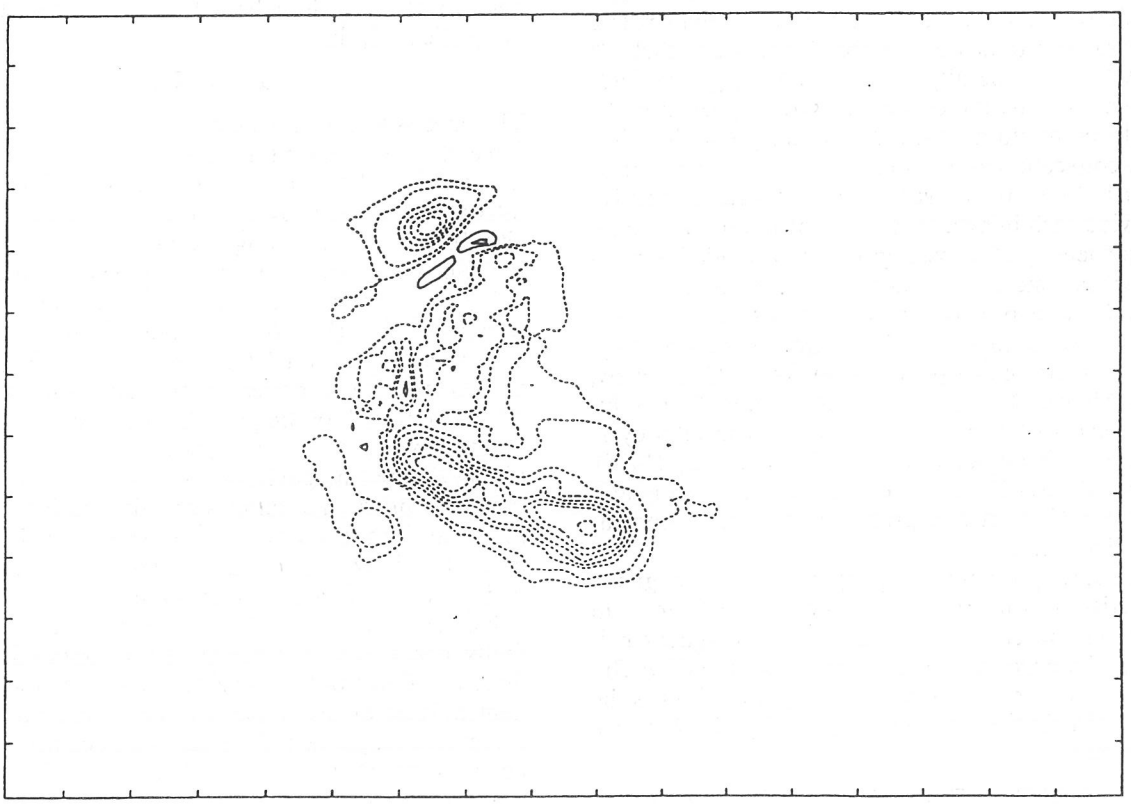

FIG. 1*b*

FIG. 1.— (*a*) Vector magnetogram of active region NOAA 6659 on 1991 June 9. The solid (dashed) contours indicate the positive (negative) longitudinal magnetic field distribution of ±20, 160, 640, 1280, 1920, 2240, 2560, and 2880 G. (*b*) Electric current helicity parameter $\boldsymbol{B}_{\parallel} \cdot (\nabla \times \boldsymbol{B})_{\parallel}$. The solid (dashed) contours indicate the positive (negative) regions of the current helicity distribution of $(\pm 0.25, 0.5, 1.0, 1.25, 1.5, 1.75, 2.0, 2.5) \times 10^{-1}\ \mathrm{G^2\ m^{-1}}$. (*c*) α-factor of the force-free field in areas where the longitudinal field is larger than 100 G. Solid (dashed) contours indicate the positive (negative) α factor distribution of $(\pm 0.5, 1.0, 2, 2.5, 3.0, 3.5, 4.0, 5.0) \times 10^{-7}\ \mathrm{m^{-1}}$. North is at the top and east is at the left.

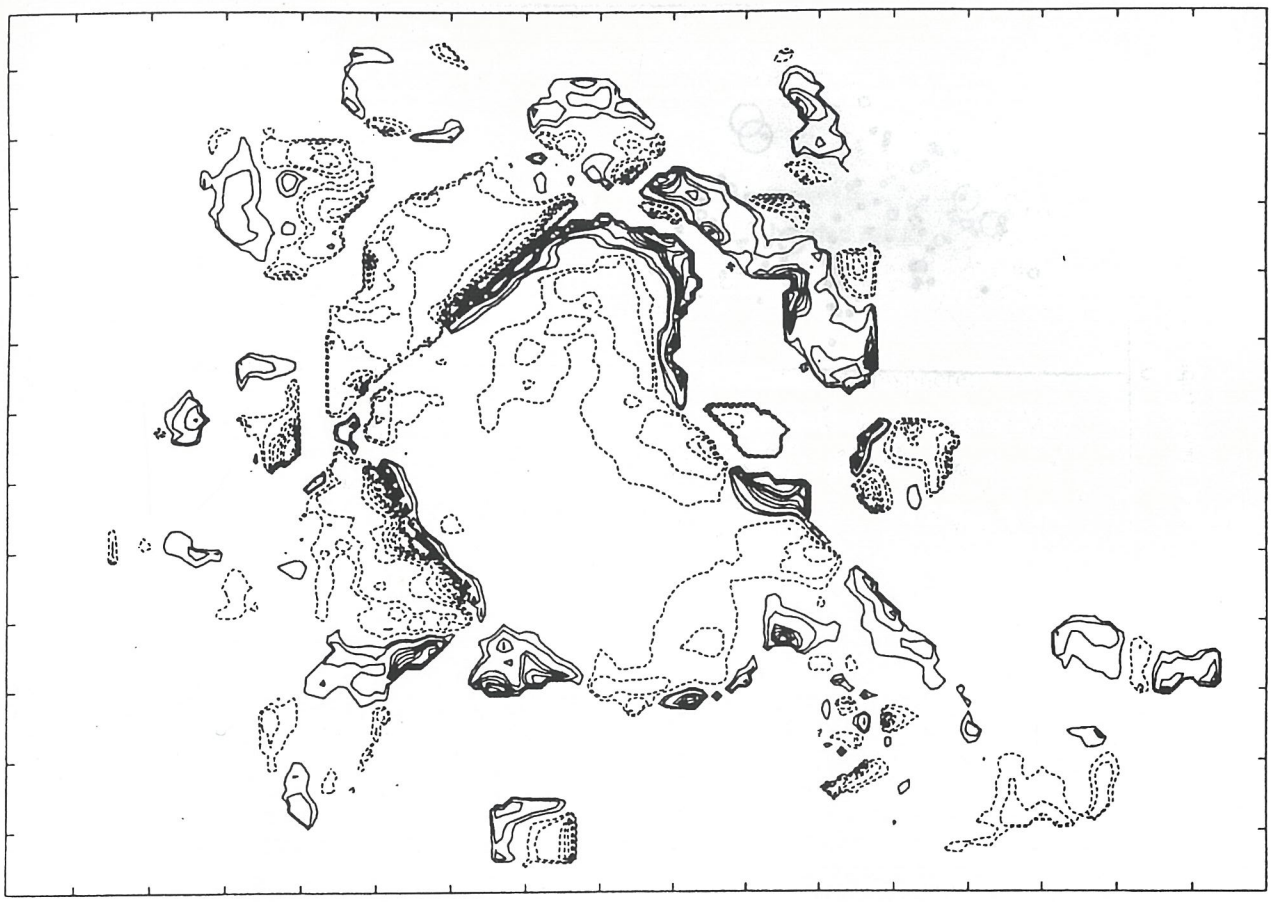

FIG. 1*c*

active region. This difference should cause the signs of the average values of two such parameters of the current helicity in some complex active regions to be opposite.

Figure 2 shows the latitudinal distribution of the mean current helicity parameter $\boldsymbol{B}_{\|} \cdot (\nabla \times \boldsymbol{B})_{\|}$ and the mean α-factor over time. Included are 422 large solar active regions that were selected from magnetograms obtained over the last 10 years. The magnetograms are used to calculate the parameters of current helicity of solar active regions located near the center of the solar disk. We notice that these are normally large active regions. This provides information on the solar activity cycle by means of current helicity. The sign rule is the following: a negative sign of current helicity normally occurs in the northern hemisphere and a positive one in the southern hemisphere. This was found by Seehafer (1990) and means that the twist of magnetic lines of force shows a global property, even if some reversed- sign (to the sign rule) regions occur in both hemispheres. Possible twists of the magnetic field lines in both hemispheres are shown in Figure 3. In Figure 2, we find that the two helicity parameters show different distributions of relative intensity. This means that some small-mean helicity regions probably have large values of α-factor. We also find that the reversed-sign regions of mean current helicity $\boldsymbol{B}_{\|} \cdot (\nabla \times \boldsymbol{B})_{\|}$ to the normal ones, following the sign rule, is less than 20% in both hemispheres, while that of the α-factor is about 30%. The value for the α-factor is consistent with the results obtained by Pevtsov et al. (1995). From the above discussion, we can find that the character of transequatorial change in the sign of the mean current helicity parameter $\boldsymbol{B}_{\|} \cdot (\nabla \times \boldsymbol{B})_{\|}$ of active regions is more obvious than the mean α-factor of the force-free field.

3. LONGITUDINAL VARIATION OF ELECTRIC CURRENT HELICITY

The longitudinal distribution of active regions and solar flares has been studied for a long time. It provides information on the solar activities and on the internal magnetic field in the solar subatmosphere. A subsequent problem is the longitudinal distribution of current helicity of active regions.

Figure 4 shows the longitudinal distribution of the electric current helicity parameter $\boldsymbol{B}_{\|} \cdot (\nabla \times \boldsymbol{B})_{\|}$ of active regions in both hemispheres with solar rotation cycles over about the last 10 years. (The latitudinal distribution of the current helicity parameters of these active regions was shown in Fig. 2.) Carefully analyzing the distribution of the electric current helicity, we find that in solar active regions longitudinal distribution tends to be uniform (even if the intensity is not distributed uniformly). However, the reversed helicity active regions show a tendency that occurs in some specific longitudes, such as the A, B, C regions in the northern hemisphere and the E, F, G, H regions in the southern hemisphere. In these longitudes, the reversed magnetic helicity of such active regions, which are dispersed over the solar surface, discontinuously keep long periods of time (20–40 solar rotation cycles, or about 1.5–3 years). This provides information on the generation of reversed current helicity in the subatmosphere brought up by emerging magnetic flux. We also notice that the existence of solar-active

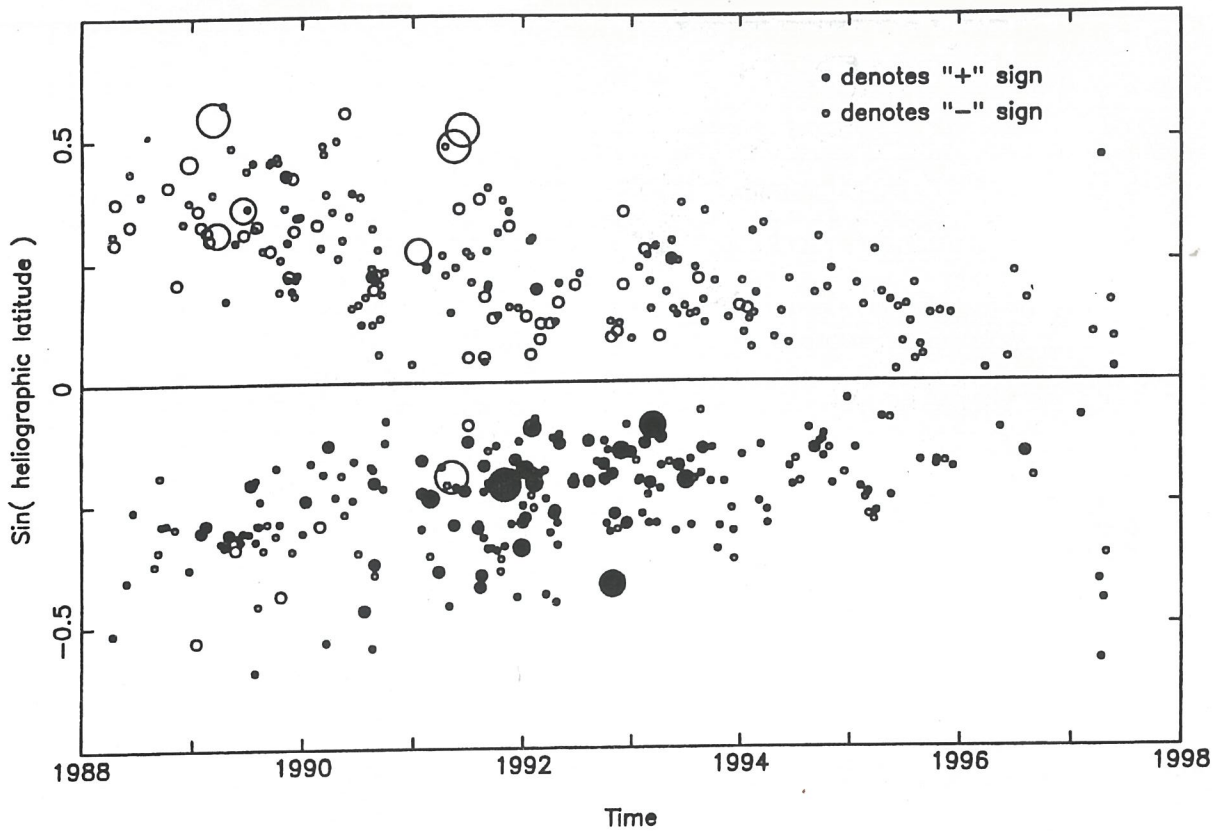

FIG. 2*a*

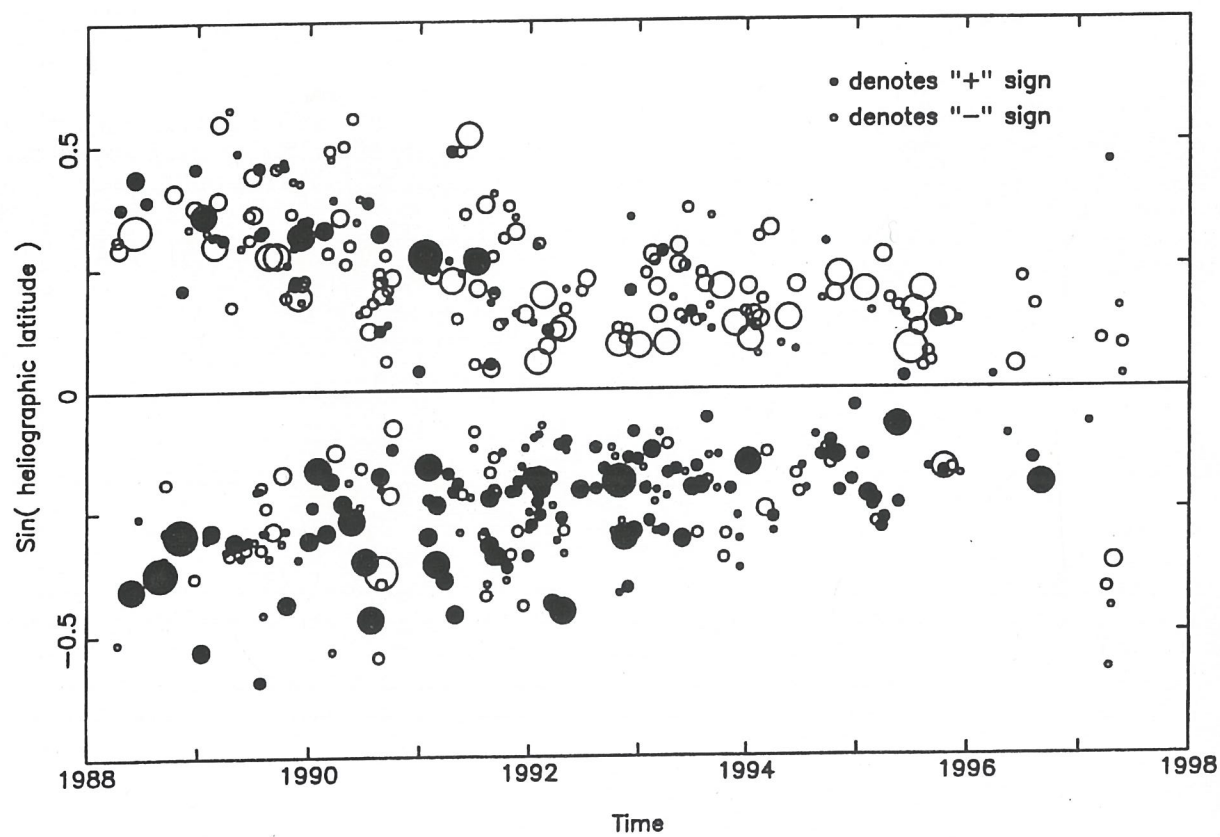

FIG. 2*b*

FIG. 2.—Butterfly diagram of the electric current helicity. (*a*) The mean density of the current helicity parameter $B_{\parallel} \cdot (\nabla \times B)_{\parallel}$ of active regions is marked by the size of the circles for grades: $(0, 1, 3, 5, 7) \times 10^{-3}$ G^2 m^{-1}. (*b*) Mean α-factor of the force-free field of active regions is marked by the size of the circles for grades: $(0, 1, 3, 5, 7) \times 10^{-8}$ m^{-1}.

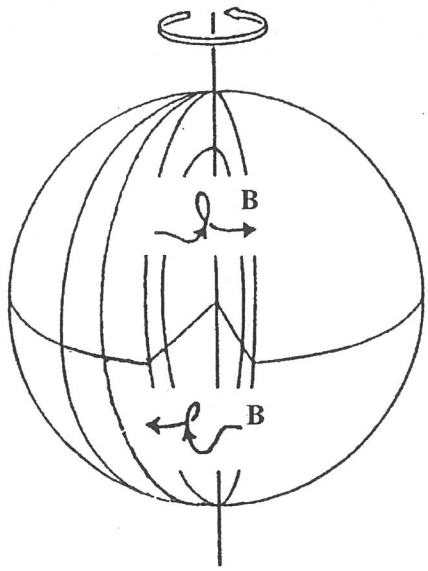

FIG. 3.—Possible schematic representation of helical twisting of magnetic field lines in convection zones

longitudes was proposed many years ago (Warwick 1965). These intense solar-active phenomena are normally related to some large (long-lived) active regions that have strong current helicity. If we analyze the distribution of current helicity with the heliographic longitudes, we conclude that there is no evidence of a statistical relationship between the distributions of the reversed helicity and the intensity of current helicity. This means that the "solar active longitudes" do not have an immediate relationship with the distribution of reversed helicity.

Figure 5 shows an example of a reversed current helicity region in the southern hemisphere. We show a vector magnetogram and corresponding maps of the electric current and current helicity parameter $\boldsymbol{B}_{\parallel} \cdot (\nabla \times \boldsymbol{B})_{\parallel}$ of a sunspot region (NOAA 5698) on 1989 September 24 and those for the same region at the next solar rotation cycle (active region NOAA 5747) on 1989 October 21. The 180° ambiguity of the transverse component of the field is normally resolved by the approach of the potential field. Analyzing the vector magnetic field, we find that a magnetic shear formed in the southern side of the magnetic main pole (N_1) of positive polarity in the active region on 1989 September 24 and that the configuration of the magnetic field changed on 1989 October 21. The magnetic shear occurred with the emergence of a magnetic flux on the northern side of the magnetic pole (N_1') of positive polarity (Wang, Xu, & Zhang 1994). Even if we cannot follow the long-term evolution of this sunspot group and detail the relationship between active regions NOAA 5698 and 5747, we notice that the transverse magnetic field twisted around the magnetic pole of the positive polarity clockwise. The electric current helicity of this sunspot group has had a negative sign for a long time, despite our sign rule of global helicity.

4. DISCUSSION AND RESULTS

It is known that the photospheric current helicity $\boldsymbol{B}_{\parallel} \cdot (\nabla \times \boldsymbol{B})_{\parallel}$ of solar active regions can be inferred by photospheric vector magnetograms, which connect the local shear or twist of the transverse magnetic field and the intensity of the longitudinal field. A similar parameter is the α-factor, introduced in the framework of force-free field theory. The difference between these helicity parameters has been discussed above, although it may not be important for analyzing the normal global properties of the twisted magnetic field in active regions.

The problem is how current helicity, which in active regions most often follows the transequatorial change in sign, is generated. Several possible models of the generation of the electric current helicity have been proposed:

1. Electric current helicity is generated by the Coriolis force, because, as helioseismological measurements have shown, much more rapid differential rotation occurs in the base of the convection zone. The radial contribution to the kinetic helicity is mainly the result of rotation and density stratification. The Coriolis forces resulting from the expansion of rising fluid cause it to twist as it rises, producing negative (positive) helicity in the northern (southern) hemisphere (Glatzmaier 1985).
2. The current helicity is caused by the subphotospheric differential rotation in the convection zone. This process is part of a larger scenario in which helicity emerges into the solar atmosphere as a twisted magnetic field and appears as coronal mass ejections and magnetic clouds (Rust & Kumar 1994).

It is generally believed that Joy's law of sunspot bipoles is caused by twisting of the magnetic bipole as it emerges, as was proposed by D'Silva (1991). If the magnetic field is generated near the base of the convection zone, the contribution of the Coriolis force to emerging magnetic flux tubes is that it twists the flux bipoles in each hemisphere in the opposite direction and the current tends to flow along the toroidal direction. Thus the current helicity has a positive (negative) sign in the northern (southern) hemisphere (Gilman 1983; Glatzmaier 1985). This is the opposite of the observational sign rule of the current helicity parameter

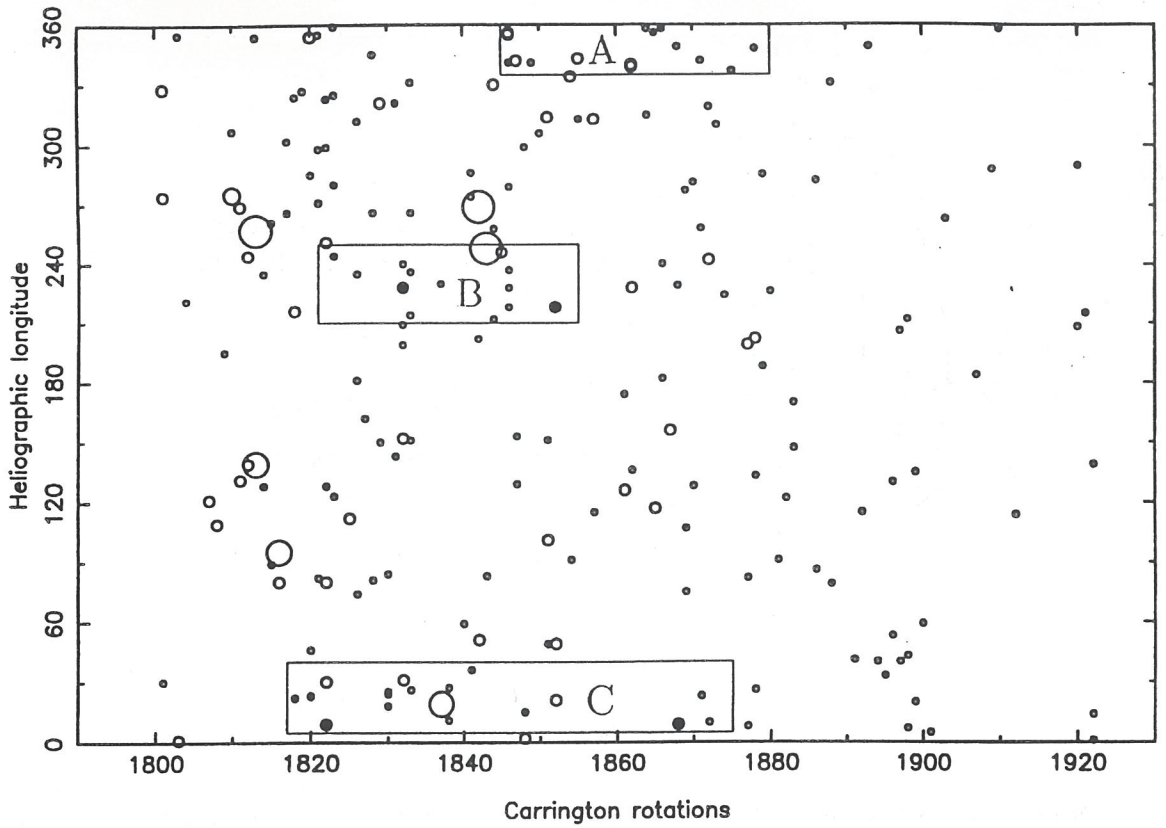

FIG. 4*a*

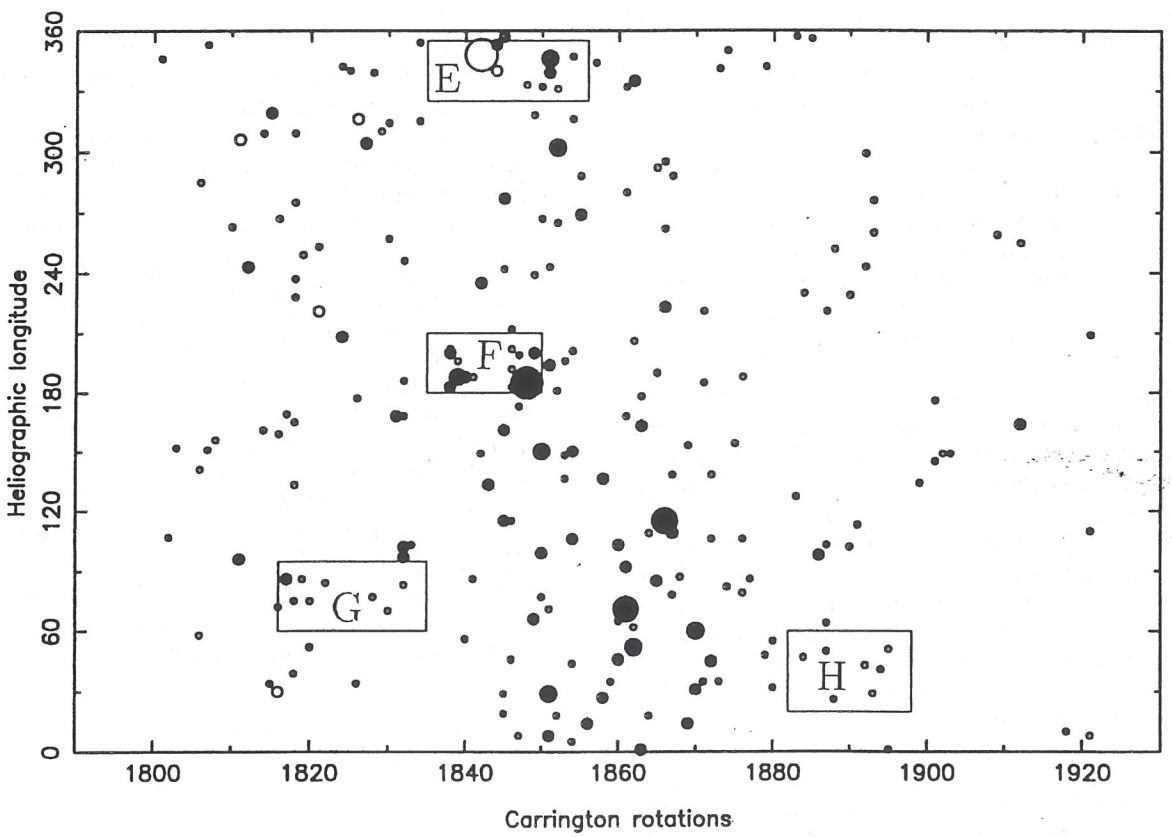

FIG. 4*b*

FIG. 4.—Distribution of the mean density of the current helicity parameter $B_{\parallel} \cdot (\nabla \times B)_{\parallel}$ of active regions with solar rotation cycles, which is marked by size of the circles for grades: (0, 1, 3, 5, 7) $\times 10^{-3}$ G^2 m^{-1}). Signs of current helicities are the same as Fig. 2. (*a*) Mean density of current helicity in the northern hemisphere. (*b*) Mean density of current helicity in the southern hemisphere.

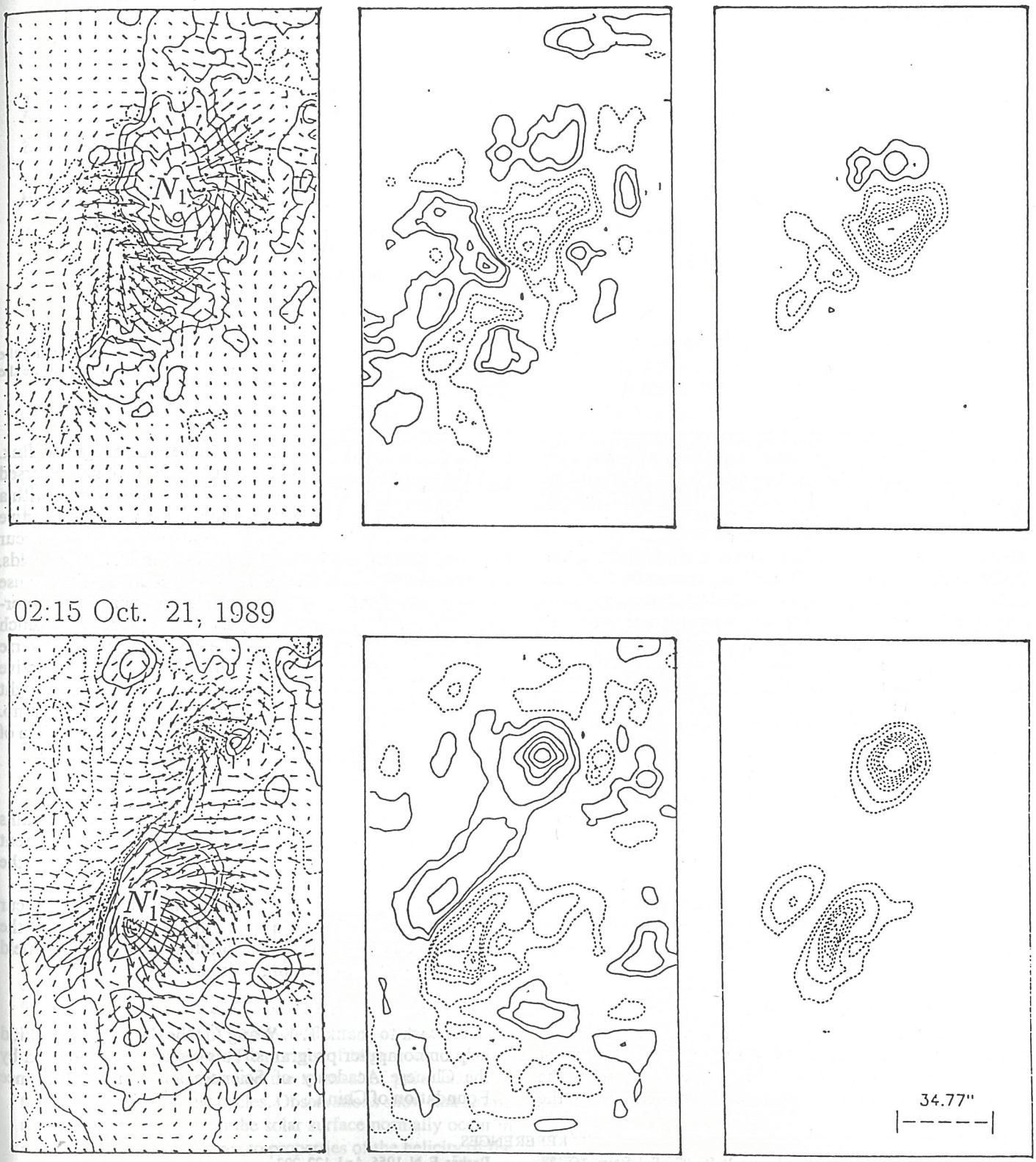

FIG. 5.—Vector magnetograms of active region NOAA 5689 (*top left*) and active region NOAA 5747. The solid (dashed) contours indicate the positive (negative) longitudinal magnetic field distribution of ± 20, 160, 640, 1280, 1920, 2240, 2560, and 2880 G. The corresponding vertical electric current is (± 0.2, 0.4, 0.8, 1.0, 1.2, 1.4, 1.6, 2.0) $\times 10^{-2}$ A m^{-2} (*middle*). Solid (dashed) contours indicate the upward (downward) flowing regions of the vertical current. Electric current helicity parameter $B_\parallel \cdot (\nabla \times B)_\parallel$ (*right*). Solid (dashed) contours indicate the positive (negative) regions of the current helicity distribution of (± 0.25, 0.5, 1.0, 1.25, 1.5, 1.75, 2.0, 2.5) $\times 10^{-1}$ G^2 m^{-1}.

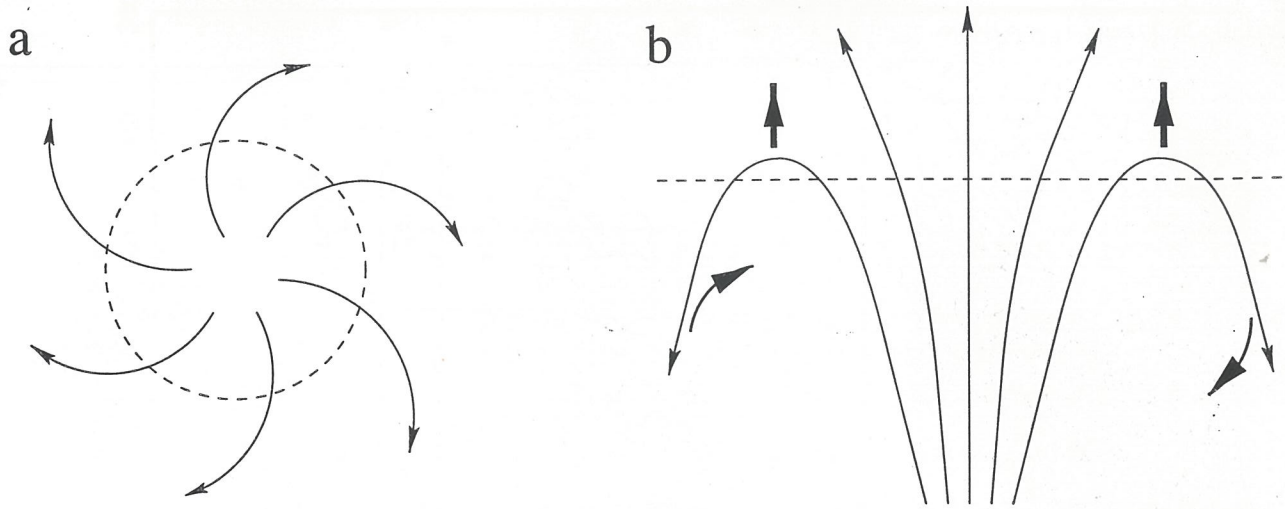

FIG. 6.—Possible model of current helicity near the solar surface in the northern hemisphere. (*a*) Transverse magnetic field twists clockwise around the magnetic main pole in the northern hemisphere viewed from the top. (*b*) Configuration of the magnetic field viewed from the side. Thick arrows indicate the direction of the magnetic lines of force.

$B_{\parallel} \cdot (\nabla \times B)_{\parallel}$ in the photosphere (Seehafer 1990). These results demonstrate that the shear of the photospheric transverse magnetic field (the local vertical electric current) in active regions is connected to the arrangement of newly emerging magnetic flux relative to the preexisting magnetic field (Zhang 1995). This means that small-scale magnetic features (bipoles) contribute to the observational current helicity as they emerge, i.e., that Coriolis forces cause the magnetic flux to tilt away from the magnetic main pole in a radial direction and to show a sign current opposite to that inferred by Gilman (1983) and Glatzmaier (1985) in the line-of-sight direction. The transverse magnetic field twists to the left (right) hand in the northern (southern) hemisphere. The configuration of the magnetic field is shown in Figure 6. Moreover, Evershed flow and the outward motion of magnetic features in the vicinity of sunspots (Wang et al. 1989; Zhang et al. 1992) are also probably important to the formation of current helicity under the action of Coriolis forces (Seehafer 1990). From the above discussion, one understands that the observational current helicity of active regions in the direction of the line of sight reflects a local property of the photosphere; this can probably provide information about the magnetic helicity normally defined in solar dynamo theories.

Another problem is how the reversed signs of current helicity of active regions in the same hemispheres are generated, because these reversed current helicity regions tend to occur at particular longitudes. This means that in these regions of the Sun, the Coriolis force probably does not dominate the magnetic flux twist as it emerges from the bottom of the convection zone and it is not caused by the random twisting process of the emerging magnetic flux. Analyzing the active regions with observational reversed current helicity, we find that they are often associated with a complex distribution of magnetic fields, as in the active region NOAA 5698 (or 5747). These regions tend to occur often in preexisting large-scale background magnetic fields. Thus, there are two mechanisms that could possibly cause the observational reversed helicity. The first is the interaction of emerging and preexisting magnetic flux, which deforms the arrangement of the photospheric transverse field in the vicinity of the emerging magnetic flux in active regions. The second is that the reversed helicity is brought up from the deep atmosphere caused by the solar dynamo. In either case, we find that accounting for the distribution of the observational helicity is a complex problem.

The main results of our analysis follow:

1. Mean $B_{\parallel} \cdot (\nabla \times B)_{\parallel}$ of the active region contains information from mean α-factor for the study of the current helicity. Naturally the current helicity will depend on the intensity of the magnetic field, while α does not.
2. The reversed sign of the current helicity tends to occur in particular heliographic longitudes. This reflects the complex configuration of the photospheric magnetic field brought up by the emerging magnetic flux.

We wish to thank T. J. Wang for the discussion and kind help on computer programs. This research is supported by the Chinese Academy of Sciences and National Science Foundation of China.

REFERENCES

Abramenko, V. I., Wang, T. J., & Yurchishin, V. B. 1996, Sol. Phys., 168, 75
Bao, S. D., & Zhang, H. Q. 1998, ApJ, 496, L43
Berger, M. A., & Field, G. B. 1984, J. Fluid Mech., 133
D'Silva, S. 1992, in ASP Conf. Ser. 27, The Solar Cycle, ed. K. L. Harvey (San Francisco: ASP), 168
Gilman, P. A. 1983, ApJS, 53, 243
Glatzmaier, G. A. 1985, ApJ, 291, 300
Goode, P. R., Frohlich, C., & Toutain, T. 1992, in ASP Conf. Ser. 27, The Solar Cycle, ed. K. L. Harvey (San Francisco: ASP), 282
Moffatt, H. K. 1978, Magnetic Field Generation in Electrically Conducting Fluids (Cambridge: Cambridge Univ. Press)
Parker, E. N. 1955, ApJ, 122, 293
Pevtsov, A. A., Canfield, R. C., & Metcalf, T. R. 1995, ApJ, 440, L109
Rust, D. M., & Kumar, A. 1994, Sol. Phys., 155, 69
Seehafer, N. 1990, Sol. Phys., 125, 219
Wang, H., Zirin, H., Pattern, A., Ai, G., & Zhang, H. Q. 1989, ApJ, 343, 489
Wang, T. J., Xu, A. A., & Zhang, H. Q. 1994, Sol. Phys., 155, 99
Warwick, C. S. 1965, ApJ, 141, 500
Zhang, H. Q. 1995, A&A, 304, 541
Zhang, H. Q., Ai, G., Wang, H., Zirin, H., & Pattern, A. 1992, Sol. Phys., 140, 307

Astron. Astrophys. 339, 880–886 (1998)

ASTRONOMY AND ASTROPHYSICS

Latitudinal distribution of photospheric current helicity and solar activities

Hongqi Zhang and Shudong Bao

Beijing Astronomical Observatory, Chinese Academy of Sciences, Beijing 100080, P.R. China

Received 8 October 1997 / Accepted 24 April 1998

Abstract. In this paper, we analyze the latitudinal distribution of the photospheric current helicity for 422 active regions, including most of the large ones observed in the last ten years. Observations show that most active regions in the northern hemisphere have negative helicities and in the southern hemisphere have positive ones. The negative maximum values of current helicity occurred in 1989 and 1991, while those positive around 1992. It is evident that the observational current helicity of active regions is normally brought up by emerging magnetic flux from the subatmosphere and probably acted by the moving mass. The result observed shows that less than 20 % of active regions have the sign opposite to that of most ones in the same hemisphere. These reversed sign regions of the current helicity are obviously related to abnormal distribution of the vector magnetic field in the active regions, due to emergence of new magnetic flux of opposite polarities.

Key words: Sun: activity – Sun: magnetic fields – Sun: photosphere

1. Introduction

A graph of the range in latitude of sunspots as a function of cycle phase (Butterfly diagram) was discovered many years ago (cf. Wilson 1994). It supplies information on the distribution of strong magnetic field regions on the solar surface within solar cycles. The evolution of the large-scale longitudinal magnetic field in the solar surface was provided by synthetic analysis with a series of full-disk photospheric magnetograms, which contains the information on the origin of large-scale magnetic fields on the solar surface and the reversal of polar magnetic field with solar magnetic cycles. Observations show that strong twisted magnetic fields on the solar surface normally occur in active regions, which relates to properties of the helicity of the magnetic field. Several previous investigations indicate trans-equatorial change in sign of the helicity of active regions in the photosphere (Seehafer 1990; Pevtsov et al. 1995; Abramenko et al. 1996). If the magnetic field consists of an ensemble of flux tubes, the helicity of the magnetic field depends on the configuration of the flux tubes. By analyzing the twisted magnetic field in the electric current picture, it is found that the formation of the electric current in the active regions obviously relates to the emergence and the evolution of new magnetic flux (Wang et al. 1994; Zhang 1995b, 1997).

The dynamo for the global magnetic field is normally assumed to operate at the base of the convection zone. A possible mechanism is the turbulent alpha effect (Parker 1955), which generates from small-scale velocity fluctuations in electromotive force parallel or anti-parallel to the mean magnetic field. The helicity of the convection motions relates to the generation of poloidal fields from toroidal fields. As the magnetic flux on the solar surface emerges from the deeper layers of the Sun, some information of the alpha effect can be inferred by the photospheric vector magnetic field. The problem is how to link the distribution of the helicity of the magnetic field on the solar surface with solar cycles and the relationship with individual current helicity regions.

In this paper, we pay attention to studying the latitudinal distribution of current helicity of active regions and their relationship with solar activity, especially for some typical active regions.

2. Definition of current helicity

Helicities are topologically a measure of the structural complexity of the corresponding fields (Moffatt 1978; Berger & Field 1984; Seehafer 1990). The helicity of magnetic fields may be characterized by several different parameters. The magnetic helicity density h_m=$\mathbf{A}\cdot\mathbf{B}$, with $\mathbf{A}$ the vector potential for magnetic field $\mathbf{B}$, measures the linkage of magnetic lines of force. The total magnetic helicity is

$$H_m = \int \mathbf{A}\cdot\mathbf{B}d^3x, \tag{1}$$

which may not be conserved when finite resistivity is present (Berger & Field 1984). However, the magnetic helicity is unmeasurable in the solar atmosphere until now. Assuming a linear Ohm's law,

$$\mathbf{E}-\frac{1}{\mathbf{c}}\mathbf{B}\times\mathbf{v}=\eta\mathbf{J}, \tag{2}$$

the helicity-dissipation rate is

$$\frac{dH_m}{dt} = -2c\int_V \eta\mathbf{J}\cdot\mathbf{B}d^3x. \tag{3}$$

The current helicity density is

$$h_c = \frac{4\pi}{c}\mathbf{B}\cdot\mathbf{J} = \mathbf{B}\cdot\nabla\times\mathbf{B} = \mathbf{B}_\perp\cdot(\nabla\times\mathbf{B})_\perp + \mathbf{B}_\parallel\cdot(\nabla\times\mathbf{B})_\parallel, \quad (4)$$

which describes the linkage of electric current. The simple relationship between h_m and h_c can be inferred in the approximation of the force-free field (Pevtsov et al. 1995), and thus the current helicity density may be written in the form

$$h_c = (B/B_\parallel)^2\mathbf{B}_\parallel\cdot(\nabla\times\mathbf{B})_\parallel. \quad (5)$$

The current helicity, however, is measurable in the solar photosphere. The mean density of current helicity in the local area of the solar surface is

$$\overline{h_c} = \frac{1}{S}\int\int \mathbf{B}\cdot\nabla\times\mathbf{B}ds, \quad (6)$$

e.g. this is an average value of the current helicity density h_c in the observing region S. Because the transverse component of the electric current cannot be inferred by the observational photospheric vector magnetograms, we will only refer to the second term $\mathbf{B}_\parallel\cdot(\nabla\times\mathbf{B})_\parallel$ of the current helicity in Eq. (4) in the following.

In the last ten years, many of vector magnetograms for active regions were observed at Huairou Solar Observing Station of Beijing Astronomical Observatory, which allows us to compute the distribution and the evolution of the current helicity. The data reduction of vector magnetograms, calculating the longitudinal electric current and the corresponding current helicity, was described by Wang et al. (1994) and Bao & Zhang (1998). For analyzing the distribution of the electric current helicity in the solar latitude, we consider 422 active regions in the last ten years. Most of the active regions belong to solar cycle 22 and a few of them belong to solar cycle 23.

3. Latitudinal variation of current helicity

The latitudinal distribution of current helicity in active regions is shown in Fig. 1. We can see that most current helicities in sunspot groups in the northern hemisphere show negative sign, while positive in the southern hemisphere, which is consistent with Seehafer's result (Seehafer 1990). The distribution of current helicity in active regions also shows the Butterfly pattern if comparing the distribution of current helicity through the solar cycle. This means that the positions of high electric current helicities are firstly in the middle latitudes at the beginning of a new solar cycle, then shift to high latitudes towards the equator with time, giving rise to the characteristic Butterfly pattern. We see that less than 20% of the active regions do not follow the general trend, but have a positive sign of the current helicity in the northern hemisphere and negative in the southern hemisphere.

The regions of high negative current helicity occurred in 1989 and 1991 which includes active regions NOAA 5395, 6659 (two super-active regions) and 6619 in the northern hemisphere, and NOAA 6615 in the southern hemisphere. The high helicity regions of positive sign occurred between the end of 1991 and the beginning of 1993. They included active regions NOAA 6891, 7321 and 7440 in the southern hemisphere. That the maximum values of current helicity in the northern hemisphere occurred in 1989 and 1991 and that in the southern hemisphere around 1992 are consistent with the configuration of two peaks of the solar activity in the solar cycle 22, which is well-known.

The imbalance of electric current helicity in an active region is defined by

$$\rho_h = \frac{\int\int h_c ds}{\int\int |h_c| ds}. \quad (7)$$

The sign of the electric current helicity may not be the same at each position in an active region. In other words, a given active region probably contains mixed signs of current helicity. The imbalance ρ_h of current helicity in an active region does not immediately relate to the amplitude of current helicity, because the total helicity of a solar active region sums the local helicities (sometimes with mixed signs) over the whole region in Eq. (7). The latitudinal distribution of imbalance ρ_h of current helicity in active regions is shown in Fig. 2.

By comparing between Figs. 1 and 2, we can find that some sunspot groups, which show low current helicity, have relatively strong imbalance of current helicity between the positive and negative signs in an active region, i.e. these regions have a predominate twisting direction of the magnetic field.

In addition, the average values of the intensity and imbalance of current helicity in active regions calculated by us are shown in Fig. 1 after data smoothing. Their distributions are a little different from one other, but show the same tendency. This means that the statistical average of the current helicity regions normally corresponds to that of the imbalance of the helicity. The average values of current helicity in 1989 occurred in the northern hemisphere, while that in 1992 in the southern hemisphere. Because most large active regions in the last ten years are included, these probably reflect the real tendency of current helicity in active regions in both hemispheres.

4. Current helicity and magnetic shear in active regions

According to the second term of Eq. (4) and Eq. (5), we can see that the density of current helicity depends on the twist of the transverse magnetic field and the intensity of the longitudinal magnetic field. The observational results of the photospheric magnetic field demonstrate that the formation of the twisting magnetic field (electric current) obviously relates to the arrangement of the magnetic field in the active regions (Zhang 1995b, 1997).

To analyze the global properties of current helicity of active regions, we define the normal current helicity which follows the global sign rule of the current helicity (i.e. in the northern (southern) hemisphere the sign of helicity is negative (positive)) and the reversal current helicity which shows the sign oppositely to the global rule. We present some examples of current helicity in the following.

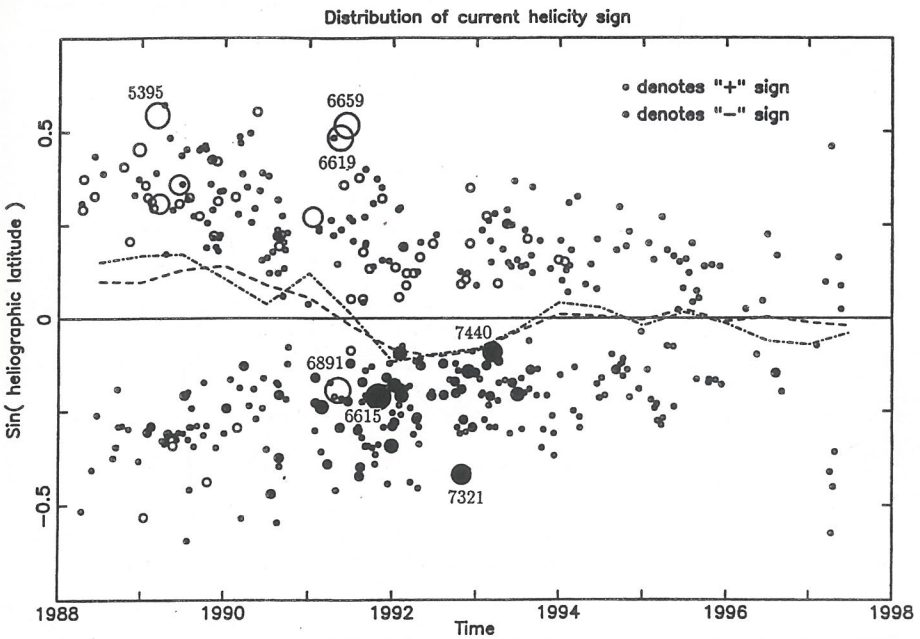

Fig. 1. Butterfly diagram of the electric current helicity. The mean density of the current helicity of active regions is marked by size of the circles for grades: 0, 1, 3, 5, 7 ($\times 10^{-3} G^2 m^{-1}$). The dashed-dotted line marks the average value of current helicity and the dashed line marks the average value of the imbalance of current helicity after the data smooth.

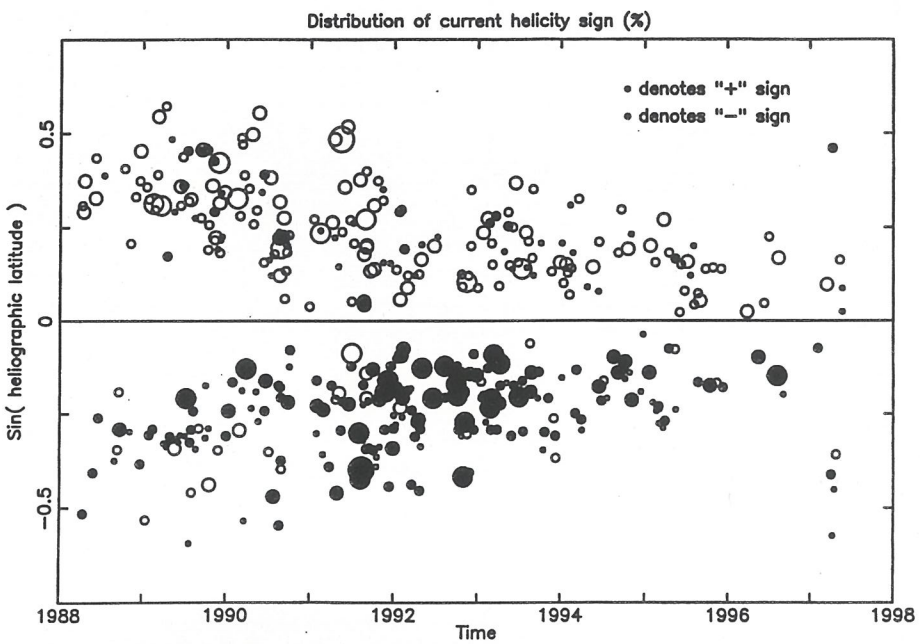

Fig. 2. Imbalance ρ_h of the current helicity. The imbalance of the current helicity is marked by sizes of the circles for grades: 0, 10, 30, 50, 70 (%).

4.1. Normal current helicity

Fig. 3a shows a vector magnetogram in the active region (NOAA 6659) on 9 June 1991. This active region was a super-active region and occurred in high latitude (N32) in the solar cycle 22. The relationship between the flares and the configuration of the magnetic field was analyzed by Zirin & Wang (1992) and Zhang (1995a, 1996) etc. The transverse magnetic field rotates counter-clockwisely towards the center of the active region and a series of highly sheared magnetic flux successively emerges near the magnetic neutral line. As comparing with the vertical electric current map (Fig. 3b), we may guess that the electric current flows up from the center of the active region towards the surrounding areas. The large-scale current helicity shows negative sign, even though a positive area is located at the north of the active region. This is a good evidence of the current helicity due to the twist of the transverse magnetic field in the northern hemisphere, which coincides with the normal sign rule of the distribution of current helicity (Seehafer 1990). By analyzing the evolution, we find that it was a mature active region and gradually drawn away by the different rotations (Schmieder et al. 1994), even though a series of highly-sheared magnetic flux emerged near the magnetic neutral line to trigger flares.

Fig. 4 shows a vector magnetogram in active region (NOAA 6772) on 12 August 1991. This active region was located at the southern hemisphere (S24) and consisted of an unipolar spot. The transverse magnetic field shows counter-clockwise vortex. The vertical electric current flows up from the center of the

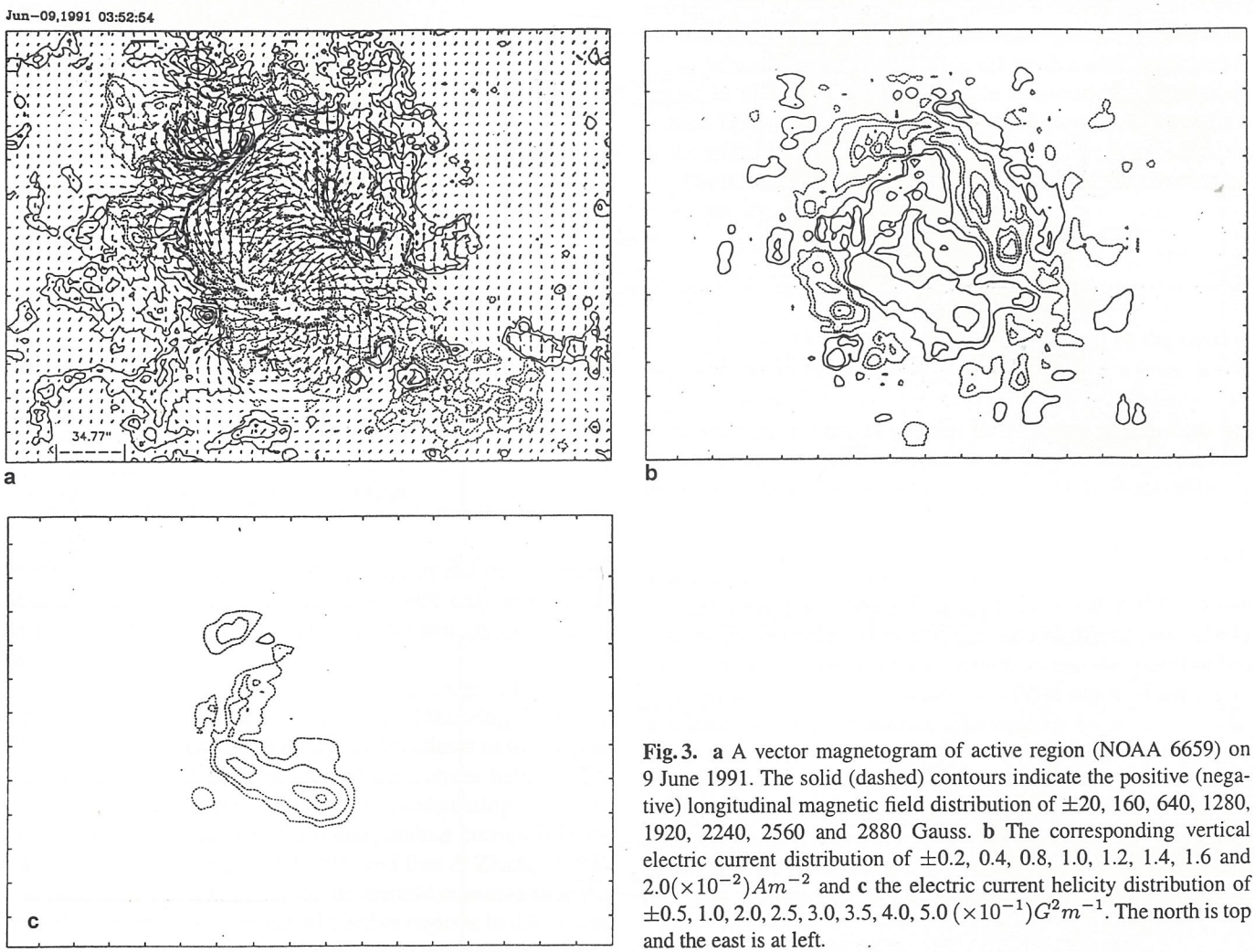

Fig. 3. **a** A vector magnetogram of active region (NOAA 6659) on 9 June 1991. The solid (dashed) contours indicate the positive (negative) longitudinal magnetic field distribution of ±20, 160, 640, 1280, 1920, 2240, 2560 and 2880 Gauss. **b** The corresponding vertical electric current distribution of ±0.2, 0.4, 0.8, 1.0, 1.2, 1.4, 1.6 and $2.0(\times 10^{-2})Am^{-2}$ and **c** the electric current helicity distribution of ±0.5, 1.0, 2.0, 2.5, 3.0, 3.5, 4.0, 5.0 $(\times 10^{-1})G^2m^{-1}$. The north is top and the east is at left.

sunspot and returns to the surrounding areas. A similar case can be found in the active region (NOAA 6767) in Fig. 5, which was also located in the southern hemisphere (S26.5) on 9 August 1991. They are decaying active regions and show obvious single sign of current helicity, which coincide with the general rule of global helicity. These are not significant trails of newly-emerging magnetic flux in these active regions. The rotation of the photospheric transverse magnetic field probably reflects the original properties of the sunspot magnetic field, which pattern may be partly distorted in some complex active regions.

4.2. Reversal current helicity

Fig. 6 shows the active region (NOAA 7070) on 25 Feb. 1992. This active region was located in the northern hemisphere (N5.6). From daily vector magnetograms, we find that the magnetic field in this active region consists of two main parts. One is magnetic poles (N_1 and S_1), another is (N_2 and S_2). The magnetic shear occurs near the magnetic neutral line between the magnetic poles (N_1 and S_1) of opposite polarity. Newly emerging magnetic flux occurs near the magnetic neutral line between magnetic poles (N_2 and S_2) of opposite polarity and pushs them apart. Thus, this active region relates to two electric current systems and contains opposite signs of the helicity, which does not completely coincide with the normal rule of the current helicity due to the emergence of magnetic flux. The development of the magnetic field in this active region is provided in a subsequent paper.

Fig. 7 shows a vector magnetogram in the active region (NOAA 6615) on 7 May 1991 and the corresponding electric current and helicity maps. This active region located in the southern hemisphere (S11.2) shows opposite sign of current helicity to the sign rule of most of the active regions in the southern hemisphere. We analyze the distribution of the vector magnetic field in the active region and its evolution, and we can find that it was a newly-growing active region. From a series of daily magnetograms, we find that two magnetic bipoles (N_3, S_3) and (N_4, S_4) emerge in the active region, and their transverse component of the magnetic field rotates clockwisely. The distribution of the vertical component of the electric current provides the information that the electric current flows towards the center of the active region from the surrounding areas.

From the results in active regions (NOAA 6615 and 7070), we find that the emergence of the magnetic flux of opposite

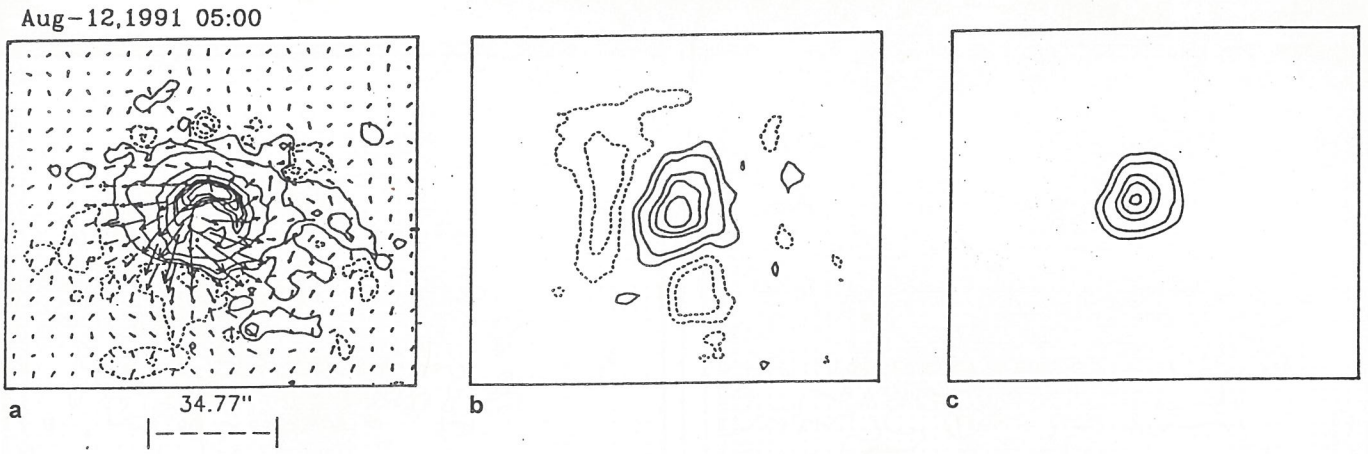

Fig. 4. a A vector magnetogram of active region (NOAA 6772) on 12 August 1991. The solid (*dashed*) contours indicate the positive (*negative*) longitudinal magnetic field distribution of ±20, 160, 640, 1280, 1920, 2240, 2560 and 2880 Gauss. **b** The corresponding vertical electric current distribution of ±0.2, 0.4, 0.8, 1.0, 1.2, 1.4, 1.6 and $2.0(\times 10^{-2})Am^{-2}$ and **c** the electric current helicity distribution of ±0.5, 1.0, 2.0, 2.5, 3.0, 3.5, 4.0, 5.0 $(\times 10^{-1})G^2m^{-1}$. The north is top and the east is at left.

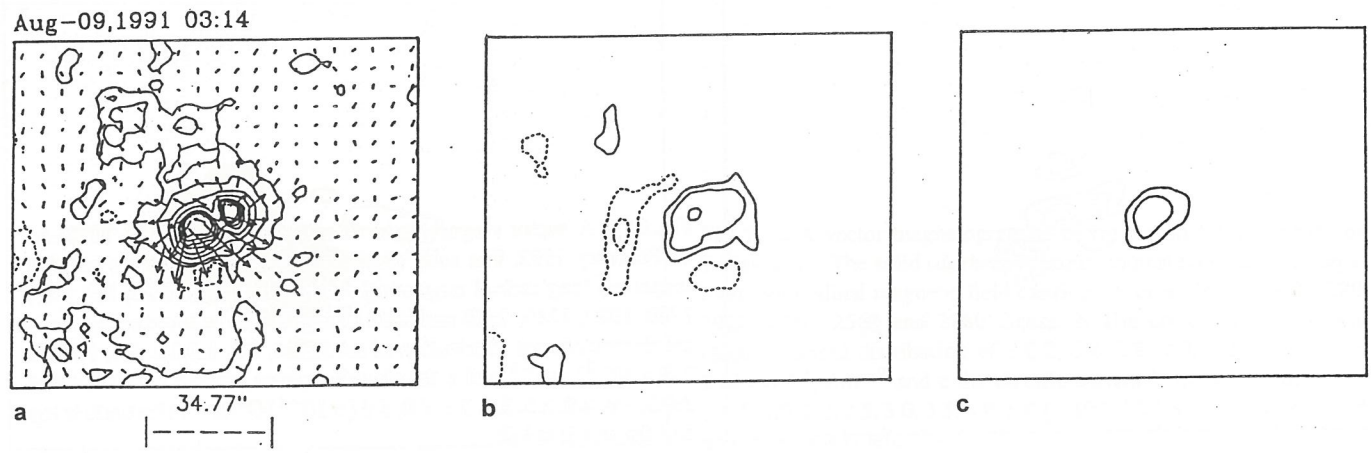

Fig. 5. a A vector magnetogram of active region (NOAA 6767) on 9 August 1991. The solid (*dashed*) contours indicate the positive (*negative*) longitudinal magnetic field distribution of ±20, 160, 640, 1280, 1920, 2240, 2560 and 2880 Gauss. **b** The corresponding vertical electric current distribution of ±0.2, 0.4, 0.8, 1.0, 1.2, 1.4, 1.6 and $2.0(\times 10^{-2})Am^{-2}$ and **c** the electric current helicity distribution of ±0.5, 1.0, 2.0, 2.5, 3.0, 3.5, 4.0, 5.0 $(\times 10^{-1})G^2m^{-1}$. The north is top and the east is at left.

polarity influences the distribution of the electric current in the photosphere (Zhang 1995b, 1996). The current helicity in these emerging flux regions trend towards the opposite sign relative to the general ones.

5. Discussion and results

The study on distribution of the current helicity and its relationship with the solar cycle is an important topic, because it provides information on the transportation of the twisted magnetic field (electric current) from the subatmosphere, which is different from that of the sunspot groups and the large-scale pattern of the longitudinal magnetic field.

The observational helicity of active regions provides a chance to analyze the twist of the strong magnetic field in the solar surface. We find that the areas of strong current helicity of opposite sign first occur in the middle latitudes of the both hemispheres at the beginning of a new solar cycle and gradually migrate from high latitude to low latitude. The signs of most current helicity in active regions coincide with the normal rule (i.e. in the northern (southern) hemisphere the sign of helicity is negative (positive)). If the atmospheric currents are generated in the (subphotospheric) region of dynamo operation before the flux ropes from which active regions result have broken away from the toroidal field belt, these currents should be generated by the alpha effect (Seehafer 1990).

The statistical results demonstrate that the distribution of current helicity in both hemispheres also connects with the solar activity, e.g. most of the powerful flare producing regions show strong current helicity, such as the active regions 5395 and 6659. This means that the helicity is an important index of the reserved magnetic energy in active regions.

We also find that the imbalance of the current helicity in the unipolar active regions (decaying active regions) is obvious,

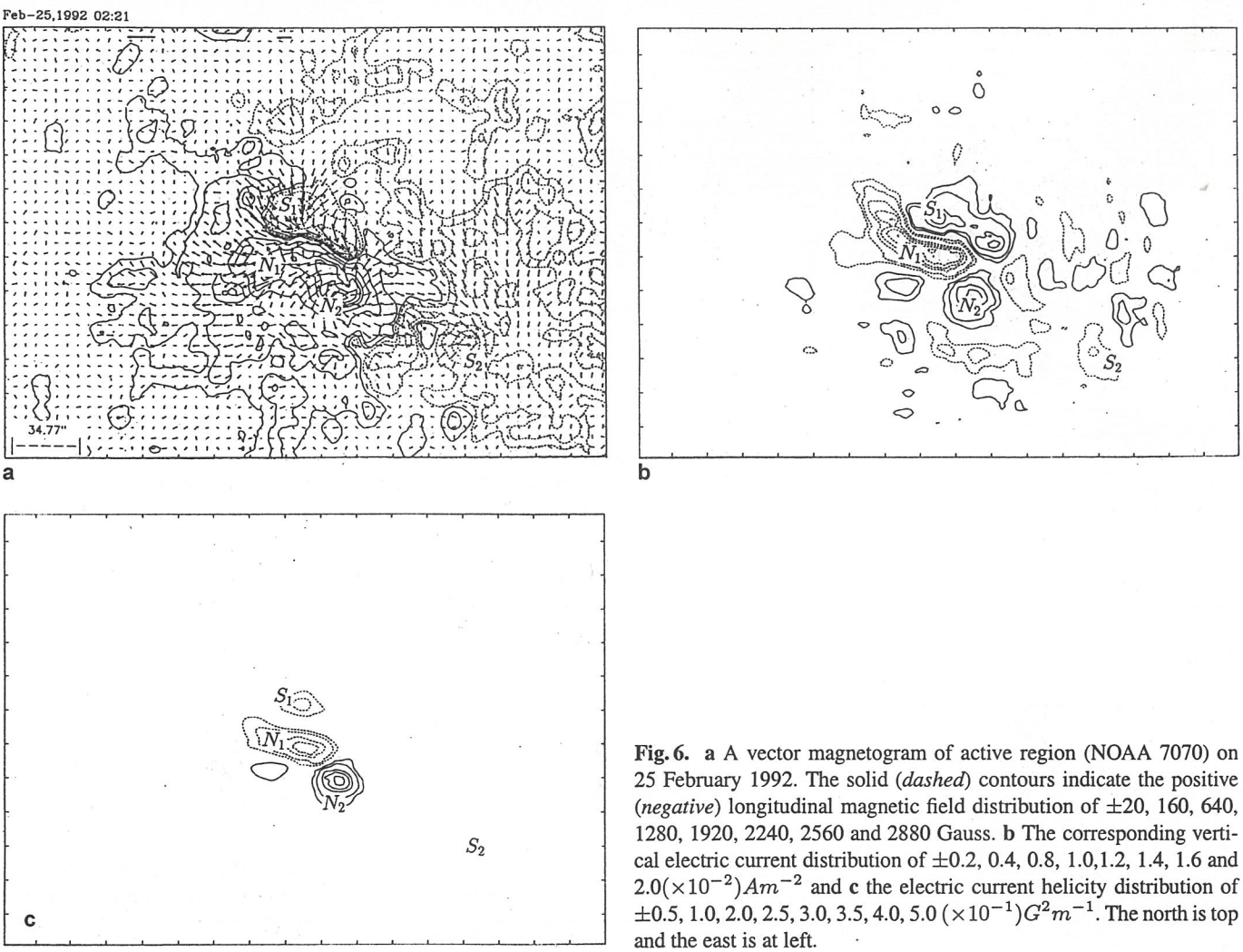

Fig. 6. **a** A vector magnetogram of active region (NOAA 7070) on 25 February 1992. The solid (*dashed*) contours indicate the positive (*negative*) longitudinal magnetic field distribution of ±20, 160, 640, 1280, 1920, 2240, 2560 and 2880 Gauss. **b** The corresponding vertical electric current distribution of ±0.2, 0.4, 0.8, 1.0,1.2, 1.4, 1.6 and $2.0(\times 10^{-2})Am^{-2}$ and **c** the electric current helicity distribution of ±0.5, 1.0, 2.0, 2.5, 3.0, 3.5, 4.0, 5.0 $(\times 10^{-1})G^2m^{-1}$. The north is top and the east is at left.

while the values of current helicity normally are not large. Evershed flow in the sunspots is probably an important reason of the twisted transverse magnetic field proposed by Seehafer (1990), due to the action of Coriolis force on the magnetic field lines. The decaying process of the magnetic main pole, which is due to the outward movement of the broken magnetic fragments, and the relationship with Evershed flow in a similar active region were demonstrated by Wang et al. (1989) and Zhang et al. (1992).

It is noticed that the signs of current helicity in some active regions reverse to the normal rule. The observational results demonstrate that the intrinsic twisting character of newly-emerging magnetic flux tubes is probably insignificant in some active regions (Zhang & Song 1992; Zhang 1995b), or hard to detect in the unresolved size. The magnetic shear in active regions is obviously caused by the emergence of magnetic flux of opposite polarities, such as in the active active regions NOAA 6615 and 7070. This means that the emerging magnetic flux of opposite polarity not only carries up the new current helicity from the subatmosphere, but also interacts with the pre-existing magnetic field and breaks up the distribution of former current helicity in active regions in the photosphere, although the current helicities brought by newly-emerging magnetic flux for most of the active regions coincide with the sign rule in both hemispheres.

From the above discussion, we find that the configuration of the current helicity of active regions and its change in the photosphere comes from two possibilities. One is caused by the emergence of new magnetic flux, which brings the new helicity into the photosphere from the subatmosphere. Another comes from the mass motion, such as the Evershed flow in sunspots near the photosphere, which changes the arrangement of the magnetic field in the action of the Coriolis force. These progressively change the distribution of the global helicity. Moreover, the twisted magnetic fields are probably ejected as CMEs and magnetic clouds, which transport the current helicity from the solar atmosphere into interplanetary space. On the other hand, even though the current helicity in active regions is interperted by us, many questions on the understanding of global properties of the helicity remain to be answered, such as we do not clarify the relationship between the helicity in active regions and that of the large-scale global field on the solar surface.

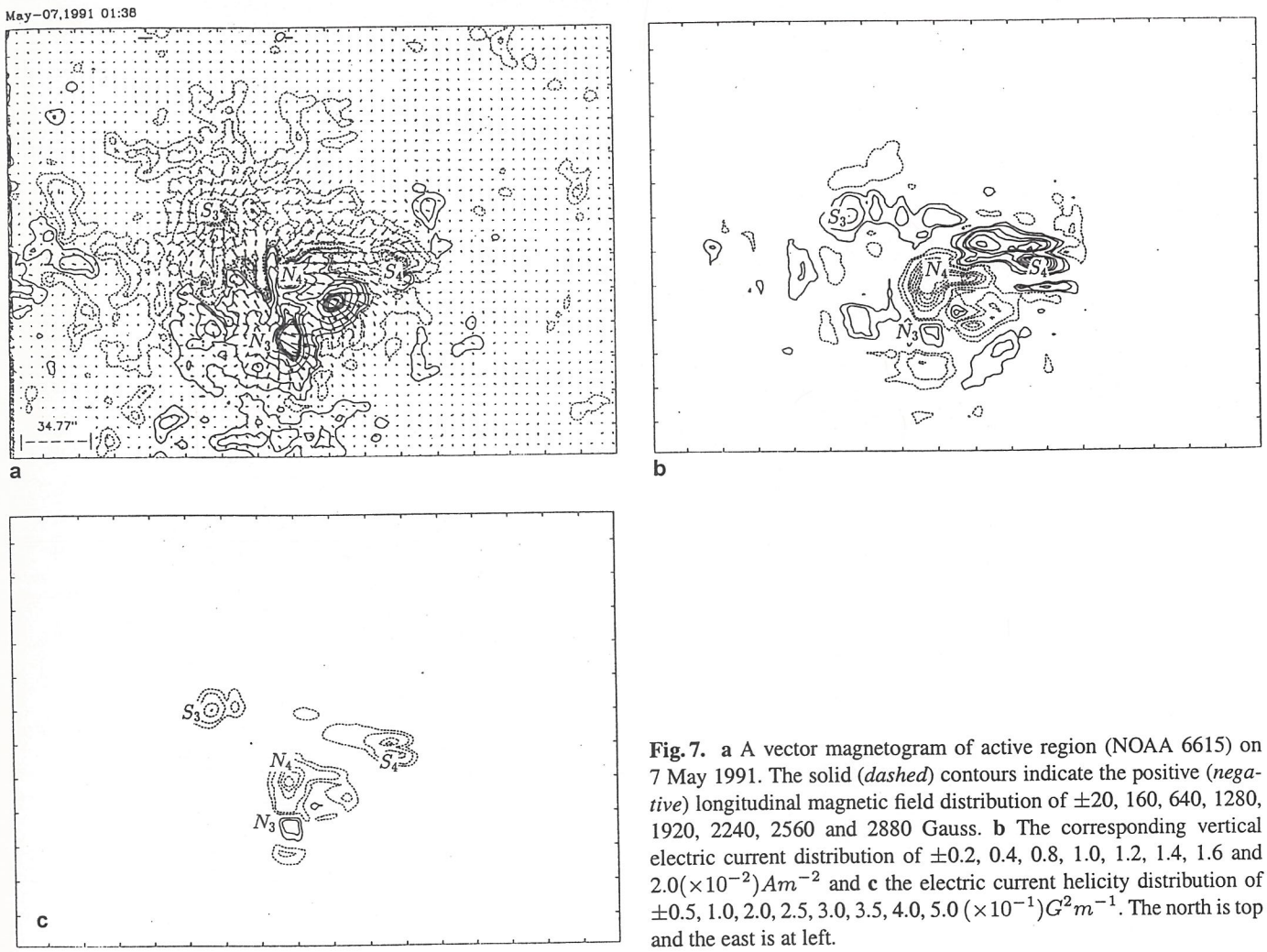

Fig. 7. **a** A vector magnetogram of active region (NOAA 6615) on 7 May 1991. The solid (*dashed*) contours indicate the positive (*negative*) longitudinal magnetic field distribution of ±20, 160, 640, 1280, 1920, 2240, 2560 and 2880 Gauss. **b** The corresponding vertical electric current distribution of ±0.2, 0.4, 0.8, 1.0, 1.2, 1.4, 1.6 and $2.0(\times 10^{-2})Am^{-2}$ and **c** the electric current helicity distribution of ±0.5, 1.0, 2.0, 2.5, 3.0, 3.5, 4.0, 5.0 $(\times 10^{-1})G^2m^{-1}$. The north is top and the east is at left.

After the analysis, the main results are as follows:

1. The average current helicity of active regions normally shows opposite signs in the two hemispheres. The maximum negative values occurred in the northern hemisphere in 1989 and 1991, while the positive ones in the southern hemisphere in about 1992 in the solar cycle 22.
2. The reverse signs of the current helicity of active regions to the normal rule in the same hemispheres are related to abnormal distribution of the vector magnetic field of active regions, due to the emerging magnetic flux of opposite polarities, which probably brings new helicity of opposite sign from the subatmosphere or breaks the sign distribution of current in both hemispheres.

Acknowledgements. We would like to thank the anonymous referee for his valuable comments which improved the manuscript. We also thank Dr. T.J. Wang for his discussion and kind help on computer programs. This research is supported by the Chinese Academy of Sciences and National Nature Science Foundation of China.

References

Abramenko, V.I., Wang, T.J. and Yurchishin, V.B. 1996, Solar Phys., 168, 75
Bao, S.D. and Zhang, H.Q. 1998, Astrophys. J. 496, L43
Berger, M.A. and Field, G.B. 1984, J. Fluid Mech., 147, 133
Moffatt, H.K. 1978, Magnetic Field Generation in Electrically Conducting Fluids, Cambridge University Press.
Parker, E.N. 1955, Astrophys. J., 122, 293
Pevtsov, A.A., Canfield, R.C. and Metchalf, T.R. 1995, Astrophys. J., 440, L109
Schmieder, B., Hagyard, H., Ai, G. et al. 1994, Solar Phys., 150, 199
Seehafer, N. 1990, Solar Phys., 125, 219
Wang, H., Zirin, H., Pattern, A., Ai, G. and Zhang, H.Q. 1989, Astrophs. J., 343, 489
Wang, T.J., Xu, A.A. and Zhang, H.Q. 1994, Solar Phys., 155, 99
Wilson, P.R. 1994, Solar and Stellar Active Cycles, Cambridge University Press.
Zhang, H.Q. 1995a, A&A 297, 869
Zhang, H.Q. 1995b, A&A 304, 541
Zhang, H.Q. 1996, Astrophys. J., 471, 1049
Zhang, H.Q. 1997, A&A 324, 713
Zhang, H.Q., Ai, G., Wang, H., Zirin, H. and Pattern, A. 1992, Solar Phys., 140, 307
Zhang, H.Q. and Song, M.T. 1992, Solar Phys., 138, 69
Zirin, H. and Wang, H., 1993, Nature, 363, 3, 426